Universitat
de les Illes Balears

DOCTORAL THESIS
2024

AGING AND MEMORY EFFECTS IN SOCIAL AND ECONOMIC DYNAMICS

David Abella Bujalance

Universitat de les Illes Balears

DOCTORAL THESIS
2024
Doctoral programme in Physics

AGING AND MEMORY EFFECTS IN SOCIAL AND ECONOMIC DYNAMICS

David Abella Bujalance

Thesis Supervisor: José Javier Ramasco Sukia
Thesis Supervisor: Maxi San Miguel
Thesis Tutor: Cristóbal López Sánchez

Doctor by the Universitat de les Illes Balears

Supervisors:
José Javier Ramasco Sukia
Maxi San Miguel

David Abella Bujalance.
Aging and memory effects in social and economic dynamics. ©
Palma de Mallorca, June 2024

A en Manuel Miranda
pel seu suport i ajuda
durant tots aquests anys.
Sempre estaràs amb mi.
i recordare sempre
el que em vas ensenyar.

Dr José Javier Ramasco of the Consejo Superior de Investigaciones Científicas (CSIC) and Dr Maxi San Miguel of the Universitat de les Illes Balears (UIB)

WE DECLARE:

That the thesis titles *Dynamics of social interactions*, presented by David Abella Bujalance to obtain a doctoral degree, has been completed under my supervision and meets the requirements to opt for an International Doctorate.

For all intents and purposes, I hereby sign this document.

Signature

Dr. José Javier Ramasco Sukia	Dr. Maxi San Miguel
Thesis Supervisor	Thesis Supervisor

Palma de Mallorca, June 2024

Acknowledgements

M'agradaria agrair aquesta tesi a totes les persones que m'han ajudat a fer-la possible. En primer lloc, vull agrair a la meva família, per tot el suport que m'han donat durant tots aquests anys. En especial, vull agrair a la meva mare, per tot el que ha fet per mi, i per tot el que ha hagut de patir per mi. També vull agrair a la meva parella, per tot el suport que m'ha donat, i per tot el que m'ha ajudat a tirar endavant. I finalment, vull agrair a tots els meus amics, per tot el suport que m'han donat, i per tots els bons moments que hem passat junts.

Des d'un primer moment, vull agrair a la meva directora, la professora Marta Arias, per haver-me donat l'oportunitat de fer aquest projecte, i per tot el suport que m'ha donat durant tot el projecte. També vull agrair al meu tutor, el professor Jordi Casas, per tot el suport que m'ha donat durant tot el projecte. I finalment, vull agrair a tots els professors que m'han ensenyat durant tots aquests anys, per tot el que m'han ensenyat, i per tot el que m'han ajudat a tirar endavant.

Tambe afegir que aquest projecte no hagués estat possible sense l'ajuda de tots els companys que han fet possible que aquest projecte sigui una realitat. Jo que soc un dels que ha fet possible que aquest projecte sigui una realitat, vull agrair a tots els companys que han fet possible que aquest projecte sigui una realitat, per tot el suport que m'han donat durant tot el projecte.

Resum

En els sistemes complexos distribuïts, els sistemes de memòria transaccional distribuïda (DTM) són una eina molt útil per a la programació concurrent. Aquests sistemes permeten als desenvolupadors de software escriure codi concurrent sense haver de preocupar-se per la gestió de la memòria compartida. A més, els DTM ofereixen una interfície molt senzilla per a la programació concurrent, ja que permeten als desenvolupadors de software escriure codi concurrent de forma semblant a com ho farien si el codi fos seqüencial. Tot i això, els DTM no són una eina perfecta, ja que tenen un rendiment molt inferior al de les estructures de dades distribuïdes. A més, els DTM no són capaços de gestionar estructures de dades distribuïdes de forma eficient. Per aquest motiu, els DTM no són una eina adequada per a la programació de sistemes distribuïts.

Resumen

En los sistemas complejos distribuidos, los sistemas de memoria transaccional distribuida (DTM) son una herramienta muy útil para la programación concurrente. Estos sistemas permiten a los desarrolladores de software escribir código concurrente sin tener que preocuparse por la gestión de la memoria compartida. Además, los DTM ofrecen una interfaz muy sencilla para la programación concurrente, ya que permiten a los desarrolladores de software escribir código concurrente de forma similar a como lo harían si el código fuera secuencial. Sin embargo, los DTM no son una herramienta perfecta, ya que tienen un rendimiento muy inferior al de las estructuras de datos distribuidas. Además, los DTM no son capaces de gestionar estructuras de datos distribuidas de forma eficiente. Por este motivo, los DTM no son una herramienta adecuada para la programación de sistemas distribuidos.

Abstract

In complex systems distributed transactional memory (DTM) systems are a very useful tool for concurrent programming. These systems allow software developers to write concurrent code without having to worry about managing shared memory. In addition, DTM systems offer a very simple interface for concurrent programming, as they allow software developers to write concurrent code in a similar way to how they would if the code were sequential. However, DTM systems are not a perfect tool, as they have a much lower performance than distributed data structures. In addition, DTM systems are not able to manage distributed data structures efficiently. For this reason, DTM systems are not a suitable tool for programming distributed systems.

Contents

List of Figures

List of publications

The list of articles detailed below, in chronological order by date of publication, form the basis of the present thesis.

1. David Abella, Maxi San Miguel, and José J. Ramasco. "Aging effects in Schelling segregation model". In: *Scientific Reports* 12.1 (Nov. 2022). ISSN: 2045-2322. DOI: 10.1038/s41598-022-23224-7. URL: http://dx.doi.org/10.1038/s41598-022-23224-7

2. David Abella, Maxi San Miguel, and José J. Ramasco. "Aging in binary-state models: The Threshold model for complex contagion". In: *Phys. Rev. E* 107 (2 Feb. 2023), page 024101. DOI: 10.1103/PhysRevE.107.024101. URL: https://link.aps.org/doi/10.1103/PhysRevE.107.024101

3. David Abella et al. "Ordering dynamics and aging in the symmetrical threshold model". In: *New Journal of Physics* 26.1 (Jan. 2024), page 013033. DOI: 10.1088/1367-2630/ad1ad4. URL: https://dx.doi.org/10.1088/1367-2630/ad1ad4

4. Idealista model for complex systems housing

5. Idealista spatial segmentation of the real state market

Other publications published during the PhD period are also included in the following list.

- David Abella, Giancarlo Franzese, and Javier Hernández-Rojas. "Many-Body Contributions in Water Nanoclusters". In: *ACS Nano* 17.3 (Jan. 2023), pages 1959–1964. ISSN: 1936-086X. DOI: 10.1021/acsnano.2c06077. URL: http://dx.doi.org/10.1021/acsnano.2c06077

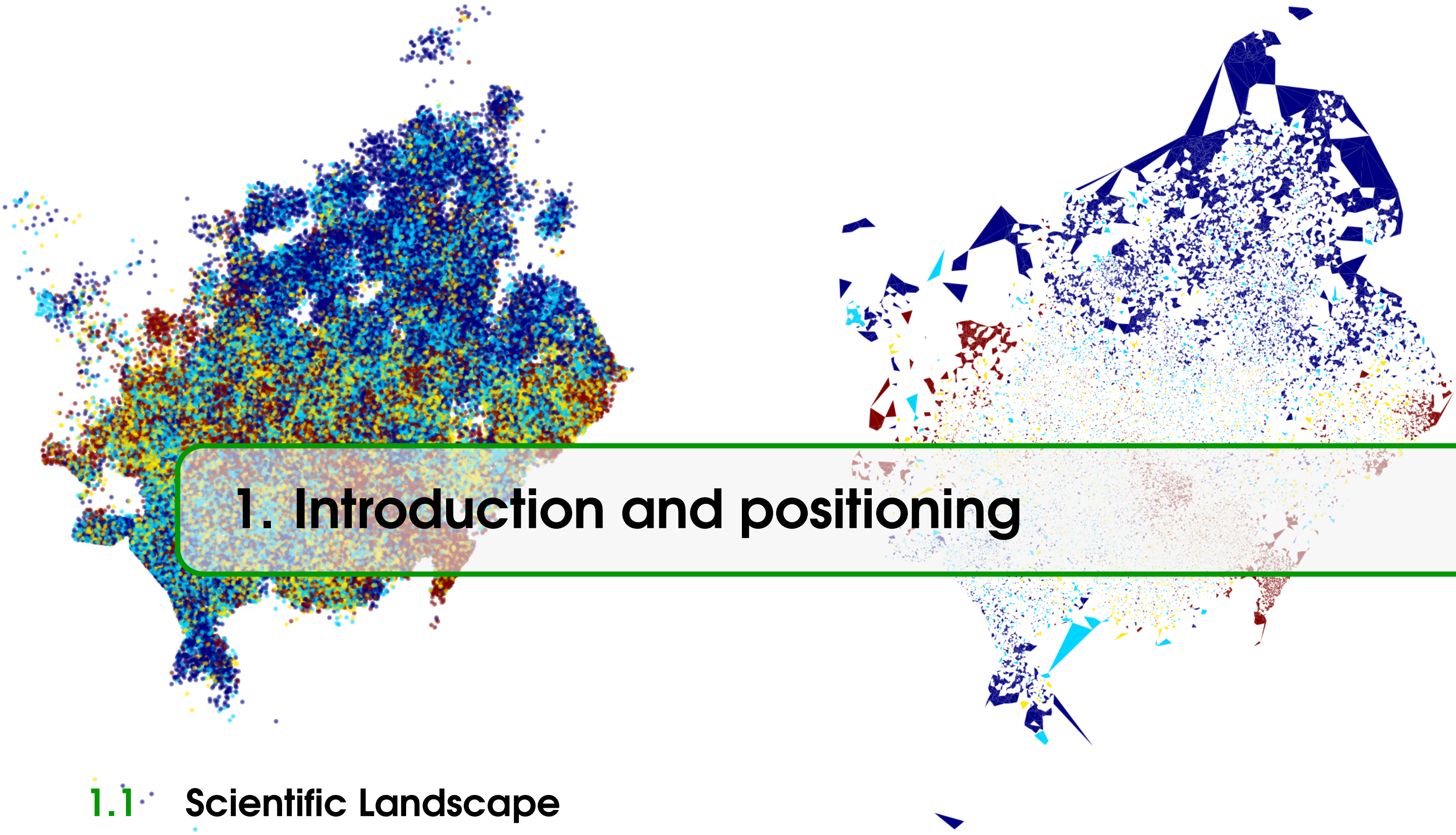

1. Introduction and positioning

1.1 Scientific Landscape

- How complex systems are studied from a physics perspective, and how the study of complex systems has evolved into the study of social systems.

- Human complex systems ....

- Nevertheless there are some challenges that are unique to the study of social systems, and that are not present in the study of physical systems and the main problem is the data availability.

- After the digital revolution, the amount of data that is generated by human activities has increased exponentially, and this data is being used to study human behavior and social systems.

- Big data is a term that is used to describe the large amount of data that is generated by human activities, and that is being used to study human behavior and social systems.

- To deal with big data, computational social science has emerged as a new field of study that uses computational methods to study human behavior and social systems.

- Also network science has emerged as a new field of study that uses network theory to study human behavior and social systems.

- This perspective is important because it allows us to understand phenomena from a different perspective, and to develop new methods to study human behavior and social systems.

- For example, the study of information spreading as a dynamical system on networks has allowed us to understand how information spreads in social networks, and to develop new methods to study information spreading in social networks.

- In particular, human interactions exhibit complex activity patterns that are difficult to understand and to model, and that are not present in the study of physical systems.

Early theoretical frameworks for understanding the contagion of ideas were heavily influenced by psychological and sociological theories. Gustave Le Bon's work on crowd psychology in the late 19th century suggested that individuals in a crowd lose their sense of self and, as a result, are more susceptible to the ideas and emotions of the crowd. Later, Gabriel Tarde's laws of imitation proposed that social change is driven by the imitation of behaviors and ideas, a process that is facilitated by close contact and communication between individuals.

1.2 Challenges of Computational Social Science

- The study of human behavior and social systems is a complex problem that requires the use of computational methods to study human behavior and social systems.

- There are some challenges that are unique to the study of human behavior and social systems, and that are not present in the study of physical systems.

1.2.1 Data availability

- The main problem is the data availability, and the fact that the data that is generated by human activities is not always available for study.

- Notice that the data sources typically used for the study of human behavior does not come from controlled experiments, but from the digital traces that are generated by human activities.

1.2.2 Data analysis

- The second problem is the data analysis, and the fact that the data that is generated by human activities is not always easy to analyze.

- The data source to analyze usually is a piece of a larger dataset, so we need to be careful to avoid biases in the analysis driven by the data size.

- Temporal windows are also a problem, because when we analyze the dynamics of a system, we need to be careful to avoid biases in the analysis driven by the temporal window.

1.2.3 Modeling

- The third problem is the modeling, and the fact that the data that is generated by human activities is not always easy to model.

- Deterministic models are not always useful to model human behavior, and we need to use stochastic models to model human behavior.

- Also, mechanistic models and data driven models is something that we need to consider when we model human behavior.

- Another possibility is to use agent-based models to model human behavior. With the advent of computational methods in the latter half of the 20th century, researchers gained powerful tools to simulate and analyze complex social systems. Agent-based modeling (ABM) emerged as a particularly influential approach, enabling scientists to create and study systems of interacting agents (individuals or collective entities) and observe emergent behaviors from simple rules of interaction.

1.2.4 Applications

- Computational social science has many applications, and it is being used to study human behavior and social systems.

- Sociotechnical systems, social networks, and human dynamics are some of the applications of computational social science.

- fake news detection, information spreading, and social influence are some of the applications of computational social science.

1.3 Terminology and general concepts

- In this section, we introduce some terminology and general concepts that are used in the study of human behavior and social systems.

Complex networks, interface density, and community structure are some of the concepts that are used in the study of human behavior and social systems.

binary state models, random networks, configuration models, and preferential attachment are some of the models that are used in the study of human behavior and social systems.

1.4 Datasets

- We used the idealista dataset

- The strong point of the idealista dataset is that it contains information about the real estate market in Spain, and that it is a large dataset that contains information about the real estate market in Spain.

- The missing point of the idealista dataset is that it contains information about the real estate market in Spain, and that it is a large dataset that contains information about the real estate market in Spain.

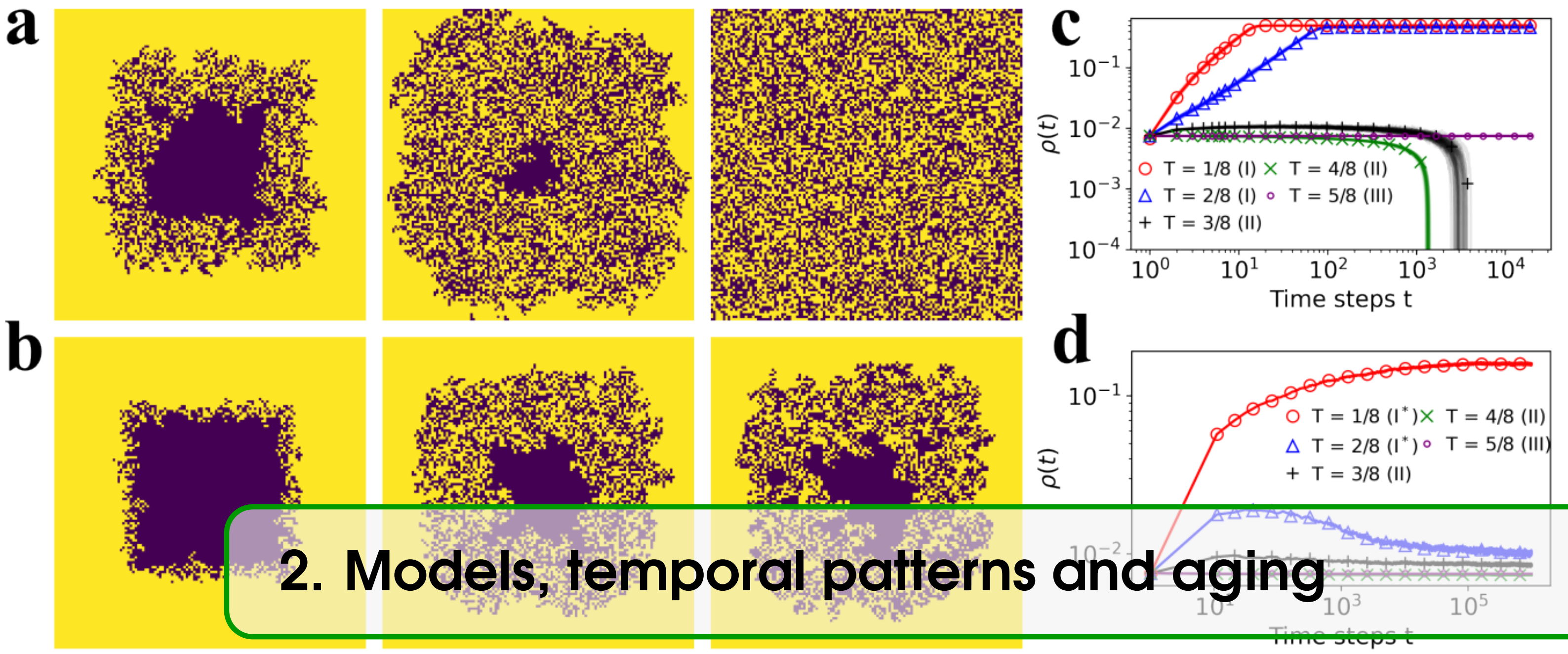

2. Models, temporal patterns and aging

2.1 Introduction

The contagion of ideas is a process that has been studied for many years and is present in many social systems, ranging from small groups and communities to large networks and societies at a global scale. This process, often referred to as social contagion, involves the spread of ideas, behaviors, innovations, and emotions among individuals and groups through various forms of social interaction. The metaphor of contagion highlights the similarities between the spread of infectious diseases and the transmission of ideas, where a single "infected" individual can influence multiple others, leading to widespread adoption of new behaviors or beliefs.

In this context, binary-state models have emerged as a versatile tool to describe a variety of natural and social phenomena in systems formed by many interacting agents. Each agent is considered to be in one of two possible states: susceptible/infected, adopters/non-adopters, democrat/republican, etc., depending on the context of the model. The interaction among agents is determined by the underlying network and the dynamical rules of the model. Examples of binary-state models include processes of opinion formation (55, 102, 132, 149), disease or social contagion (72, 123), among others. Extended and modified versions of these models can lead to very different dynamical behaviors than in the original model. As examples, the use of multi-layer (7, 46, 47) or time-dependent networks (163), higher-order interactions (8, 27, 87), non-linear collective phenomena (26, 125), noise (23) and non-Markovian (31, 126, 153, 162) effects induce significant changes to the dynamics.

With the advent of network theory and the increasing availability of large-scale data from online platforms, researchers have been able to study the contagion of ideas with unprecedented precision and detail. Duncan Watts and Steven Strogatz's small-world model (168) and Albert-László Barabási and Réka Albert's work on scale-free networks provided foundational insights into the structure of social networks and their role in facilitating or hindering the spread of information and ideas (12).

Recent studies have focused on the mechanisms of social contagion in digital environments, where ideas can spread rapidly and widely through social media platforms (39, 118). Analyses have identified emotional engagement and practical value as key drivers of sharing behavior (56, 157). Additionally, the role of social influence on online platforms has been explored, demonstrating how peer effects can significantly impact individuals' decisions to adopt new products or ideas (91).

The contagion of ideas also plays a critical role in the diffusion of innovations. Rogger's seminal work outlines a theory of how, why, and at what rate new ideas and technology spread through

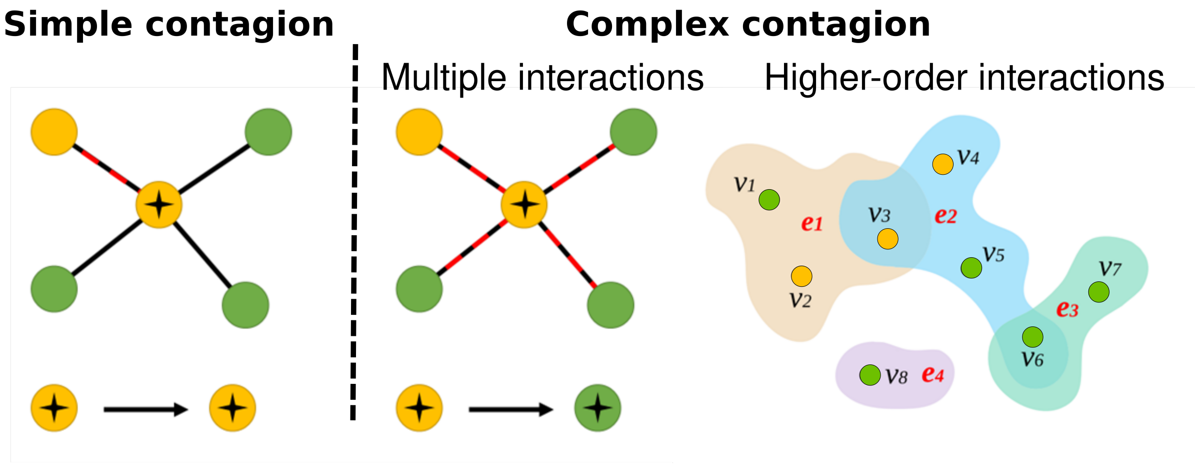

Figure 2.1: Comparison between the different types of social interaction. **Simple contagion**, where the agent considers just the pairwise interaction with one social contact (interaction highlighted with a dashed red line) and **Complex contagion**, where the agent considers the interaction with multiple social contacts. There are two distinguishable types of Complex contagion: **Multiple pairwise interactions**, where the agent considers the interaction with multiple social contacts (interactions highlighted with dashed red lines) and **Higher-order interactions**, where the agent considers the interaction with a group of social contacts, all at once, in a single interaction (not pairwise). The green, yellow colors represent the state (idea, position, political party...). (The hypergraph representation is from Ref. (8)).

cultures, highlighting the importance of social networks and opinion leaders in the spread of new ideas (133). Peer effects and social influence have been shown to play a significant role in the adoption of new technologies, with individuals more likely to adopt new products or services if they see others in their social network doing the same (21, 161).

2.2 Simple and Complex Contagion

In the study of social contagion, researchers distinguish between two main types of contagion processes: simple contagion and complex contagion. Simple contagion refers to the spread of ideas, behaviors, or innovations primarily through single exposures or interactions, much like the transmission of infectious diseases. This process is characterized by the principle that an individual's likelihood of adopting a new idea or behavior increases with each additional exposure to that idea or behavior within their social network (34, 58, 72). In contrast, complex contagion involves multiple exposures or reinforcements from different sources within the network, often requiring a critical mass of adopters before an individual is influenced to adopt the idea or behavior (29, 30).

Simple contagion is often described as a process that involves only dyadic interactions, where the adoption of an idea or behavior is facilitated by direct contact between two individuals. This type of contagion is fundamental to understanding how information, rumors, or diseases spread through populations via direct, pairwise connections (112, 122). The dynamics of simple contagion are crucial for the rapid dissemination of information and the efficient spread of both beneficial and detrimental behaviors across social ties (34, 58).

In contrast, complex contagion occurs in scenarios where adoption is not merely a result of dyadic interactions but also involves group dynamics and the reinforcement from multiple sources within the network. This type of contagion often requires a critical mass or threshold of adopters within an individual's social network to trigger the adoption of the idea, behavior, or innovation (29, 30). Granovetter's work on threshold models of collective behavior further illuminates this concept by exploring how individual thresholds for action or adoption depend on the proportion of others adopting the behavior, highlighting the nonlinear nature of social influence and the importance of group interaction in complex contagion processes (72).

The multiple exposure necessary that characterizes complex contagion can be understood in two ways: (i) as a reinforcement of the idea or behavior from multiple pairwise (dyadic) interactions (29, 30), or (ii) as a reinforcement from multiple sources in a group interaction (higher-order interactions) (8, 15, 87). In the first case, the peer pressure, characteristic of complex contagion processes, is included into the model, which is designed to be used a simple network of dyadic social contacts. In the second case, the group interaction is included in the higher-order network, which is a more general representation of the social contacts, where the interactions are not restricted to dyads (8). See Fig. 2.1 for a graphical representation of the different types of social interactions.

Moreover, real-world processes are influenced not solely by either simple or complex contagion mechanisms but by a complex interaction between the two (Hybrid contagion). Such multifaceted interactions give rise to varied outcomes, including phenomena like criticality, tricriticality, and echo chambers (48, 107), all of which profoundly affect how information is spread, how behaviors are adopted, and how collective actions are formed.

There have been attempt to extract the simple/complex nature of a process from real data. For example, by analyzing the correlation between the infection order of network nodes and their local topology, it is possible to infer the type of contagion process that is taking place (28). This approach relies on observing a single instance of spreading to classify the contagion as simple, threshold-driven, or influenced by higher-order interactions, without requiring extensive data or knowledge of the network's global structure. Nevertheless, the classification of contagion processes remains a challenging task, as the dynamics of social contagion are influenced by a multitude of factors and high-quality data related to the infection process is often scarce.

2.3 Granovetter-Watts threshold model

In this thesis, we focus on the dynamics of complex contagion driven by multiple interactions in a network of dyadic social contacts (no higher-order interactions). In particular, we focus on a particular category of complex contagion models called **threshold models**.

Threshold models represent a critical conceptual framework in understanding how individual behaviors aggregate to produce collective outcomes, especially in contexts where decisions are influenced by the actions of others (72, 74). By defining a "threshold" — the point at which an individual's perception of the collective behavior of others prompts them to act — these models offer insights into the pivotal role of social influence and network structure in driving large-scale changes from small initial actions (50). Rooted in the interdisciplinary nexus of sociology, economics, and network theory, these models illuminate the mechanics behind phenomena as diverse as social movements, technological adoption, market dynamics, and even cascading failures within infrastructures. All these phenomena share a common thread: the need for a critical mass of adopters or actors to trigger a collective response, a threshold that must be crossed to initiate a cascade of actions or behaviors (29, 30).

When we talk about threshold models, the model that comes to our minds is the threshold mdoel introduced by Mark Granovetter in 1978 (72), highlighting how individuals' actions are influenced by the number of others participating in a behavior. In this model, each individual has a threshold that determines the number of neighbors they need to observe adopting a behavior before they themselves adopt it. This threshold can be interpreted as a measure of an individual's susceptibility to social influence, capturing the idea that some people are more likely to adopt a behavior if they see many others doing the same, while others may require more convincing or reinforcement before they act. Duncan J. Watts in 2002 (167) built upon Granovetter's concept, applying mathematical analysis to explore the model within complex networks. His work, particularly on how minor initial actions can lead to large cascades, further elucidated the relationship between individual thresholds and network structures. This model,

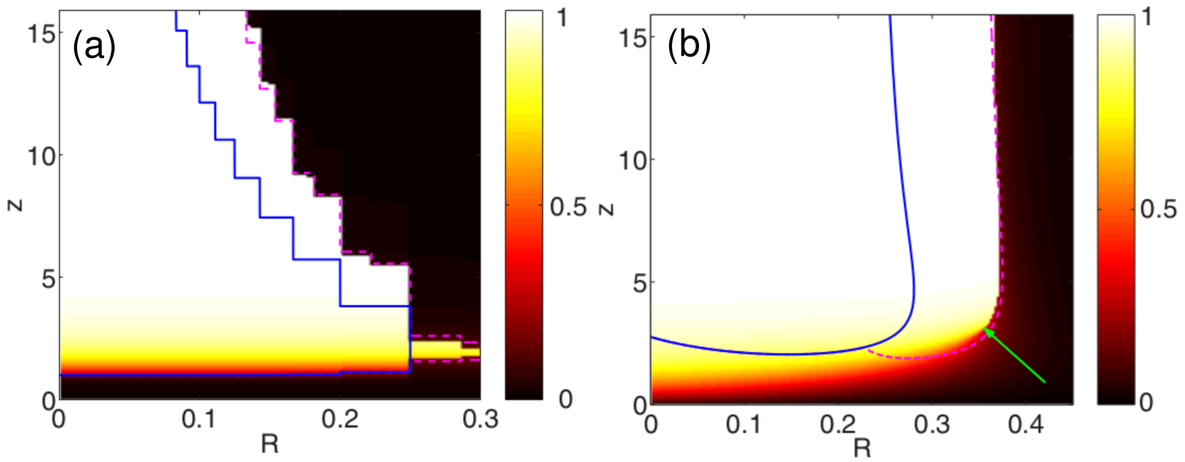

Figure 2.2: Average density n of active nodes in a Poisson random graph of mean degree z and uniform threshold value R **(a)** and threshold distributed is Gaussian with mean R and standard deviation 0.2 **(b)** (from Ref. (67)). Seed fraction is set $n_0 = 0.01$. Lines show approximations to the global cascade boundaries. The phase transition is discontinuous.

known as the Granovetter-Watts threshold model, has since become a cornerstone of research on social contagion and collective behavior, offering a powerful lens through which to study the dynamics of complex contagion in social networks.

Update rules — Granovetter-Watts model. An individual time step of the model is defined as follows:

1. Each node i has a threshold R_i.
2. At each time step, a node i is selected at random.
3. If the fraction of active neighbors of i is greater than R_i, then i becomes active.

The Granovetter-Watts model exhibits a phase transition from a regime where the adoption is rare, where there are only small cascades and none of them is global, to a regime where the adoption is widespread, where there are large cascades that reach all the system. This phase transition is discontinuous (67, 167), and it is characterized by a critical threshold value R_c that separates the two regimes (refer to Fig. 2.2). In the regime where the global cascades are rare, the system is in a supercritical state $R > R_c$, and the cascades are small and localized. In the regime where all the system reaches adoption, the system is in a subcritical state $R > R_c$, and the cascades are fast and global. The phase transition is driven by the interplay between the individual thresholds (homogeneous or heterogeneous) and the network structure, and it is a result of the collective dynamics of the system.

The exploration of this model has been widespread, encompassing studies on various types of networks including regular lattices and small-world networks (30), as well as on random graphs (67). It has also been examined within the contexts of networks with modular and community structures (64), networks that exhibit clustering (80, 81), hypergraphs (8), and networks characterized by homophily (48), among others. In addition, the literature has expanded to cover the effects of varying the rules for adoption, such as incorporating social reinforcement across multiple layers (32), examining the influence of opinion leaders and initial seed size on the process (103, 148), the introduction of on-off thresholds (49), and analyzing the dynamics when simple contagions compete with complex ones (40, 48, 107). Further, empirical data have been used to test the predictions of the Granovetter-Watts model, demonstrating its applicability across a wide range of real-world situations (29, 76, 94, 96, 97, 111, 135, 160).

2.4 The Sakoda-Schelling model

- Thomas C. Schelling (1975) proposed a model to study the dynamics of segregation based on the idea that individuals have a threshold that needs to be reached in order to move to a different location.

- This model become very popular because it was able to reproduce the segregation patterns that are observed in many cities, just as an emergent phenomena from individual decisions.

- On the other hand, this model was already studied by Sakoda in 1971, in a paper that was published in Japanese, and that was not known by the scientific community. In this work, the author proposed a model to study the dynamics of segregation based on the idea that individuals have a threshold that needs to be reached in order to move to a different location.

Update rules — Sakoda-Schelling model. An individual time step of the model is defined as follows:

1. Each node i has a tolerance threshold T_i.
2. At each time step, a node i is selected at random.
3. If the fraction of different kind neighbors of i is greater than T_i, then i moves to a location where the fraction of different kind neighbors is less than T_i.
   - If there is no available location, then i remains in the same location.

- Schelling model is a particular case of the Sakoda model.

- This model exhibits a phase transition from a regime where the segregation is low to a regime where the segregation is high. This phase transition is discontinuous.

Thomas Schelling introduced a simple segregation model (82, 141, 142, 143) in which agents of two colors are distributed randomly on a chess-board, leaving some locations free. Agents are unsatisfied if more than a half of the eight nearest neighbors have different color. Randomly, the unsatisfied agents will move to available satisfying locations of the neighborhood. This model has had a very significant impact for several reasons: The "hand-made" simulations performed by T. Schelling by moving pawns on a chessboard are an early precedent of the use of agent-based simulations in Social Sciences. It is also one of the first social models to show emergent behavior as a result of simple interactions among agents, a characteristic of complex systems.

- Despite the many variants of the model that have been proposed, the phase transition emergent in this model is very robust.

In particular, the Sakoda-Schelling model has been studied from a Statistical Physics point of view due to its close relation to different forms of Kinetic Ising-like models (155, 156), and also addressing general questions of clustering and domain growth phenomena, as well as for the existence of phase transitions from segregated to non-segregated phases. For example, the relation with phase separation in binary mixtures has been considered (41, 165), as well as the connection with the phase diagram of spin-1 Hamiltonians (19, 60, 61, 140). In this context a useful classification of models is to distinguish between two possible types of dynamics (41): "constrained", where agents just move to satisfying vacancies (if possible), and "unconstrained", where agents' motion does not prevent them to remain unsatisfied. In addition, the motion can be short-range (only to neighboring sites, as in the original model) or long-range. Constrained motion has been named "solid-like" because it generally leads to frozen small clusters, while unconstrained motion has been considered "liquid-like" because it allows for large growing clusters (165). Including the motion of satisfied agents leads to a noisy effect playing the role of temperature in a statistical physics approach.

2.5 Bursty Human Dynamics

- All models previously described are based in an important assumption regarding to its dynamics: the interactions between individuals occur at a constant rate.

- This constant rate assumption is assuming that the stochastic interactions follow a Poisson process.

- However, from the analysis of many datasets of human interactions, it has been observed that the interactions between individuals are not constant, but bursty.

- The bursty behaviour is characterized by power law interevent time distributions, and it is present in many human activities, such as e-mail communication, face-to-face interactions, and phone calls.

- The modeling of bursty human dynamics is important because it allows us to understand how the bursty behaviour of human interactions affects the dynamics of social systems.

- Previous literature has several approaches to model bursty human dynamics: temporal networks, activity-driven models, aging . . .

2.6 Aging mechanism

- The aging mechanism is a mechanism that has been proposed to model the bursty behaviour of human interactions.

- Aging mechanism is based on the idea that the probability of an individual to interact with another individual decreases with the time since the last interaction.

- Attachment to previous beliefs or habits is a common feature in human behavior. Granovetter (1973) discussed

- Instead of the constant rate assumption, the aging mechanism assumes that the interactions between individuals occur at a rate that decreases with the time since the last interaction.

- The focus on this approach is to include the bursty dynamics in the individuals attempts to interact with others, rather than in the interactions themselves (as in the activity-driven models or temporal networks).

It is known that human interactions do not occur at a constant rate. They rather show a bursty character with a non-Poissonian inter-event time distribution that reflects a memory from past interactions. (11, 88, 99, 119, 137, 174) However, most social simulations, including simulations of variants of the Sakoda-Schelling model, implicitly assume a constant rate of interactions or state updating. "Aging" is one form of memory effect on which the rate of interactions depends on the persistence time of an agent in a state, modifying the transition to a different state (20, 53, 130). This concept of aging, or "social inertia" (151), constrains the transitions in a way that the longer an agent remains in a given state, the smaller the probability to change it. Aging has been already shown to modify social dynamics very significantly. For example, in opinion dynamics, aging is able to produce coarsening towards a consensus state in the voter model (53, 128) or to induce a continuous phase transition in the noisy voter model (10).

Aging is an important non-Markovian effect that we address in this chapter for binary-state models. Aging accounts for the influence that the persistence time of an agent in a given state modifies the transition rate to a different state (20, 31, 53, 130, 152), so that, the longer an agent remains in a given state, the smaller is the probability to change it.

Aging effects have been already shown to modify binary-state dynamics very significantly. For example, aging is able to produce coarsening towards a consensus state in the Voter model (53, 127), to induce continuous phase transitions in the noisy Voter model (10, 126).

2.7 Aging in Simple Contagion Models

- Aging in the Voter model has been studied by many authors, and it has been shown that the aging mechanism affects the dynamics of the model.

- The aging mechanism has been shown to affect the dynamics of the Voter model, and to change the phase transition of the model.

- Aging in the noisy voter model is able to change the phase transition of the model, and to make the phase transition continuous.

- Aging in the SI model is able to change the cascade size distribution of the model, and to make the cascade size distribution follow a power law (see the work of Karsai et al. 2011).

I Aging in threshold models

3. Aging effects in the Sakoda-Schelling segregation model

The results in this chapter are published as:

David Abella, Maxi San Miguel, and José J. Ramasco. "Aging effects in Schelling segregation model". In: *Scientific Reports* 12.1 (Nov. 2022). ISSN: 2045-2322. DOI: 10.1038/s41598-022-23224-7. URL: http://dx.doi.org/10.1038/s41598-022-23224-7

We incorporate aging into the Sakoda-Schelling model by making the probability of agents to move inversely proportional to the time they have been satisfied in their present location. This mechanism simulates the development of an emotional attachment to a location where an agent has been satisfied for a while. The introduction of aging has several major impacts on the model statics and dynamics: the phase transition between a segregated and a mixed phase of the original model disappears, and we observe segregated states with a high level of agent satisfaction even for high values of tolerance. In addition, the new segregated phase is dynamically characterized by a slow power-law coarsening process similar to a glassy-like dynamics.

3.1 Introduction

As it was introduced in section 2.4, a robust result of the Sakoda-Schelling model is that segregation occurs even when individuals have a very mild preference for neighbors of their own type, so collective behavior is not to be understood in terms of individual intentions. In addition, the model introduced the concept of behavioral threshold that inspired a number of other models of collective social behavior (71). But still currently, Schelling's model is at the basis of fundamental studies of the micro-macro paradigm in Social Sciences (75), while it continues to have important implications for social and economic policies addressing the urban segregation problem (36, 37, 100, 139). A main limitation of the Sakoda-Schelling model is that it has no history or memory by which, for example, residents might prefer to maintain their present location (146).

As a result of the notable implications of this model and the robustness of the emerging segregation, there exists a vast literature around Schelling's results. Many variants of the original Sakoda-Schelling model have been reported modifying the rules that govern the dynamics, the satisfaction condition, or including other mechanisms, network effects, or specific applications (5, 6, 13, 41, 51, 60, 61, 70, 83, 84, 92, 101, 120, 121, 134, 144, 155, 156, 164, 165).

With the motivation of established relevant effects of aging in the previous chapter, our goal is to characterize how "aging" modifies the segregation dynamics of the Sakoda-Schelling model. In this context, aging must be understood as an emotional/economic attachment to a certain location linked to the persistence time in this location. This attachment balances the memory-less and purely rational considerations of the original model (73). The aging-induced inertia, which results in resistance to movement, is minimalist modeling of behavior with many different possible causes. Besides the moving out cost due to the housing market fluctuations, aging accounts for the links established with the neighborhood's public goods, venues, schools, etc, which are known to be highly relevant in this context (33, 146, 166). These urban elements are also a major consideration when households locate (35, 38, 42, 147) and aging also accounts for the memory of this decision.

In this chapter, aging is introduced in the Sakoda-Schelling model by considering that agents are less prone to change their location as they get older in a satisfying place. In other words, aging is introduced giving a smaller probability for satisfied agents to "move-out" the longer they have remained in a satisfying neighborhood. We implement this aging mechanism in the long-range noisy constrained version of the Schelling Model (60), for which a detailed phase diagram was reported. We study how this phase diagram is modified by the aging mechanism, finding that aging inhibits a segregated-mixed phase transition. This implies that aging favors segregation, a counter-intuitive result. We also describe the coarsening dynamics in the segregated phase showing that aging gives rise to a slower coarsening that breaks the time-translational invariance.

3.2 Aging in the Sakoda-Schelling model

The model considered here is a variant of the noisy constrained Sakoda-Schelling model (60) in which we explicitly include aging effects. For simplicity, we refer to this variant as the Sakoda-Schelling model during the rest of the paper to compare with the model presented here: the Sakoda-Schelling model with aging. For both, the system is established on a $L \times L$ Moore lattice with 8 neighbors per site and periodic boundary conditions, where agents of two kinds (representing, for instance, wealth levels, race, language, etc) occupy the sites. There are also empty sites (vacancies), where agents can move to, depending on their state and on the vacancy neighborhood. The condition of each site i of the lattice will be described with a variable σ_i that takes three possible values: $\sigma_i = \pm 1$ for the two kinds of agents and $\sigma_i = 0$ for vacancies. In addition, depending on the local environment, agents can be in two states: satisfied or unsatisfied. In our case, agents are satisfied if their neighborhood is constituted by a fraction of unlike agents lower than a fixed homogeneous threshold T. Otherwise, they are unsatisfied. Therefore, this control parameter T is a measure of how tolerant the population of the system is. We also need a non-zero vacancy density, $n_0 > 0$, for agents to change their location. This n_0 is understood as an extra parameter of the model. The initial configuration is built by randomly distributing the agents ($N_{\text{agents}} = L^2(1 - n_0)$). We always consider initially one half of agents of each kind.

In the Sakoda-Schelling model considered in this study, an agent chosen by chance moves to a random satisfying vacancy (if any exists) independently of his/her initial state and of the distance. This process is repeated until the system reaches a stationary state. The movement of unsatisfied agents behaves as a driver for the system dynamics, while the motion of satisfied agents plays the role of noise. When tolerance T becomes larger, more satisfying vacancies are present in the system and the noise consequently increases.

The aging mechanism in our model is introduced by considering an activation probability of the agents inversely proportional to the time spent at a satisfied location, motivated by the definition for opinion dynamics (10). This methodology was proposed to mimic the power-law like inter-event time distributions observed in real-world social systems (11, 53). If an agent j is initially satisfied in her neighborhood, the internal time is set $\tau_j = 0$. Then, in every time step, a randomly chosen agent j follows different rules depending on whether she is originally satisfied or not. If unsatisfied, j moves to any random satisfying vacancy of the system. If satisfied, she moves to another satisfying vacancy with an activation probability $p_j = 1/(\tau_j + 2)$. In both cases, if no vacancy has a satisfying neighborhood, the agent j remains in the initial site. As before, these rules are iterated until the system reaches a stationary state (if possible). The time is counted in Monte-Carlo steps; after each Monte-Carlo step, that is after N_{agents} iterations, the internal time increases for all satisfied agents in one unit, $\tau_j \to \tau_j + 1$. Notice that, when an unsatisfied agent becomes satisfied due to the neighbor's motion, an internal time $\tau_j = 0$ is set for that agent. As for the Sakoda-Schelling model, there is a noise effect associated with the motion of satisfied agents. In this case, the intensity of this noise is related not only to the tolerance parameter T, but to the presence of aging as well. In fact, aging introduces more constraints to the movements and contributes to decreasing the noise.

Given the number of neighbors available in the Moore lattice, numerical simulations are only performed for a finite set of meaningful tolerance values: $\{1/8, 1/7, 1/6, \cdots, 6/7, 7/8\}$. During all our analysis, we focus on the low vacancy density region of the phase diagram.

3.3 Segregation coefficient

Many metrics have been introduced in the literature to discern if the final state is segregated or not (60, 101, 150, 171). The number of clusters is known to be directly related to the segregation because a high presence of small clusters indicates a mixing between agents. As for the Sakoda-Schelling model(60), we compute the following metric related to the second moment of the cluster size distribution:

$$s = \frac{2}{(L^2(1-n_0))^2} \sum_{\{c\}} m_c^2, \tag{3.1}$$

where the index of the sum c runs over all the clusters $\{c\}$ and m_c is the number of agents in the cluster c. The average of s over realizations after reaching a stationary state is defined as the segregation coefficient $\langle s \rangle$. This metric is bounded between 0 and 1: $\langle s \rangle \to 1$ if there are only 2 equally-sized clusters, and $\langle s \rangle \to 0$ if the number of clusters tends to the number of agents. The cluster detection is performed using the Hoshen-Kopelman algorithm (85).

Another metric of segregation is the interface density (41), defined as the fraction of links connecting agents of different kinds. The calculation is done in two steps: estimating the interface density for each agent j, ρ_j, and then the average over all the agents ρ:

$$\rho_j = \frac{1}{2}\left(1 - \frac{\sigma_j \sum_{k\in\Omega_j} \sigma_k}{\sum_{k\in\Omega_j} \sigma_k^2}\right) \quad \text{and} \quad \rho = \frac{1}{\mathrm{N_{agents}}} \sum_{\mathrm{j=1}}^{\mathrm{N_{agents}}} \rho_{\mathrm{j}}, \tag{3.2}$$

where the indices k run over the neighborhood of agent j, Ω_j. If an agent j is surrounded only by vacant sites, we define by convention $\rho_j = 0$. Performing a realization average of ρ, we obtain the average interface density $\langle \rho \rangle$ in the stationary state is denoted as $\langle \rho_{\mathrm{st}} \rangle$. The time evolution of this metric, not present in literature, allows us to study the coarsening process.

3.4 Results

3.4.1 Phase diagram

To discuss the phase diagram of our model, we focus on the region of parameters with a vacancy density $n_0 < 50\%$ to avoid diluted states with a majority of vacancies. For this region, the Sakoda-Schelling model presents 3 different phases (60): frozen, segregated and mixed. For low tolerance values, the system freezes in a disordered state, given that there are no satisfying vacancies for any kind of agent. With increasing tolerance, the system undergoes a transition toward a segregated state, which is characterized by a 2-clusters dynamical final state. Finally, for high values of T, after another transition, we find a dynamical disordered (mixed) state, in which a vast majority of vacancies are satisfying for both kinds of agents, and small clusters are continuously created and annihilated.

These three phases are characterized by measuring the segregation coefficient $\langle s \rangle$ and the average interface density $\langle \rho_{\mathrm{st}} \rangle$ at the final state. The results for the original model are depicted as a function of the tolerance T in Fig. 3.1a for the interface density and in Fig. 3.1b for the segregation coefficient. At low values of T, both indicators show a disordered state that falls in the

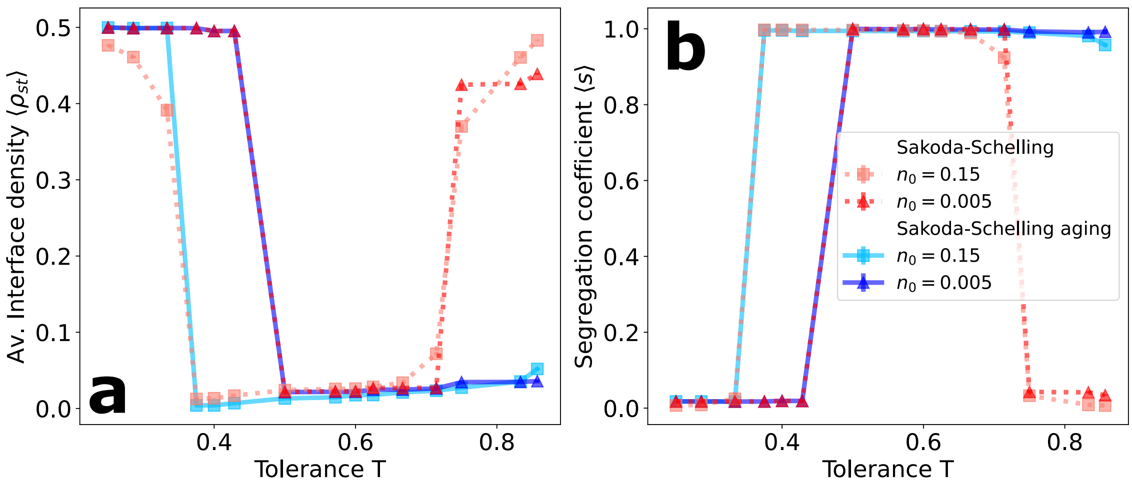

Figure 3.1: Average interface density $\langle \rho_{\rm st} \rangle$ (**a**) and segregation coefficient $\langle s \rangle$ (**b**) at the stationary regime as a function of the tolerance parameter T for two values of the vacancy density $n_0 = 0.5\%$ and 15%. Results are shown for both the Sakoda-Schelling model and the variant with aging introduced in this paper. Simulations are performed on an 80×80 lattice and averaged over $5 \cdot 10^4$ realizations.

frozen phase. We also observe a dependence of the transition point with the vacancy density. On the other hand, for high T values, the transition point between segregated and mixed states has no dependence on the parameter n_0. Notice that mixed and frozen states present a very similar value of $\langle s \rangle$ but can be differentiated by the stationary value of the average interface density $\langle \rho_{\rm st} \rangle$. These results are in agreement with the results reported for the Sakoda-Schelling model(60), with the extra information provided by the average interface density.

The first quite dramatic effect of including aging in the system is the disappearance of the mixed state from the phase diagram. In both metrics, the difference between the models with and without aging is clearly manifested. For low T values, the frozen-segregated transition behaves similarly to the original model since aging has no implications as the system gets quickly frozen. Nevertheless, for high values of the tolerance $T > 0.5$, the segregated-mixed transition disappears, and the segregated phase is always present. This is not an intuitive effect and one would think that aging, contributing to difficult agent's mobility, should prevent the system from forming fully developed segregated clusters. However, it is just the opposite, and it favors cluster prevalence.

3.4.2 Segregated phase: final state

To gain further insights into the differences in the system dynamics that lead to the extended segregated phase, we compute the fraction of unsatisfied agents at the stationary regime n_u (see Fig. 3.2a). This metric plays a role as a marker for the frozen-segregated transition, as shown for the 1D Sakoda-Schelling model (41). The frozen phase presents a big majority of unsatisfied agents for both models. After the transition, this parameter decays to very low values in the segregated phase, where a majority of agents are satisfied. In this phase, we observe a step-like increasing behavior of the unsatisfied agents with T. As the tolerance grows, the number of satisfying vacancies increases and the noisy movement of satisfied agents drives the system evolution, creating eventual unsatisfied agents in the sites that they abandon or target. However, in the Sakoda-Schelling model, the transition to a mixed state at $T = 0.75$ inhibits the creation of clear fronts between agents of different kinds, and it is also associated to a sharp increase of $n_u \simeq 0.05$ (red squares in Fig. 3.2a). The Sakoda-Schelling model with aging, on the other hand, shows a lower fraction of unsatisfied agents during all values of the tolerance above the

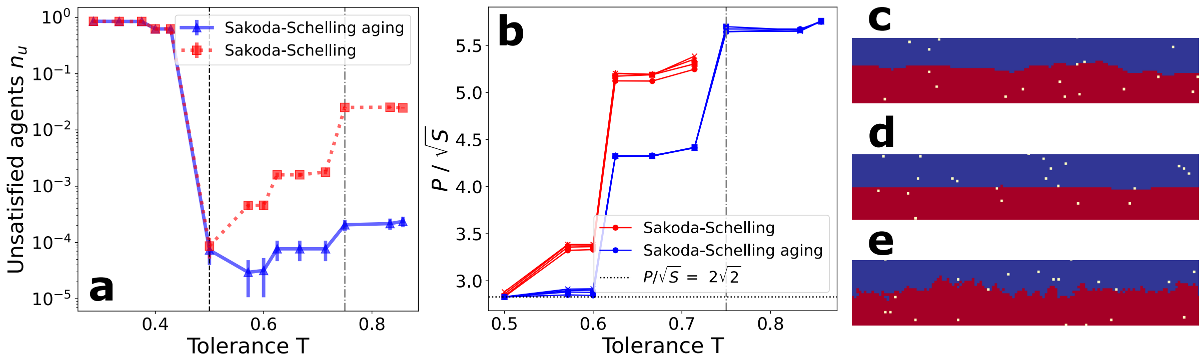

Figure 3.2: (**a**) Fraction of unsatisfied agents n_u at the stationary regime as a function of the tolerance parameter T. (**b**) Measure of the interface roughness between clusters of different kind of agents at the final stationary state $P/\sqrt{S}$ as a function of the tolerance parameter T. Different markers indicate different system sizes: $L = 40$ (circles), 60 (squares), 80 (triangles) and 100 (crosses). Results are shown for both the Sakoda-Schelling model with and without aging. Numerical simulations are performed for $n_0 = 0.5\%$ and averaged over $5 \cdot 10^4$ realizations. The frozen-segregated transition (dashed black line) and the segregated-mixed transition (gray dot-dashed line) are highlighted to differentiate the phases that the Sakoda-Schelling model exhibits. There are no values of $P/\sqrt{S}$ for the Sakoda-Schelling model above $T = 3/4$ because the segregated-mixed transition occurs. (**c**) Final state interface zoom snapshot for $T = 0.57$ using the original model. (**d**) Final state interface zoom snapshot for $T = 0.57$ using the model with aging. (**e**) Same as c for $T = 0.86$.

frozen-segregated transition (blue triangles in Fig. 3.2a). So much so, that many realizations reach $n_u = 0$ and this causes the large error bars in Fig. 3.2a after the transition. In a counterintuitive way, the introduction of aging causes a higher global satisfaction when compared with the original model in both the segregated and the mixed phases.

The creation of new unsatisfied agents at the final stationary state occurs at the interface, where different kind agents meet. This is why we study the interface roughness (perimeter) P as a function of the tolerance parameter. To compute this measure, we compute the number of agents of one kind in contact with different kind agents. To perform this calculation, we smooth the interface by considering vacancies surrounded by a majority of agents of a certain kind as members of that kind. In our system of $L \times L$ with periodic boundary, the minimum interface size (perimeter) P between clusters of agents of different kind is $P = 2L$. To avoid the L dependency, we calculate an adimensional magnitude $P/\sqrt{S}$, where S is the number of agents of each kind $S = N_{\text{agents}}/2 = L^2(1 - n_0)/2$ (surface). This metric $P/\sqrt{S}$ is computed starting from a flat interface as an initial condition and evolving it for $t_{\max} = 10^4$ MC steps to reach well within the stationary state. With the metric $P/\sqrt{S}$, we are able to estimate how close is the final state interface of our system to the flat interface ($P/\sqrt{S} = 2\sqrt{2}$). The results show an increasing dependence of roughness with the tolerance parameter T (see Fig. 3.2b). This growth can be explained as an increase in tolerance means that agents are satisfied with fewer "same-kind" neighbors. Therefore, the interface is able to be rougher, keeping the agents in a satisfied state. In addition, notice that all values with different L collapse, so the dependence on the system size has been eliminated.

Comparing both models, one observes a lower interface roughness for the Sakoda-Schelling model with aging, regardless of the value of T. The closest value to the flat interface occurs for the first values of T after the frozen-segregated phase transition (shown in Fig. 3.2d). In the original model, we observe higher values of $P/\sqrt{S}$ due to the noise produced by the satisfied agents' behavior (see Fig. 3.2c). Moreover, aging allows us to obtain a segregated phase with even larger interface roughness than the maximum observed in the original model for large values of T (see Fig. 3.2e). We remark that, when aging is introduced, agents try to join those of their own kind but are less and less prone to change location as time passes. Thus, in the

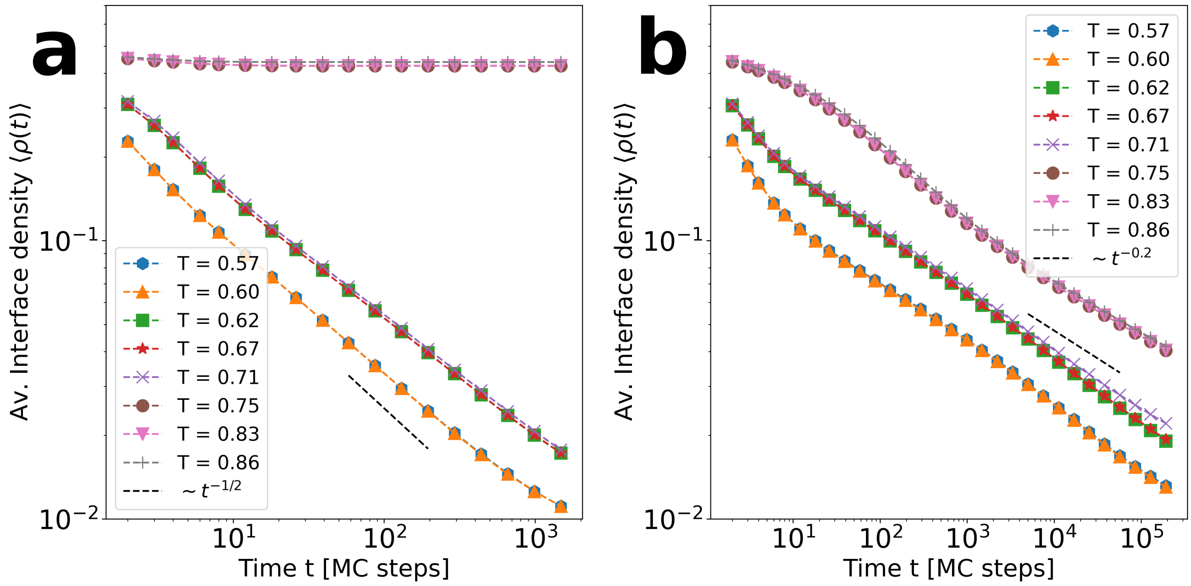

Figure 3.3: Average interface density $\langle\rho(t)\rangle$ as a function of time steps for different values of the tolerance parameter T using the Sakoda-Schelling model (**a**) and the version with aging (**b**). Average performed over $5 \cdot 10^3$ realizations. Fitted power-law in a black dashed line highlighting the estimated exponent value. We set system size $L = 200$ and $n_0 = 0.005$.

Sakoda-Schelling model with aging, agents in the bulk of the clusters mainly do not move and those moving more often are located at the interface between agent kinds. At medium and large scales, this phenomenon leads to ergodicity breaking in the final state dynamics.

3.4.3 Segregated phase: coarsening dynamics

Diverse versions of the original Schelling Model exhibit different behaviors in terms of coarsening dynamics. Recent publications report a power-law like domain growth (6, 41). We monitor here the evolution of the interface density $\langle\rho(t)\rangle$, which, in the segregated phase, decreases as $\langle\rho(t)\rangle \sim t^{-\alpha}$ so the domains should grow in our model following a power-law with time.

The coarsening process of the Sakoda-Schelling model at the segregated phase ($0.5 \leq T < 0.75$) is displayed in Fig. 3.3a and Fig. 3.4. We find that the average interface density follows a power-law decay with an exponent $\alpha \simeq 0.5$ for the limit of small vacancy density $n_0 \to 0$, in agreement with the value reported for close variants of the Sakoda-Schelling model (41). This exponent value is curious since the coarsening in the presence of a conserved quantity (but with local interactions) exhibits an exponent $\alpha = 1/3$ (77). Nevertheless, the interactions in this model are not local, and the coarsening exponent is more similar to the one in systems with a non-conserved order-parameter ($\alpha = 1/2$). Fig. 3.3a shows as well how coarsening changes with the tolerance parameter. Even though the exponent α does not depend on T, we observe a certain delay when increasing T from 0.6 to 0.62. In the system evolution of Fig. 3.4, one can see how the behavior of the satisfied agents for higher tolerance values is translated into rougher interfaces, causing such delay. For $T > 0.75$, the system exhibits a transition towards a mixed state where the interface density fluctuates around $\rho = 0.5$, indicating that the state is constantly disordered.

The Sakoda-Schelling model with aging shows very different behavior (Fig. 3.3b). As expected, the average interface density exhibits a power-law decay with time for all values of the tolerance T after the frozen-segregated transition. Still, the decay is slower than for the Sakoda-Schelling model, with $\langle\rho(t)\rangle \sim t^{-0.2}$. A mechanism that could be behind this behavior is that the model with aging counts more satisfied agents than the original model, and their probability to move

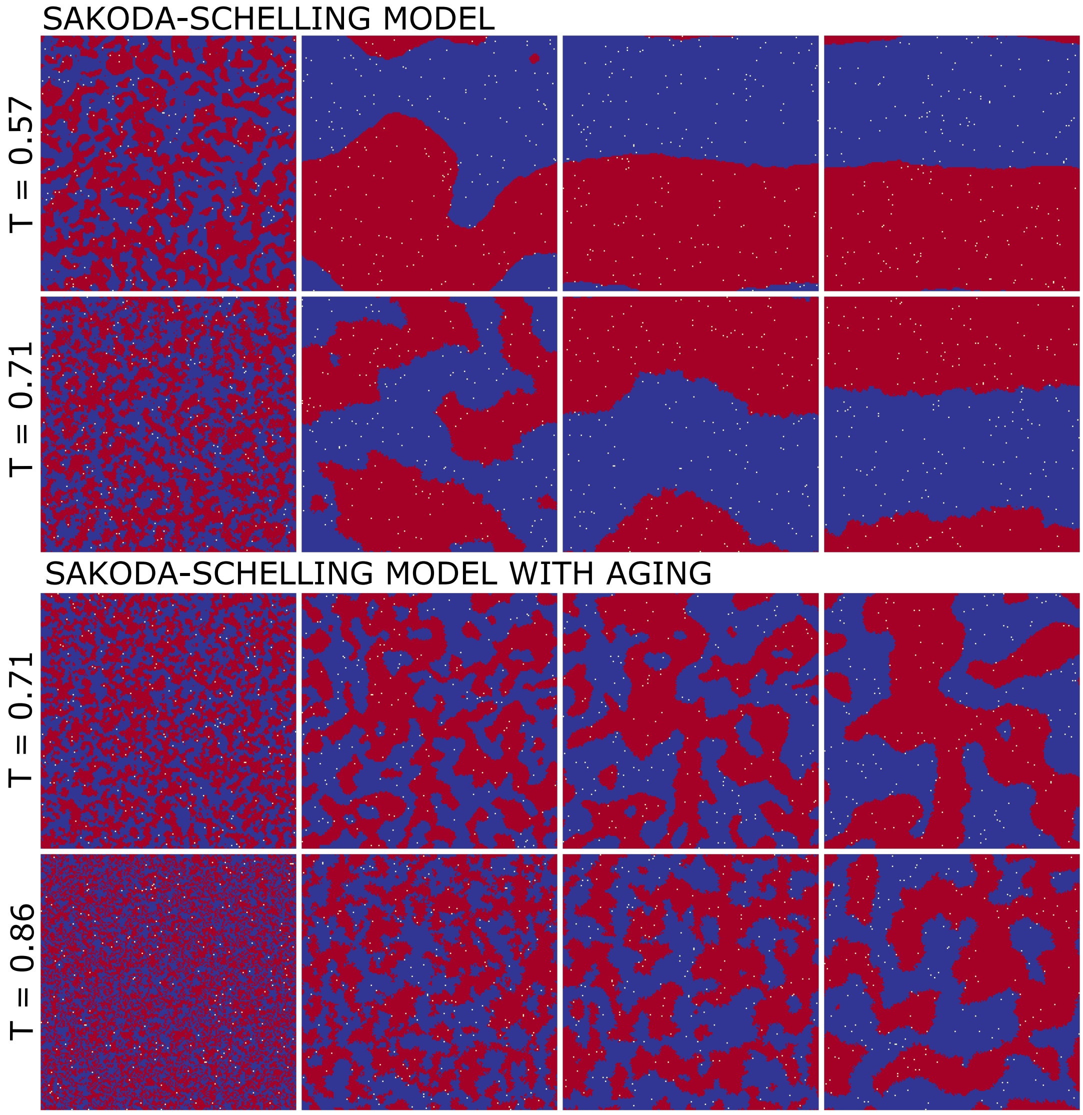

Figure 3.4: Coarsening towards the segregated state at two different values of T for both models. Snapshots are taken for 5, 500, 5000 and 50000 time steps ordered from left to right. We set system size $L = 200$ and $n_0 = 0.005$.

becomes lower as time goes by. Moreover, satisfied agents inside a cluster will not move and the dynamics of the model take place at the interface. It is, therefore, more difficult for separated clusters to collide and merge, an effect that slows down the decay of the interface density. The persistence of small clusters becomes clear when the snapshots' evolution is compared for both models at the same tolerance value $T = 0.71$ (see Fig. 3.4). Moreover, while for the original model the initial clustering for $t = 500$ steps does not determine the final state, in the case of aging the bigger clusters present at the beginning of the evolution are the ones that keep growing, determining the shape of the system configuration after 50000 time steps. This is a dynamical effect, because the system in both cases tends to a final configuration with 2-clusters.

In the case of the Sakoda-Schelling model with aging, we observe an early cross-over in the dynamics (Fig. 3.3b). For $T < 0.75$, the coarsening starts with an initial decay of $\langle \rho(t) \rangle$ faster than $t^{-0.2}$. This occurs because in this regime it is necessary sometimes for the aging effects to become relevant, and initially the system behaves as in the original model. Similarly, for $T \geq 0.75$, $\langle \rho(t) \rangle$ decays slowly for a moment before reaching the power-law behavior for large t values. Confirming this scenario, Fig. 3.4 shows that for $T = 0.86$, the system starts evolving similarly to a mixed state until some clusters are created. At this moment, aging prevents the clusters' desegregation, leading the system very slowly to coarsening dynamics and, eventually, to a fully segregated state.

Regarding the relaxation time to the final state, we see in Fig. 3.4 how for $T = 0.71$, the stationary state of the Sakoda-Schelling model is reached after approximately $t = 5000$ time steps. In contrast, the version with aging needs much more than 50000 steps to attain it. This highlights the important temporal difference between both models in terms of domain growth dynamics, which strongly increases the computational cost of the study of the stationary state of the model with aging. We have been thus able to study only medium and small system sizes in this final regime.

The dynamics studied thus far are performed considering the limit $n_0 \to 0$, but the analysis can be extended to higher vacancy densities. For the particular case of high n_0 and low T, aging leads to the formation of a vacancy cluster at the interface between domains (see details in Appendix A).

3.4.4 Aging breaks the asymptotic time-translational invariance

Here, we explore further time translational invariance (TTI) in the model dynamics. For this, we start by defining the two-time autocorrelation function $C(\tau, t_\mathrm{w})$ (172) as

$$C(\tau, t_\mathrm{w}) = \left\langle \frac{1}{M} \sum_{i=1}^{N} \sigma_i(t_\mathrm{w} + \tau)\, \sigma_i(t_\mathrm{w}) \right\rangle, \tag{3.3}$$

where N is the system size, $\langle \cdot \rangle$ refers to averages over realizations, t_w is the waiting time to start the autocorrelation measurements, τ a time interval after t_w and M is a normalization factor defined as

$$M = \sum_{i=1}^{N} (\sigma_i(t_\mathrm{w} + \tau)\, \sigma_i(t_\mathrm{w}))^2. \tag{3.4}$$

which is computed at each realization.

The autocorrelation function is displayed for the Sakoda-Schelling model with $T = 0.75$ in Fig. 3.5a. We observe the curves decreasing with τ as expected, and that after a characteristic time period ($t_\mathrm{w}^* \approx 5000$ for a system size of 80×80) they collapse into a single curve. This is the regime in which the dynamics becomes TTI, implying that the autocorrelation function does not depend any more on the waiting time, $C(\tau, t_\mathrm{w}) = C(\tau)$ for $t_\mathrm{w} > t_\mathrm{w}^*$.

For the Sakoda-Schelling model with aging, the dynamics show some different features (Figs. 3.5b and 3.5c). First, the autocorrelation functions decay slower with τ in all the cases, which is connected to the long-lived small clusters mentioned previously. We do not find in the simulations any value of t_w^* for the systems to fall into a TTI regime. Not only that, but a scaling relation including both τ and t_w can be applied to collapse the autocorrelation curves (see insets Figs. 3.5b and 3.5c). This behavior is similar to glassy systems (172), therefore it is useful to use the mathematical description for those systems in our case. In this type of dynamics, a final stationary state is not attainable in the thermodynamic limit, and it is possible to decompose the autocorrelation function into an equilibrium part and an "aging" part (aging in the sense of non-equilibrium dynamics in glassy systems) (17, 172):

$$C(\tau, t_\mathrm{w}) \simeq C_\mathrm{eq}(\tau)\, C_\mathrm{aging} u(\tau, t_w) = C_\mathrm{eq}(\tau)\, C_\mathrm{aging} \left(\frac{h(\tau)}{h(t_\mathrm{w})} \right), \tag{3.5}$$

where C_eq describes the fast relaxation of the system components within each domain (TTI term), C_aging is a scaling function and $u(\tau, t_w)$ is a normalization factor which, in some cases, can be written as the quotient of an unknown function $h(t)$ at the two times τ and t_w. This function $h(t)$ is known to be related to the dynamical correlation length (17, 57). In our case, we use $h(t) = t$ to scale the results in Fig. 3.5b (see inset). This scaling is valid for values of $T \in [0.5, 0.75)$. Nevertheless, higher values of T do not hold a linear scaling, and we need to turn to other functional forms

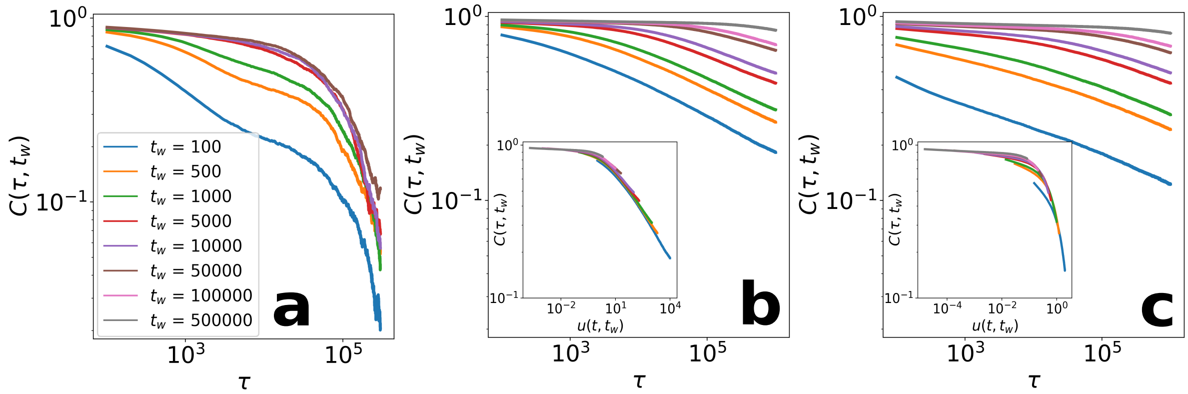

Figure 3.5: Two-times autocorrelation $C(\tau, t_\mathrm{w})$ as a function of the time period passed since the waiting time t_w. First, the autocorrelation is shown for the Sakoda-Schelling model at $T = 0.71$ in **a**, and for the version with aging at $T = 0.71$ in **b** and $T = 0.86$ in **c**. The insets are the result of the collapse using $u(\tau, t_w) = \tau/t_w$ (**b**) and $u(\tau, t_w) = \log(\tau + t_w)/\log(t_w) - 1$ (**c**). The curves correspond to different values of the waiting time t_w. Calculations performed on a 100×100 lattice averaged over $5 \cdot 10^4$ realizations.

as the normalization factor $u(\tau, t_w) = \log(\tau + t_w)/\log(t_w) - 1$ used in Fig. 3.5c. This indicates that for $T > 0.75$, the dynamical correlation length evolves in a different and slower way.

3.5 Summary and discussion

We have studied the effect of aging on a 3-state threshold model (with two symmetrical states $\sigma_i = \pm 1$), which combines long-range mobility with local short-range interactions. Specifically, taking as basis the noisy constrained Sakoda-Schelling model, we assign to the agents an internal clock counting the time spent in the same satisfying location. The probability of changing state decreases then inversely proportional to this time. Therefore, older satisfied agents are less prone to update resident locations. The original model displays a transition between a segregated phase and a mixed one as the tolerance control parameter T increases. This transition disappears when aging is introduced into the system, the mixed phase is replaced by a segregated phase even for high values of the tolerance parameter T. As a result, the model with aging presents a higher global satisfaction than without this effect for all values of the tolerance.

On the dynamical perspective, the relaxation towards the segregated phase features a coarsening phenomena characterized by a power-law decay of the average interface density with time $\langle \rho \rangle \sim t^{-\alpha}$. For the original model in the limit of low vacancy density, the exponent is around $\alpha = 1/2$. This exponent is also reported in other variants of the Sakoda-Schelling model (6, 41). Aging gives rise to long-lived small clusters and a slower coarsening, reducing the exponent to $\alpha \simeq 0.2$. We investigated the autocorrelation functions in the segregated phase and found that aging breaks the asymptotic time-translational invariance of the dynamics. This result, along with a nontrivial scaling of the autocorrelation functions, establish close similarities with low-coarsening systems, such as glassy systems, and our Sakoda-Schelling model with aging for high values of the tolerance parameter. Moreover, this work studies the case for equal size populations ignores effects arising from the competition between different population sizes. Further work would be to study a joint effect of minority population and aging.

As for the implications of our results from a social perspective, we must note that the fact that aging favors segregation, inhibiting the segregation-mixed phase transition, is rather counter-intuitive, but gives support to the argument that segregation is a stochastically stable state and may prevail in an all-integrationist world (173). Our model predicts the appearance of segregation even for tolerance values close to one. Additionally, the model relaxation time multiplies manifold, which implies that if aging is present the natural state of this system seems to be generically out of equilibrium.

4. Aging in binary state dynamics: The Approximate Master Equation

The results in this chapter are published as:

David Abella, Maxi San Miguel, and José J. Ramasco. "Aging in binary-state models: The Threshold model for complex contagion". In: *Phys. Rev. E* 107 (2 Feb. 2023), page 024101. DOI: 10.1103/PhysRevE.107.024101. URL: https://link.aps.org/doi/10.1103/PhysRevE.107.024101

The Approximate Master Equation (AME) is a general mathematical equation that allows to describe binary state models in complex networks. Here, we extend the traditional mathematical framework to include aging effects, which account for the influence of the persistence time of an agent in a given state on the transition rate to a different state. When aging is considered, the Markovia assumption is no longer valid, and the AME must be modified to include non-Markovian dynamics. We derive the AME for binary-state models with aging effects, including aging and resetting events, and show how it can be reduced to the original Markovian dynamics when the rates are not dependent on the internal time. We also demonstrate how the heterogeneous mean-field approximation can be derived from the master equation. The results presented in this chapter provide a comprehensive framework for studying aging effects in binary-state models, offering a more accurate description of the dynamics of complex networks. In the following chapters of this thesis, we apply this framework to describe the aging implications in two binary-state models: the Granovetter-Watts model and the Symmetrical Threshold model.

4.1 Introduction

Binary-state models are a versatile tool to describe a variety of natural and social phenomena in systems formed by many interacting agents. Each agent is considered to be in one of two possible states: susceptible/infected, adopters/non-adopters, democrat/republican, etc, depending on the context of the model. The interaction among agents is determined by the underlying network and the dynamical rules of the model. There are many examples of binary-state models, including processes of opinion formation (55, 102, 132, 149), disease or social contagion (72, 123), etc. Extended and modified versions of these models can lead to very different dynamical behaviors than in the original model. As examples, the use of multi-layer (7, 46, 47) or time-dependent networks (163), higher-order interactions (8, 27, 87), non-linear collective phenomena (26, 125), noise (23) and non-Markovian (31, 126, 153, 162) effects induce significant changes to the dynamics.

Theoretical and computational studies of stochastic binary-state models usually rely on a Markovian assumption for its dynamics. This implies that events depend only on the present state, i.e., dynamical rules are memoryless. Markovian processes exhibit exponential distributions in the upcoming events times and the number of events in a given time interval follows a Poisson distribution. However, there is strong empirical evidence against this assumption in human interactions. For example, bursty non-Markovian dynamics with heavy-tail inter-event time distributions, reflecting temporal activity patterns, have been reported in many studies (9, 89, 95, 99, 137, 174). The understanding of these non-Markovian effects is in general a topic of current interest (126, 127, 153, 162). In particular, for the threshold models, memory effects have been included as past exposures' memory (50), message-passing algorithms (145), memory distributions for retweeting algorithms (68) and timers (116).

Aging is an important non-Markovian effect that we address in this chapter for binary-state models. We here provide a general theoretical framework to discuss aging effects building upon a general Markovian approach for binary-state models (65, 66). We build an Approximate Master Equation (AME)[1] for any binary-state model with aging effects (including aging and resetting events). We show how the AME can be reduced to the original Markovian dynamics when the rates are not dependent on the age of the agents. We also show how the heterogeneous mean-field approximation can be derived from the master equation. The results presented in this chapter provide a solid foundation for future studies on aging effects in binary-state models, offering a more accurate description of the dynamics of complex networks.

4.2 Derivation of the Approximate Master Equation for binary-state models with aging

We consider binary-state dynamics on static, undirected, connected networks assuming a locally tree-like structure and in the limit of $N \to \infty$, following closely the approach used in Ref. (66) for binary-state dynamics in complex networks. The new ingredient is to consider the nodes with different "age" or "internal time" as different sets, what allows us to treat as Markovian the memory effects introduced by aging (126, 127). We define $x^{\pm}_{k,m,j}(t)$ as the fraction of nodes that are in state ± 1 and have degree k, m infected neighbors and age j at time t. The networks have degree distribution p_k and have been generated by the configuration model (110, 113). For the models considered in this thesis, the initial condition is set such that all agents have age $j = 0$ and there is a randomly chosen fraction x^-_0 of nodes in state -1:

$$\begin{aligned}
&\text{For } j>0 \qquad x^+_{k,m,j}(0) = 0 \qquad && x^-_{k,m,j}(0) = 0, \\
&\text{For } j=0 \qquad x^+_{k,m,0}(0) = (1-x^-_0)\,B_{k,m}[x^-_0] \qquad && x^-_{k,m,0}(0) = x^-_0\,B_{k,m}[x^-_0],
\end{aligned} \tag{4.1}$$

where $B_{k,m}[x^-_0]$ is the binomial distribution with k attempts, m successes and x^-_0 is the initial fraction of agents in state -1 (as the probability of success of the binomial). Now, we examine how $x^+_{k,m,j}$ changes in a time step. We consider 3 possible events:

- An agent changes state from $+1$ to -1 and resets the internal time to $j = 0$, with probability $T^+(k,m,j)$.
- An agent remains at its state and resets its internal time to $j = 0$, with probability $R^+(k,m,j)$.
- An agent remains at its state and ages, with probability $A^+(k,m,j)$.

The probability to change state and to age make sense in the context of aging. The reset probability is introduced to account for "exogenous" aging, in which an external influence forces the node to attempt a change of state but the node remains in its current state. Moreover, notice that we assume all the probabilities to be a function of the degree k, the number of neighbors in state -1 m and the time spent in the actual state (or since a reset) j. Now, taking into account this possible events, we write the possible transitions for the set $x^+_{k,m,j}$, for $j > 0$ (see

[1] We use here the term "master equation" for consistency with Refs. [65, 66], but the word "master" has a different meaning than the one used to describe an equation for the probability distribution [124, 159]

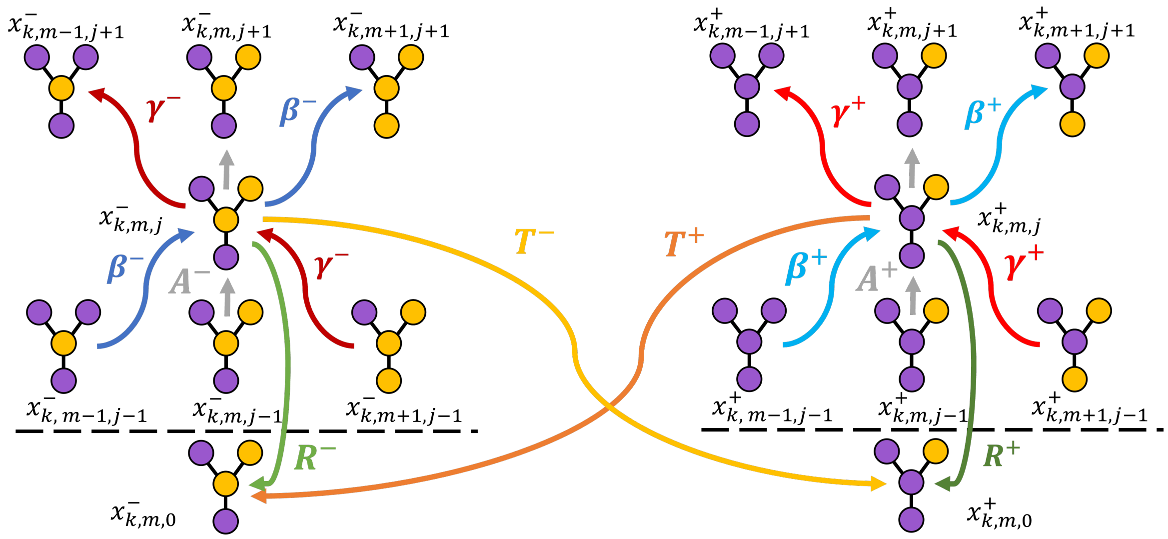

Figure 4.1: Schematic representation of the transitions to or from the set $x^-_{k,m,j}$ (left) and $x^+_{k,m,j}$ (right) ($j > 0$). We show the central node with some neighbors ($k = 3$) for different values m and j. Purple nodes are in state susceptible or non-adopters or $+1$, and yellow are in state infected or adopters or -1.

Fig. 4.1 for a schematic representation of transitions involving $x^+_{k,m,j}$ and $x^-_{k,m,j}$):

$$\begin{aligned}x^+_{k,m,j}(t+dt) =& x^+_{k,m,j}(t) - T^+(k,m,j)x^+_{k,m,j}\,dt - R^+(k,m,j)x^+_{k,m,j}\,dt - A^+(k,m,j)x^+_{k,m,j}\,dt \\ &+ A^+(k,m,j-1)x^+_{k,m,j-1}\,dt - \omega(x^+_{k,m,j} \to x^+_{k,m+1,j+1})x^+_{k,m,j}\,dt \\ &- \omega(x^+_{k,m,j} \to x^+_{k,m-1,j+1})x^+_{k,m,j}\,dt + \omega(x^+_{k,m+1,j-1} \to x^+_{k,m,j})x^+_{k,m+1,j-1}\,dt \\ &+ \omega(x^+_{k,m-1,j-1} \to x^+_{k,m-1,j-1})x^+_{k,m-1,j-1}\,dt.\end{aligned} \tag{4.2}$$

The case $j = 0$ needs to be treated differently from $j > 0$ because there is an injection of nodes into this set due to the resetting and changing state events. We write the possible transitions for the set $x^+_{k,m,0}$ as follows:

$$\begin{aligned}x^+_{k,m,0}(t+dt) =& x^+_{k,m,0}(t) - T^+(k,m,0)x^+_{k,m,0}\,dt + \sum_{l=0}^{\infty} T^-(k,m,l)x^-_{k,m,l}\,dt + \sum_{l=1}^{\infty} R^+(k,m,l)x^+_{k,m,l}\,dt \\ &- T^+(k,m,0)x^+_{k,m,0}\,dt - \omega(x^+_{k,m,0} \to x^+_{k,m+1,1})x^+_{k,m,0}\,dt - \omega(x^+_{k,m,0} \to x^+_{k,m-1,1})x^+_{k,m,0}\,dt.\end{aligned} \tag{4.3}$$

Similar equations can be found considering transitions for $x^-_{k,m,j}$ and $x^-_{k,m,0}$. Notice that we have considered no transition increasing (or decreasing) the number of -1 neighbors m, keeping constant the age j. This is because the age j is defined as the time spent in the current state (or since a reset). Therefore, if a node remains in its state and the number of neighbors in state -1 changes ($m \to m\pm 1$), the age of the node must increase ($j \to j+1$). To determine the rate of these events, we use the same assumption as in Ref. (66): we assume that the number of $++$ (edges between agents in state $+1$) edges change to $+-$ edges at a time-dependent rate β^+. Therefore, the transition rates are:

$$\begin{aligned}\omega(x^+_{k,m,j} \to s_{k,m+1,j+1}) &= (k-m)\,\beta^+, \\ \omega(s_{k,m-1,j-1} \to x^+_{k,m,j}) &= (k-m+1)\,\beta^+.\end{aligned} \tag{4.4}$$

To determine the rate β^+, we count the change of $++$ edges that change to $+-$ in a time step. This change is produced by a neighbor of a node in state $+1$ changing state from $+1$ to -1. Thus, we can extract this information from the transition probability $T^+(k,m,j)$:

$$\beta^+ = \frac{\sum_{j=0}^{\infty}\sum_{k=0}^{\infty} p_k \sum_{m=0}^{k}(k-m)\,T^+(k,m,j)\,x^+_{k,m,j}}{\sum_{j=0}^{\infty}\sum_{k=0}^{\infty} p_k \sum_{m=0}^{k}(k-m)\,x^+_{k,m,j}}. \tag{4.5}$$

A similar approximation is used to determine the transition rates at which $+-$ edges change to $++$ edges. We write:

$$\begin{aligned}\omega(x^+_{k,m,j} \to x^+_{k,m-1,j+1}) &= m\,\gamma^+,\\ \omega(x^+_{k,m+1,j-1} \to x^+_{k,m,j}) &= (m+1)\,\gamma^+,\end{aligned} \tag{4.6}$$

where the rate γ^+ is computed using the opposite transition probability $T^-(k,m,j)$:

$$\gamma^+ = \frac{\sum_{j=0}^{\infty}\sum_{k=0}^{\infty} p_k \sum_{m=0}^{k}(k-m)\,T^-(k,m,j)\,x^-_{k,m,j}}{\sum_{j=0}^{\infty}\sum_{k=0}^{\infty} p_k \sum_{m=0}^{k}(k-m)\,x^-_{k,m,j}}. \tag{4.7}$$

Taking the limit $dt \to 0$ of Eqs. (4.2)-(4.3), we obtain the approximate master equation (AME) for the evolution of the different sets $x^{\pm}_{k,m,j}$ and $x^{\pm}_{k,m,0}$:

$$\begin{aligned}\frac{dx^{\pm}_{k,m,j}}{dt} &= -\left(T^{\pm}(k,m,j)+A^{\pm}(k,m,j)+R^{\pm}(k,m,j)\right)x^{\pm}_{k,m,j} - (k-m)\,\beta^{\pm}\,x^{\pm}_{k,m,j}\\ &\quad - m\,\gamma^{\pm}\,x^{\pm}_{k,m,j} + (k-m+1)\,\beta^{\pm}\,x^{\pm}_{k,m-1,j-1} + (m+1)\,\gamma^{\pm}\,x^{\pm}_{k,m+1,j-1} + A^{\pm}(k,m,j-1)\,x^{\pm}_{k,m,j-1},\\ \frac{dx^{\pm}_{k,m,0}}{dt} &= -\left(T^{\pm}(k,m,0)+A^{\pm}(k,m,0)+R^{\pm}(k,m,0)\right)x^{\pm}_{k,m,0} - (k-m)\,\beta^{\pm}\,x^{\pm}_{k,m,0} - m\,\gamma^{\pm}\,x^{\pm}_{k,m,0}\\ &\quad + \sum_{l=0}^{\infty} T^{\mp}(k,m,l)\,x^{\mp}_{k,m,l} + \sum_{l=0}^{\infty} R^{\pm}(k,m,l)\,x^{\pm}_{k,m,l},\end{aligned} \tag{4.8}$$

where β^- (γ^-) are time-dependent rates that account for the transitions at which $-+$ ($--$) edges change to $--$ ($-+$) edges:

$$\beta^- = \frac{\sum_{j=0}^{\infty}\sum_{k=0}^{\infty} p_k \sum_{m=0}^{k} m\,T^+(k,m,j)\,x^+_{k,m,j}}{\sum_{j=0}^{\infty}\sum_{k=0}^{\infty} p_k \sum_{m=0}^{k}(k-m)\,x^-_{k,m,j}} \qquad \gamma^- = \frac{\sum_{j=0}^{\infty}\sum_{k=0}^{\infty} p_k \sum_{m=0}^{k} m\,T^-(k,m,j)\,x^-_{k,m,j}}{\sum_{j=0}^{\infty}\sum_{k=0}^{\infty} p_k \sum_{m=0}^{k} m\,x^-_{k,m,j}}. \tag{4.9}$$

Equations 4.8 define a closed set of deterministic differential equations that can be solved numerically using standard computational methods for any complex network and any model aging via the transition, reset and aging probabilities (a general script in Julia is available in a GitHub repository (62)).

4.3 Reduction to Markovian dynamics

When there are neither resetting nor aging events ($R^{\pm}(k,m,j) = A^{\pm}(k,m,j) = 0$) and the transition probabilities do not depend on the internal time j, $T^{\pm}(k,m,j) = T^{\pm}(k,m)$, our dynamics are Markovian. In this case, if we are not interested in the solutions $x^{\pm}_{k,m,j}(t)$, Eq. 4.8 can be reduced by summing variable j. We define $x^{\pm}_{k,m} = \sum_j x^{\pm}_{k,m,j}$ as the fraction of nodes that are in state ± 1 and have degree k and m infected neighbors. The equations for the variables $x^{\pm}_{k,m}$ are:

$$\begin{aligned}\frac{dx^{\pm}_{k,m}}{dt} = \frac{dx^{\pm}_{k,m,0}}{dt} + \sum_{j=1}^{\infty}\frac{dx^{\pm}_{k,m,j}}{dt} &= -T^{\pm}(k,m)\,x^{\pm}_{k,m} + T^{\mp}(k,m)\,x^{\mp}_{k,m} - (k-m)\,\beta^{\pm}\,x^{\pm}_{k,m} - m\,\gamma^{\pm}\,x^{\pm}_{k,m}\\ &\quad + (k-m+1)\,\beta^{\pm}\,x^{\pm}_{k,m-1} + (m+1)\,\gamma^{\pm}\,x^{\pm}_{k,m+1},\end{aligned} \tag{4.10}$$

where the rates $\beta^{\pm}$ and $\gamma^{\pm}$ are redefined as follows:

$$\beta^{+} = \frac{\sum_{k=0}^{\infty} p_k \sum_{m=0}^{k} (k-m)\, T^{+}(k,m)\, x_{k,m}^{+}}{\sum_{k=0}^{\infty} p_k \sum_{m=0}^{k} (k-m)\, x_{k,m}^{-}}, \qquad \gamma^{+} = \frac{\sum_{k=0}^{\infty} p_k \sum_{m=0}^{k} (k-m)\, T^{+}(k,m)\, x_{k,m}^{+}}{\sum_{k=0}^{\infty} p_k \sum_{m=0}^{k} m\, x_{k,m}^{+}},$$
$$\beta^{-} = \frac{\sum_{k=0}^{\infty} p_k \sum_{m=0}^{k} m\, T^{+}(k,m)\, x_{k,m}^{+}}{\sum_{k=0}^{\infty} p_k \sum_{m=0}^{k} (k-m)\, x_{k,m}^{-}}, \qquad \gamma^{-} = \frac{\sum_{k=0}^{\infty} p_k \sum_{m=0}^{k} m\, T^{-}(k,m)\, x_{k,m}^{-}}{\sum_{k=0}^{\infty} p_k \sum_{m=0}^{k} m\, x_{k,m}^{-}}. \tag{4.11}$$

Notice that this reduction is not an approximation and there is no loss of accuracy. The reduction to Markovian dynamics is a consequence of the chosen model. Eq. 4.10 correspond to the equations derived by J.P. Gleeson (66) for Markovian binary-state dynamics in complex networks. This is a set of $(k_{\max}+1)(k_{\max}+1)$ differential equations that can be solved numerically using standard computational methods for any complex network and any model via the transition probabilities $T^{\pm}(k,m)$.

4.4 Heterogeneous mean-field approximation (HMF)

Moreover, from Eqs. (4.10), we can perform a heterogeneous mean-field approximation (HMF) to reduce our system to $k_{\max}+1$ differential equations (66). This appoximation assumes a solution $x_{k,m}^{\pm} = x_k^{\pm} B_{k,m}[\omega]$, where $\omega = \langle k x_k^{-} \rangle / \langle k \rangle$ is the probability that one end of a randomly chosen edge is in state -1. Using this ansatz, the AME can be reduced to the following set of equations:

$$\frac{d}{dt} x_k^{-} = \quad -x_k^{-} \sum_{m=0}^{k} T_{k,m}^{-} B_{k,m}[\omega] + \left(1 - x_k^{-}\right) \sum_{m=0}^{k} T_{k,m}^{+} B_{k,m}[\omega], \tag{4.12}$$

This system of $(k_{\max}+1)$ differential equations, coupled via ω, cannot be solved analytically in general. However, it can be solved numerically using standard computational methods.

4.5 Summary and discussion

This chapter has expanded traditional binary-state models to include the effects of aging, providing a deeper insight into the dynamic behavior of complex networks. The mathematical framework developed here lays the groundwork for future studies to explore various aspects of aging in other dynamic systems, potentially leading to more accurate predictions and control strategies in both natural and engineered networks. The results presented in this chapter are a significant step forward in understanding the role of aging in binary-state dynamics, and we hope that they will inspire further research in this area.

Further work in this area could include the inclusion of other non-Markovian effects, such as memory kernels (138) or extended to 3-state dynamics, which could be useful to understand the phase diagram of the Sakoda-Schelling model with aging, described in previous chapter. Moreover, the AME was improved in Ref. (127) to include finite-size and stochastic effects in binary-state models, which could be extended to include aging effects. Finally, the framework developed in this chapter could be useful to describe aging dynamics in threshold models, since these models need for a mathematical framework that needs to go beyond mean-field approximations to capture the dynamics of the system (67).

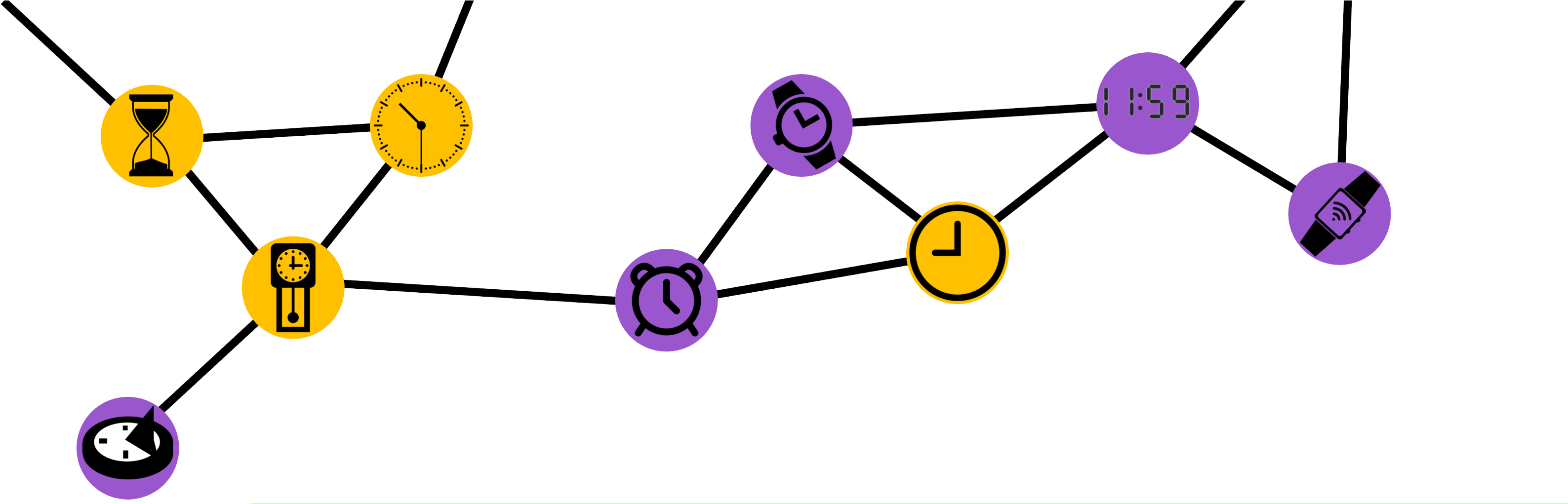

5. Impact of Aging in the Granovetter-Watts model

The results in this chapter are published as:

David Abella, Maxi San Miguel, and José J. Ramasco. “Aging in binary-state models: The Threshold model for complex contagion”. In: *Phys. Rev. E* 107 (2 Feb. 2023), page 024101. DOI: 10.1103/PhysRevE.107.024101. URL: https://link.aps.org/doi/10.1103/PhysRevE.107.024101

In this chapter, we analyze the aging implications in one of the most simple binary-state treshold models: the Granovetter-Watts model. Our analytical approximations give a good description of extensive Monte Carlo simulations in Erdős-Rényi, random-regular and Barabási-Albert networks. While aging does not modify the cascade condition, it slows down the cascade dynamics towards the full-adoption state: the exponential increase of adopters in time from the original model is replaced by a stretched exponential or power law, depending on the aging mechanism. Under several approximations, we give analytical expressions for the cascade condition and for the exponents of the adopters' density growth laws. Beyond random networks, we also describe by Monte Carlo simulations the effects of aging for the Granovetter-Watts model in a two-dimensional lattice.

5.1 Introduction

The Granovetter-Watts model (72, 167), is a well-known binary-state model for Complex contagion processes, such as rumor propagation, adoption of new technologies, riots, stock market herds, political and environmental campaigns... The discontinuous phase transition and the cascade condition exhibited by the Granovetter-Watts model were predicted with analytical tools in Ref. (167). This model has been extensively studied in regular lattices and small-world networks (30), random graphs (67), modular and community structure (64), clustered networks (80, 81), hypergraphs (8), homophilic networks (48), etc. Moreover, recent studies also include variants of the adoption rules including the impact of opinion leaders (103) and seed-size (148), on-off threshold (49) and the competition between simple and complex contagion (40, 48, 105, 107, 108). Additionally, the Granovetter-Watts model has been confronted with several sources of empirical data (29, 76, 94, 96, 97, 111, 135, 160).

Previous studies of the Granovetter-Watts model usually rely on a Markovian assumption for its dynamics. This implies that events depend only on the present state, i.e., dynamical rules are memoryless. Markovian processes exhibit exponential distributions in the upcoming events times and the number of events in a given time interval follows a Poisson distribution. However, there is strong empirical evidence against this assumption in human interactions and thus, the understanding of these non-Markovian effects is in general a topic of current interest (126, 127, 153, 162). In particular, for the threshold models, memory effects have been included as past exposures' memory (50), message-passing algorithms (145), memory distributions for retweeting

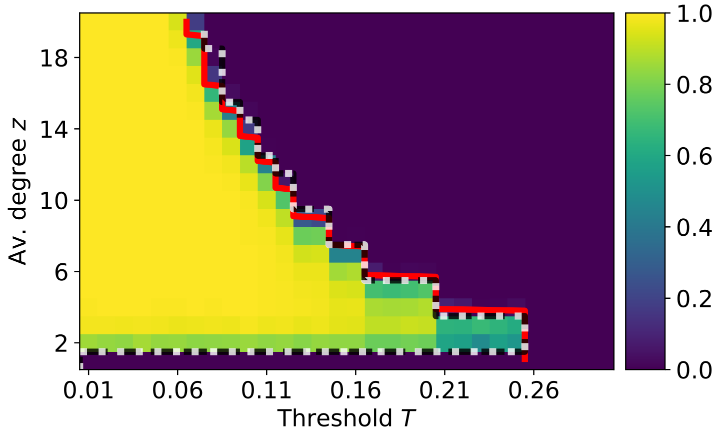

Figure 5.1: Average density x^- of adopters for an Erdős-Rényi graph of mean degree z using a model with threshold T. Color-coded values of x^- are from Monte Carlo simulations of the model without aging in a graph with $N = 10,000$ agents. Black dashed and white dotted lines correspond to T_c value obtained numerically for the model with exogenous and endogenous aging, respectively. Monte Carlo simulations are averaged over $M = 5\times10^4$ realizations. The red solid line is the analytical approximation of the cascade boundary, from Eq. (5.17), which is the same with and without aging.

algorithms (68) and timers (116).

In the specific context of innovation adoption, mechanisms of inertia or resistance to adopt the technology have been already introduced. In fact, the original approach of Rogers (133) considers a fraction of "laggards" that will resist innovating until a large majority of the population has already adopted it. Similar articles highlight the importance of timing interactions (14) and the effect of "contrarians" (tendency to act against the majority), which has an important impact on the dynamics (59, 69). In Ref. (69), it is discussed how different technologies may show different adoption cascades regarding the balance between advertisement and resistance to change.

In this chapter, we incorporate the aging mechanism into the Granovetter-Watts model, characterizing both the cascade condition and dynamics towards the fully adopted state. We propose two different aging mechanisms giving rise to heterogeneous activity patterns, characterized by flat-tail inter-event time distributions. To describe the results, we use the general master equation for any binary-state model with temporal activity patterns previously described in chapter 4. For the particular case of the Granovetter-Watts model, we are able reduce the dimensionality of the full system without loss of accuracy. Theoretical predictions are matched with extensive Monte Carlo simulations in different networks. For completeness, the role of both aging mechanisms is also studied in a two-dimensional Moore lattice.

The chapter is organized as follows. In the next section, we describe the original Granovetter-Watts model and introduce exogenous and endogenous aging in the model. In section 5.3, numerical results are reported and contrasted with theoretical predictions for different complex networks. For completeness, in section 5.4 the case of a 2D-lattice is analyzed. The final section contains a summary and a discussion of the results.

5.2 Aging in the Granovetter-Watts model

As it was introduced before (see 2.3), the standard Granovetter-Watts model (72, 167) considers a network of N interacting agents, where each node of the network represents an agent i with a binary-state variable $\sigma_i = \{0,1\}$ and a given threshold T $(0 < T < 1)$. The state indicates if the agent has adopted a technology (or joined a riot, spread a meme or fake news, etc.) or not.

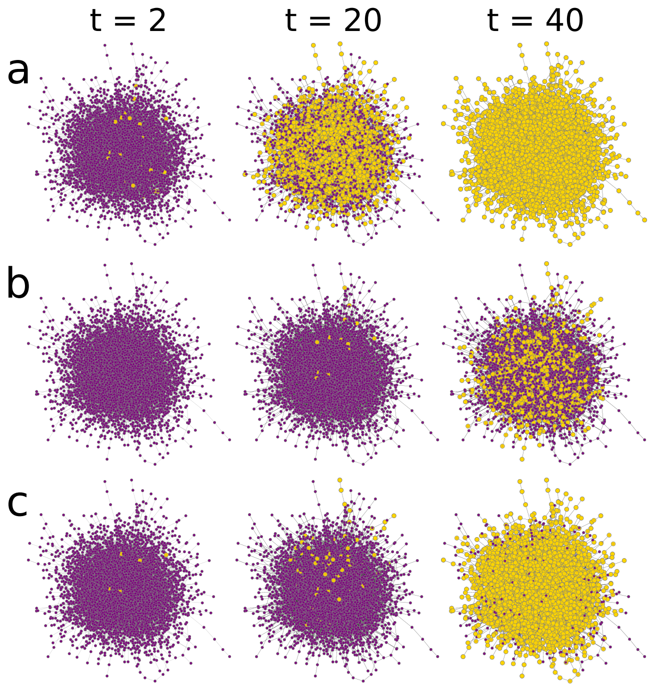

Figure 5.2: Cascade spreading for the original Granovetter-Watts model **(a)**, and the versions with endogenous **(b)** and exogenous **(c)** aging. Yellow nodes are adopters and purple nodes are non-adopters. Time increases from left to right. Monte Carlo simulations are performed in an Erdős-Rényi network with mean degree $z = 3$ and $T = 0.22$. System size is $N = 8,000$.

We use the wording of a technology adoption process for the rest of the chapter. If a node i (with k neighbors) has not adopted ($\sigma_i = 0$) the technology, becomes adopter ($\sigma_i = 1$) if the fraction m/k of neighbors adopters exceeds the threshold T. Adopter nodes cannot go back to the non-adopter state.

In the Granovetter-Watts model with aging, each agent has an internal time $j = 0, 1, 2, ...$ (in Monte-Carlo units) as in Refs. (10, 31, 53, 54, 126, 127, 130, 152). As initial condition, we set $j = 0$ for all nodes. In Monte Carlo simulations, we follow a Random Asynchronous Update in which agents are activated in discrete time steps with probability $p_A(j) = 1/(j+2)$. When a non-adopter agent is activated, she changes state according to the threshold condition $m/k > T$. We will consider two different aging mechanisms, endogenous and exogenous aging (53), which account for the power law inter-event time distributions empirically observed in human interactions (9). For endogenous aging, the internal time measures the time spent in the current state: If an agent in an updating attempt is not activated or does not adopt, the internal time increases by one unit. Therefore, the longer an agent has remained without adopting the technology, the more difficult it is for her to adopt it.

For exogenous aging, the internal time accounts for the time since the last attempt to change state: In each updating attempt in which the agent is activated, the internal clock resets to $j = 0$ even if there is no adoption. In this case, aging is understood as a resistance to adopt the technology the longer the agent has not been induced to consider adoption by some external influence.

5.3 Results on Complex networks

In this section we discuss the Granovetter-Watts model with endogenous and exogenous aging in three different complex networks: random-regular (RR) (170), Erdős-Rényi (ER) (52) and Barabási-Albert (BA) (12).

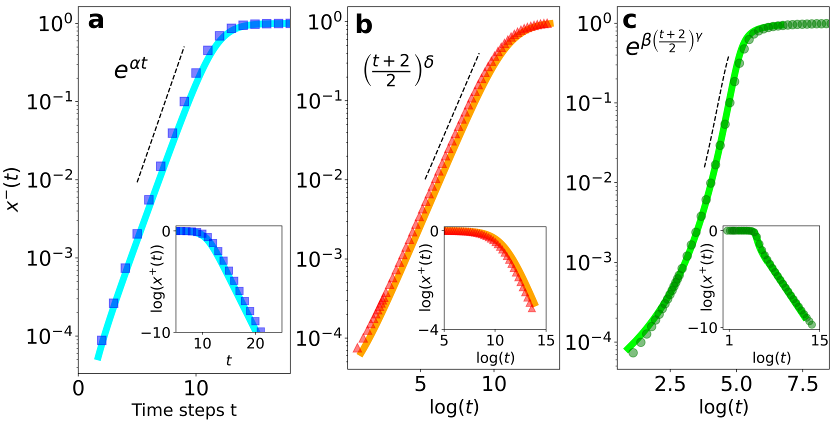

Figure 5.3: Cascade dynamics and fall to the full-adopt state ($x^- \sim 1$) of the Granovetter-Watts model without aging **(a)** and the versions with endogenous **(b)** and exogenous **(c)** aging effects. At (b-c), the evolution is plotted as a function of the logarithm of time $\log(t)$ in Monte Carlo steps, as in the insets. The underlying network is a 3-regular random graph and the threshold is $T = 0.2$. The exponent values are $\alpha \simeq 1.0$, $\beta \simeq 1.14$, $\gamma \simeq 0.38$ and $\delta \simeq 1.0$. Numerically integrated solutions of Eq. (5.4) (solid lines) describe accurately the numerical results. Monte Carlo simulations are averaged over $M = 5 \times 10^4$ realizations in a network of $N = 1.6 \times 10^5$ nodes.

5.3.1 Numerical results

For the networks considered, the Granovetter-Watts model undergoes a discontinuous phase transition at a certain critical value T_c (cascade condition) (167). For $T < T_c$, a small initial seed of adopters triggers a global cascade where, on average, a significant proportion of agents in the system adopt the technology (change from $\sigma_i = 0$ to 1). In our analysis, the initial condition is set to favor cascades: one agent i with degree $k_i = z$ is selected randomly and all her neighbors are initially adopters, as in Ref. (30, 148). For $T > T_c$, there are few cascade occurrences and none of them is global. The cascade condition dependence with the average degree z of the underlying network has been studied in Refs. (67, 167). For the two aging mechanisms considered, Monte Carlo simulations in random graphs show that the T_c dependence on z is very similar to the one for the model without aging (see Fig. 5.1). Therefore, for random networks, tends to the same cascade condition derived for the original model (which for ER graphs is $T_c = 1/z$ (167)). Similar results were found for RR and BA graphs. This result is not obvious a priory because aging has been shown to modify the final state in several models (10, 31, 53, 54, 126, 127, 130, 152).

Even though aging in the Granovetter-Watts model does not modify the cascade condition, it has a large impact in the complex contagion cascade dynamics (Fig.5.2). From Monte Carlo simulations in a random regular graph we find that, without aging, the average fraction of adopters, denoted by x^-, follows an initial exponential increase with time (see Fig. 5.2a and 5.3a),

$$x^-(t) \sim x_0^- e^{\alpha t}, \tag{5.1}$$

where x_0^- is the initial fraction of adopters (seed). This behavior is universal for all values of the control parameters z and T below the cascade condition. In addition, we investigated the approach to the full-adopt state ($x^- = 1$) and we found that the fraction of non-adopters, denoted by x^+, follows an exponential decay $x^+(t) =\sim e^{-t}$ for all values of the control parameters (see inset in Fig.5.3a).

When aging is introduced, the cascade dynamics are much slower than an exponential law (see Fig. 5.2b). For endogenous aging, all non-adopters agents have the same activation probability $p_A(j)$, which decreases at each time step. This gives rise to cascade dynamics

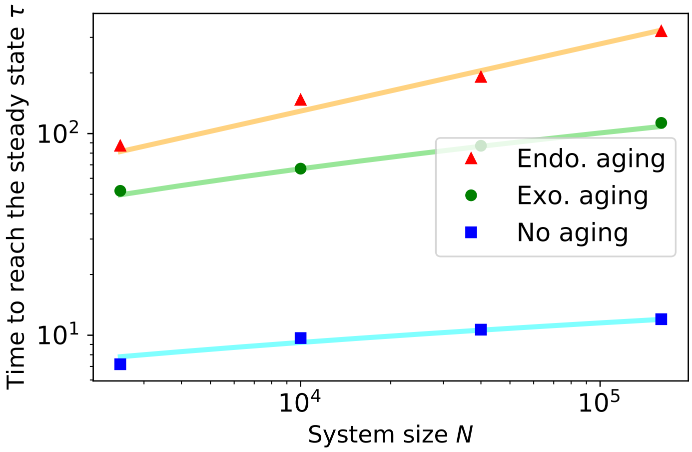

Figure 5.4: Average time to reach the steady state ($x^- > 0.9$) τ as a function of the system size N for the original Granovetter-Watts model and the versions with endogenous and exogenous aging. The underlying network is a 5-regular random graph and the threshold is $T = 0.12$. Monte Carlo simulations are averaged over $M = 5\times 10^4$ realizations. Solid lines are the system size-dependent timescale: For the original model, $\tau_{\text{NOAG.}} = (1/\alpha)\log(N)$, for the endogenous ($\tau_{\text{ENDO}} = 2N^{1/\delta} - 2$) and for the exogenous aging ($\tau_{\text{EXO}} = 2(\log(N)/\beta)^{1/\gamma} - 2$), which follows from the dynamics from Eq. (5.1), (5.2) and (5.3). The exponents α, β, γ and δ are fitted exponents from numerical simulations.

well-fitted by a power law increase (see Fig. 5.3b),

$$x^-(t) \sim x_0^- \left(\frac{t+2}{2}\right)^{\delta}. \tag{5.2}$$

For exogenous aging, we observe a slow adoption spread at the beginning followed by a cascade where almost all agents adopt the technology (Fig. 5.2c). This behavior is well-fitted with a stretched exponential increase of the number of adopters (see Fig. 5.3c),

$$x^-(t) \sim x_0^- e^{\beta\,((t+2)/2)^{\gamma}}. \tag{5.3}$$

For both aging mechanisms, in the last stages of evolution, a few "stubborn" non-adopters remain, although the environment favors the adoption. Due to the chosen activation probability, the number of non-adopters decay with a power law $x^+(t) \sim 1/(t+2)$ in both cases (see insets at Fig. 5.3(b-c)).

Comparing the evolution of the original model with one of the versions with aging, we observe an important separation of time scales. While for the original model, the time to reach the steady state follows a logarithmic increase with the system size, the versions with endogenous and exogenous aging show a power law and a power-logarithmic dependence, respectively (see Fig.5.4). Therefore, the time scale separation between the original model and the versions with aging increases as we increase the system size, and thus, the aging effects are more relevant for large systems.

The power law and the stretched exponential dynamics for endogenous and exogenous aging, respectively, are observed for z and T below the cascade condition ($T < T_c$) and for many different system sizes. This is shown in Fig. 5.5 for a random regular, Erdős-Rényi and Barabási-Albert networks. In particular, we show that the time-dependent behavior for different system sizes collapses to a single curve when time is scaled with the system size-dependent timescale (previously analyzed in Fig. 5.4) that follows from either the power law dynamics ($\tau_{\text{ENDO}} = 2N^{1/\delta} - 2$) or the stretched exponential law ($\tau_{\text{EXO}} = 2(\log(N)/\beta)^{1/\gamma} - 2$). Notice that the scaling of the y-axis is necessary for Fig.5.5(d-f) to show a linear dependence due to the stretched

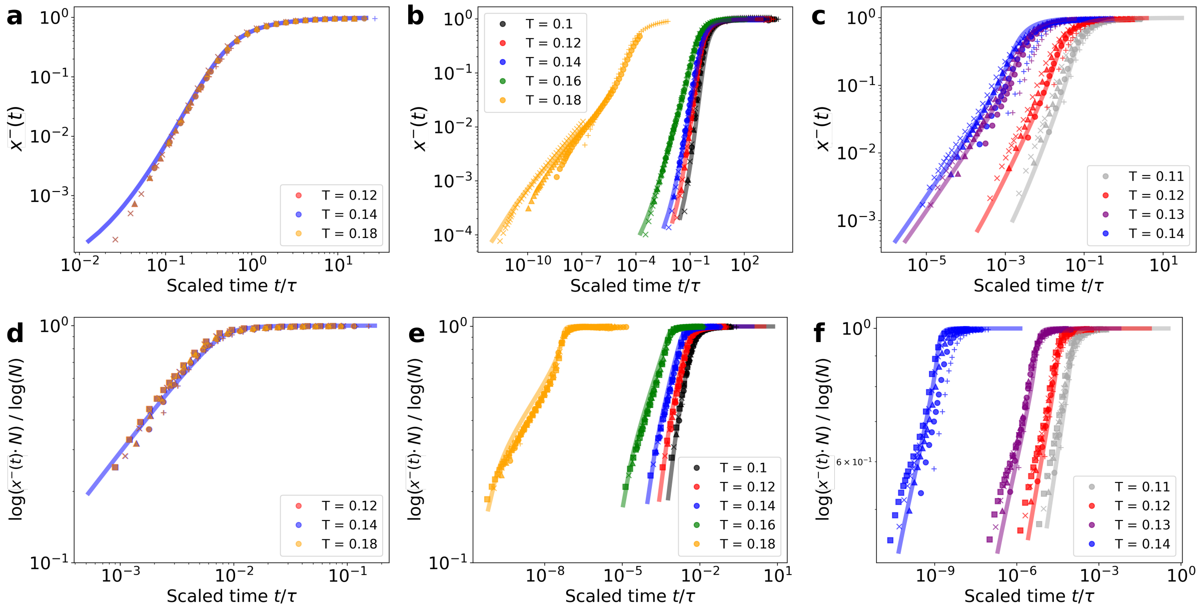

Figure 5.5: Cascade dynamics of the Granovetter-Watts model with endogenous (a - c) and exogenous (d - f) aging. From the left column to the right: a random regular graph with degree $z = 5$ (a and d), an Erdős-Rényi graph with average degree $z = 5$ (b and e) and a Barabási-Albert graph with average degree $z = 8$ (c and f). Different colors indicate different values of T and markers correspond to different system sizes: $N = 2,500$ (plus), $10,000$ (circles), $40,000$ (triangles), $160,000$ (crosses) and $640,000$ (squares). Time is scaled according to the system size for each model: $\tau_{\text{EXO}} = 2(\log(N)/\beta)^{1/\gamma} - 2$, $\tau_{\text{ENDO}} = 2N^{1/\delta} - 2$, where β, γ and δ are the fitted exponents from the behavior according to Eq. (5.2) and (5.3). Solid lines are obtained from the solutions of Eq. (5.13). Monte Carlo simulations are averaged over $M = 5 \times 10^4$ realizations.

exponential increase.

A different question is the dependence of the exponents of the power law and stretched exponential with the parameters z and T. Numerical results from fitted Monte Carlo simulations for $\alpha(z,T)$, $\delta(z,T)$ and $\gamma(z,T)$ are shown in Figs. 5.6 and 5.7. For a random-regular graph, as apparent from Fig. 5.5, the exponents do not depend on the parameter T up to T_c (so the exponents are dependent only on z, $\alpha(z)$, $\gamma(z)$ and $\delta(z)$), while for Erdős-Rényi and Barabási-Albert networks the value of the exponents decrease with T when approaching T_c, indicating a slowing down of the dynamics. Also, for these two latter networks, the exponents present a maximum value at a certain value of z. This maximum value at a certain z for a fixed T can be understood as being between the two critical lines of Fig. 5.1.

5.3.2 General mathematical description

To account for the non-Markovian dynamics introduced by the aging mechanism, we need to go beyond the standard mathematical descriptions of the Granovetter-Watts model (64, 66, 67). We do so using a Markovian description by enlarging the number of variables (126, 127). Namely, we classify the agents with degree k, number of adopter neighbors m and age j as different sets in a compartmental model in a general framework for binary-state dynamics in complex networks, as described in chapter 4. To write down the AME for the Granovetter-Watts model with aging, we need to consider the following possible transitions:

- A node i, in state $\sigma_i = \pm 1$, changes state and resets internal age with probability $T^{\pm}(k,m,j)$;
- A node i, in state $\sigma_i = \pm 1$, remains in the same state and resets internal age to zero ($j \to 0$) with probability $R^{\pm}(k,m,j)$;
- A node i, in state $\sigma_i = \pm 1$, remains in the same state and ages ($j \to j+1$) with probability

$A^{\pm}(k,m,j)$.

For the specific case of the Granovetter-Watts model, dynamics are monotonic and $T^{-}(k,m,j)=0$ (no adopter becomes a non-adopter). Moreover, when an agent becomes an adopter, there are neither resetting nor aging events $R^{-}(k,m,j)=A^{-}(k,m,j)=0$. This means as well that equations for the non-adopters $x^{+}_{k,m,j}$ and adopters $x^{-}_{k,m,j}$ nodes are independent. Thus, we can write the following rate equations for the evolution of the fraction $x^{+}_{k,m,j}(t)$ of k-degree non-adopters nodes with m infected neighbors and age j:

$$\frac{dx^{+}_{k,m,j}}{dt} = -x^{+}_{k,m,j} - (k-m)\,\beta^{s}\,x^{+}_{k,m,j} + (k-m+1)\,\beta^{s}\,x^{+}_{k,m-1,j-1} + A^{+}(k,m,j-1)\,x^{+}_{k,m,j-1}, \tag{5.4}$$
$$\frac{dx^{+}_{k,m,0}}{dt} = -x^{+}_{k,m,0} - (k-m)\,\beta^{s}\,x^{+}_{k,m,0} + \sum_{l=0} R^{+}(k,m,l)\,x^{+}_{k,m,l},$$

where β^{s} is a non-linear function of $x^{+}_{k',m',j'}$ for all values of k',m' and j' (see Eq. (4.5)). The remaining step is to define explicitly the transition probabilities for our aging mechanisms. For both exogenous and endogenous aging, the adoption probability is the probability that an agent is activated and has a fraction of adopters that exceeds the threshold T, which means that

$$T^{+}(k,m,j) = p_A(j)\,\theta(m/k-T), \tag{5.5}$$

where $\theta(\cdot)$ is the Heaviside step function.

The reset and aging probabilities for endogenous and exogenous aging mechanisms are different. The simplest case is endogenous aging where there is no reset $R^{\pm}(k,m,j)=0$ and agents increase by one the age with probability

$$A^{+}(k,m,j) = 1 - T^{+}(k,m,j) = 1 - p_A(j)\,\theta\,(m/k-T)\,. \tag{5.6}$$

When aging is exogenous, the reset probability is the probability to activate and not adopt

$$R^{+}(k,m,j) = p_A(j)\,(1-\theta\,(m/k-T))\,. \tag{5.7}$$

Thus, agents that age are just the ones that do not activate, $A^{+}(k,m,j)=1-p_A(j)$.

Using these definitions, we have integrated numerically Eq. (5.4) for the Granovetter-Watts model with both endogenous and exogenous aging. Numerical solutions give good agreement with Monte Carlo simulations (see Fig. 5.3). However, in a general network, considering a cutoff for the degree $k=0,\ldots,k_{\max}$ and age $j=0,\ldots,j_{\max}$, the number of differential equations to solve is $(k_{\max}+1)\,(k_{\max}+1)\,(j_{\max}+1)$ according to the three subindexes of the variable $x^{+}_{k,m,j}$. This number grows with the largest degree square and largest age considered and thus, some further approximations are needed to obtain a convenient reduced system of differential equations.

As an ansatz, we assume that timing interactions can be effectively decoupled from the adoption process so the solution of Eq. (5.4) can be written as

$$x^{+}_{k,m,j}(t) = x^{+}_{k,m}(t)\,G_j(t), \tag{5.8}$$

where $x^{+}_{k,m}$ is the fraction of non-adopters with degree k and m infected neighbors $x^{+}_{k,m}=\sum_j x^{+}_{k,m,j}$ and there is an age distribution $G_j(t)$, independent of the adoption process.

If we sum over the variable age j in Eq. (5.4), we can rewrite the following rate equations for the variables $x^{+}_{k,m}$

$$\frac{dx^{+}_{k,m}}{dt} = -\langle p_A\rangle\,\theta(m-kT)\,x^{+}_{k,m} - (k-m)\,\beta^{s}\,x^{+}_{k,m} + (k-m+1)\,\beta^{s}\,x^{+}_{k,m-1}, \tag{5.9}$$

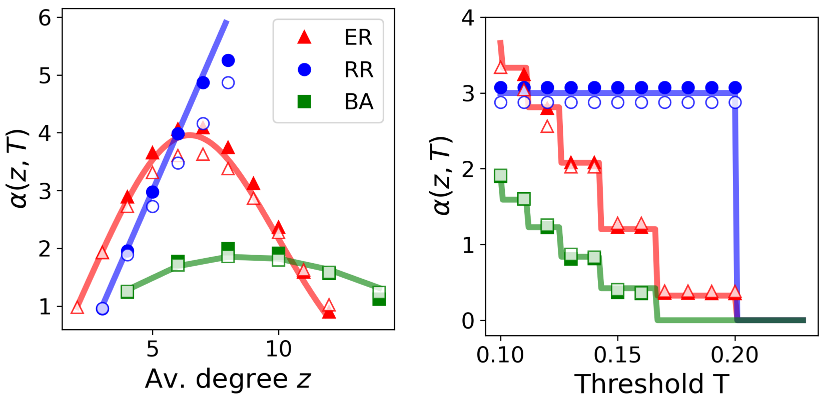

Figure 5.6: Exponent α for the original Granovetter-Watts model (empty markers) and δ for the version with endogenous aging (filled markers) for different values of the average degree z (and $T = 0.1$) **(left)** and as a function of T for fixed z **(right)**. Different markers indicate results from Monte Carlo simulations with different topologies: red triangles indicate an Erdős-Rényi (ER) graph, blue circles indicate a random regular (RR) graph and green squares indicate a Barabási-Albert (BA) graph. In the right panel, the average degree is fixed $z = 5$ for ER and RR, and $z = 8$ for the BA. Predicted values by Eq. (5.22) (solid lines) fit the results for each topology. System size is fixed at $N = 4\times 10^6$ for the original model and $N = 3.2\times 10^5$ for the version with aging.

where aging effects are just included in $\langle p_A\rangle(t)$:

$$\langle p_A\rangle(t) = \sum_{j=0}^{\infty} p_A(j)\, G_j(t). \tag{5.10}$$

Using the definition of the fraction of k-degree adopters $x_k^-(t)$,

$$x_k^-(t) = 1 - \sum_{j=0}^{\infty}\sum_{m=0}^{k} x_{k,m,j}^+, \tag{5.11}$$

and along the lines of Ref. (66), we use the following ansatz

$$x_{k,m}^+ = (1 - x_k^-(0))\, B_{k,m}[\phi], \tag{5.12}$$

where $B_{k,m}[\phi]$ is the binomial distribution with k attempts, m successes and with success probability ϕ. From this point, we derive from Eq. (5.9) a reduced system of two coupled differential equations for the fraction of adopters $x^-(t) = \sum_k p_k x_k^-(t)$ and an auxiliary variable $\phi(t)$ (see details in Ref. (66)):

$$\frac{dx^-}{dt} = \langle p_A\rangle[h(\phi) - x^-], \qquad \frac{d\phi}{dt} = \langle p_A\rangle[g(\phi) - \phi], \tag{5.13}$$

where $\phi(t)$ can be understood as the probability that a randomly chosen neighbor of a non-adopter node is an adopter at time t. The functions $h(\phi)$ and $g(\phi)$ are nonlinear functions of this variable ϕ

$$\begin{aligned} h(\phi) &= \sum_{k=0}^{\infty} p_k \left(x_k^-(0) + (1 - x_k^-(0)) \sum_{m=kT}^{k} B_{k,m}[\phi] \right), \\ g(\phi) &= \sum_{k=0}^{\infty} \frac{k}{z} p_k \left(x_k^-(0) + (1 - x_k^-(0)) \sum_{m=kT}^{k} B_{k-1,m}[\phi] \right). \end{aligned} \tag{5.14}$$

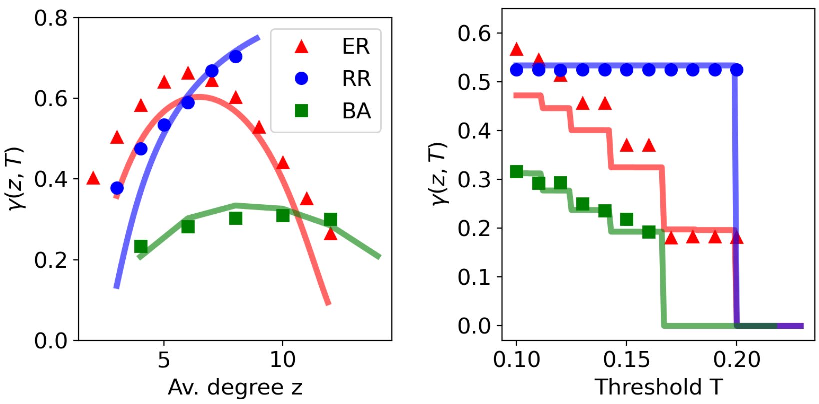

Figure 5.7: Exponent γ for the Granovetter-Watts model with exogenous aging for different values of the average degree z $(T = 0.1)$ **(left)** and as a function of T for fixed z **(right)**. Different markers indicate results from Monte Carlo simulations with different topology: red triangles indicate an Erdős-Rényi (ER) graph, blue circles indicate a random regular (RR) graph and green squares indicate a Barabási-Albert (BA) graph. In the right panel, the average degree is fixed $z = 5$ for ER and RR, and $z = 8$ for the BA. Predicted values by numerical integration of Eqs. (5.13) (solid lines) fit approximately the results for each topology. System size is fixed at $N = 3.2 \times 10^5$.

When $\langle p_A \rangle$ is replaced by a constant, Eqs. (5.13) reduce to previous results for the original model (64).

Determining the distribution $G_j(t)$ a priori is not easy. For endogenous aging, all non-adopters have the same age at each time step and $G_j(t) = \delta(j-t)$ (where $\delta(\cdot)$ is the Dirac delta function). Therefore, $\langle p_A \rangle = 1/(t+2)$. The numerical solution of Eq. (5.13) gives a good agreement with Monte Carlo simulations (see Fig. 5.5(a-c)). For the case of exogenous aging, the reset of the internal clock makes more difficult a choice for $G_j(t)$. Inspired on the stretched exponential behavior of $x^-(t)$ observed from Monte Carlo simulations, we propose $\langle p_A \rangle = 1/(t+2)^\mu$. For $\mu = 0.75$, the numerical solutions of Eq. (5.13) gives a very good agreement with our Monte Carlo simulations (see Fig. 5.5 (d-f)).

5.3.3 Analytical results

To obtain an analytical result for the cascade condition and for the exponents of the predicted exponential, stretched-exponential and power law cascade dynamics that we fitted from Monte Carlo simulations, we need to go a step beyond the numerical solution of our approximated differential equations (Eqs. (5.4) and (5.13)).

For a global cascade to occur, it is needed that the variable $\phi(t)$ grows with time. If we assume a small initial seed ($x_k^-(0) \to 0$), Eq. (5.13) can be rewritten as in Ref. (67)

$$\frac{d\phi}{dt} = \langle p_A \rangle \left(-\phi + \sum_{k=1}^{\infty} \frac{k}{z} p_k \sum_{m=kT}^{k} B_{k-1,m}[\phi] \right). \tag{5.15}$$

Rewriting the sum term as $\sum_{l=0}^{\infty} C_l \phi^l$, with coefficients

$$C_l = \sum_{k=l}^{\infty} \sum_{m=0}^{l} \binom{k-1}{l} \binom{l}{m} (-1)^{l+m} \frac{k}{z} p_k \, \theta\left(m/k - T\right), \tag{5.16}$$

we linearize Eq. (5.15) around $\phi = 0$:

$$\frac{d\phi}{dt} \approx \langle p_A \rangle \left(C_1 - 1\right) \phi. \tag{5.17}$$

The solution for Eq. (5.17) is then

$$\phi(t) = x_0^- \, e^{(C_1-1)\int_0^t \langle p_A\rangle(s)\,ds}, \tag{5.18}$$

given that $\phi(0) = x_0^-$.

Linearization is useful to determine the time dependence of the cascade process. Assuming a small initial seed and rewriting the term $h(\phi)$ as $\sum_{l=0}^{\infty} K_l\,\phi^l$, the linearized equation for the fraction of adopters $x^-(t)$ becomes

$$\frac{dx^-}{dt} \approx \langle p_A\rangle\,(K_1-1)\,\phi, \tag{5.19}$$

where the coefficients K_l are

$$K_l = \sum_{k=l}^{\infty}\sum_{m=0}^{l} \binom{k}{l}\binom{l}{m}(-1)^{l+m}\,p_k\,\theta\,(m/k-T). \tag{5.20}$$

A solution for the fraction of adopters $x^-(t)$ can be obtained from Eqs. (5.18) and (5.19). For the case of the Granovetter-Watts model without aging, setting $\langle p_A\rangle = 1$, the solution is an exponential cascade dynamics

$$x^-(t) = x_0^- \, e^{(C_1-1)\,t}. \tag{5.21}$$

Therefore, the number of adopters $x^-(t)$ follows an exponential increase with exponent $\alpha(z,T)$:

$$\alpha(z,T) = C_1 - 1 = \sum_{k=0}^{\lfloor 1/T\rfloor} \frac{k\,(k-1)}{z}\,p_k - 1, \tag{5.22}$$

where C_1 is computed from Eq. (5.16).

For endogenous aging, the same derivation is valid to determine the exponents $\delta(z,T)$. Using $\langle p_A\rangle = 1/(t+2)$, the fraction of adopters follows a power law dependence,

$$x^-(t) = x_0^- \left(\frac{t+2}{2}\right)^{(C_1-1)}. \tag{5.23}$$

The exponent reported for the power law cascade dynamics $\delta(z,T)$ turns out to be, therefore, the same exponent as the one for the exponential behavior where there is no aging: $\delta(z,T) = \alpha(z,T) = C_1 - 1$. Fig. 5.6 compares the prediction of Eq. (5.22) with the results computed from Monte Carlo simulations. There is a good agreement for both Barabási-Albert and Erdős-Rényi networks for all values of T and z. For a random-regular graph, the predicted dependence, $\alpha(z) = z-2$, is not a good approximation for large z. This is because the presence of small cycles increases importantly in a random-regular graph as the average degree z grows (169) and the locally-tree assumption made for the derivation of the rate equations (Eq. (5.4)) is not valid anymore. A different approach is necessary for clustered networks (as in Ref.(98) for the Granovetter-Watts model).

Moreover, from Eq. (5.17), we can extract the cascade condition for the Granovetter-Watts model in general. Since $\langle p_A\rangle(t)$ is always positive, global cascades occur when $(C_1-1) > 0$, so the cascade condition is:

$$T < T_c = \frac{1}{\sum_{k=0}^{\infty}\frac{k\,(k-1)}{z}\,p_k}. \tag{5.24}$$

This cascade condition does not depend on the aging term $\langle p_A\rangle(t)$ and thus, it is the same as for the Granovetter-Watts model without aging. In Fig. 5.1, the red solid line is the result of this analytical calculation, and it is in good agreement with the numerical results.

For exogenous aging, an analytical expression for the exponent $\gamma(z,T)$ is not obtained following this methodology. Still, we can fit the exponent from the numerical solutions in Fig. 5.5 (d-f). Fig.5.7 shows a good comparison between the exponent calculated from the numerical solutions and the one calculated from Monte Carlo simulations. The dependence of $\gamma(z,T)$ with

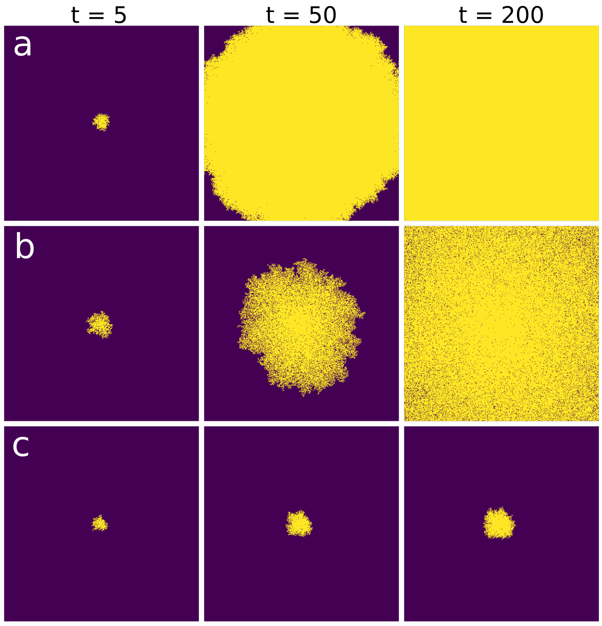

Figure 5.8: Cascade spreading of the original Granovetter-Watts model **(a)** and the versions with exogenous **(b)** and endogenous **(c)** aging on a Moore neighborhood lattice with size $N = L \times L$, $L = 405$. Yellow and purple nodes are adopters and non-adopters, respectively. Time increases from left to right. Initial seeds are selected favoring cascades: one agent and all him/her neighbors are set as adopters at the center of the system.

the parameters z and T is qualitatively similar to the dependence of $\alpha(z,T)$.

5.4 Results on a Moore lattice

The Granovetter-Watts model in a two-dimensional regular lattice with a Moore neighborhood (nearest and next nearest neighbors) has a critical threshold (cascade condition) $T_c = 3/8$ (30). Below this value, cascade dynamics follows a power law increase in the density of adopters $x^-(t)$, which does not depend on the threshold value T (30). In Fig. 5.8a, we show a typical realization of this model: From an initial seed, the adoption radius increases linearly with time until all agents adopt the technology.

When aging is considered, cascade dynamics become much slower and a dependence on T appears. When the aging mechanism is exogenous, Monte Carlo simulations indicate cascade dynamics following a power law $x^-(t) \approx t^{\zeta(T)}$. Qualitatively, we observe that while in the case without aging there was a soft interface between adopter and non-adopters, aging causes a strong roughening in the interface and the presence of non-adopters inside the bulk (see Fig. 5.8b). In addition, the exponent values fitted from Monte Carlo simulations allow us to collapse curves for different system sizes (see Fig. 5.9a). Due to finite size effects, the interface between adopters and non-adopters eventually reaches the borders of the system and the remaining non-adopters, in the bulk, will slowly adopt with the density of adopters following the functional shape $x^-(t) = 1 - 1/(t+2)$.

Fig.5.8c shows the dynamics towards global adoption for endogenous aging. In comparison with the case of exogenous aging, we do not observe strong interface roughening between adopters and non-adopters, because non-adopters are not present in the bulk. Monte Carlo simulations indicate a very slow increase of the density of adopters x^-, similar to a power-logarithmic growth $x^-(t) \approx (\log(t))^{\nu}$, with a threshold dependent exponent $\nu(T)$ (Fig. 5.9b). Our general approximation used for complex networks assumes a tree-like network, and it is not appropriate for the Moore lattice.

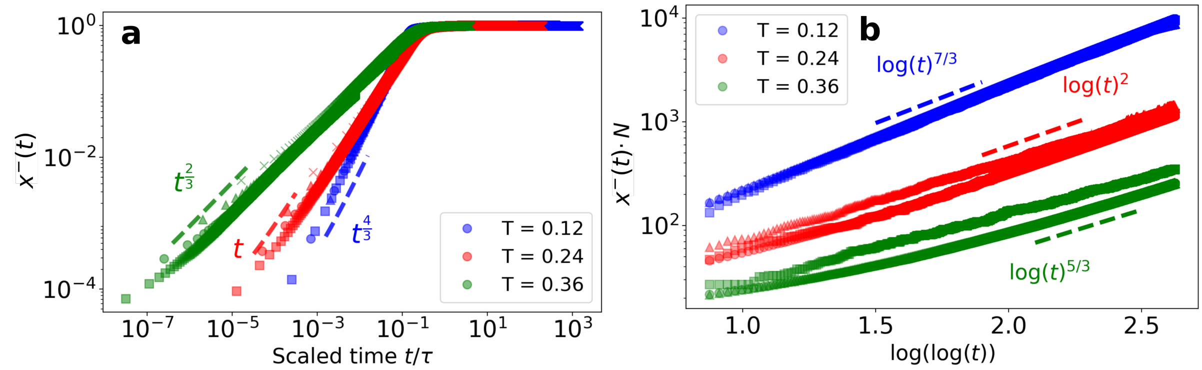

Figure 5.9: Cascade dynamics of the Granovetter-Watts model with exogenous **(a)** and endogenous **(b)** aging on a Moore neighborhood lattice. Different colors indicate different values of the threshold T. Different markers indicate the results of Monte Carlo simulations with different system size $N = L \times L$: $L = 50$ (crosses), 100 (triangles), 200 (circles) and 400 (squares). In (a), time is scaled according to size $\tau = L^{2/\zeta}$. Discontinuous solid lines indicate a power law behavior with exponent $\zeta = 4/3$ (blue), 1 (red) and $2/3$ (green). In (b), the system sizes are not scaled due to the slow dynamics. Discontinuous solid lines indicate a power-logarithmic behavior, $x^-(t)N \sim \log(t)^\nu$, with exponent $\nu = 7/3$ (blue), 2 (red) and $5/3$ (green).

5.5 Summary and discussion

We have addressed in this chapter the role of aging in general models with binary-state agents interacting in a complex network. Temporal activity patterns are incorporated by means of a variable that represents the internal time of each agent. We have developed an approximate Master Equation for this general situation. In this framework, we have explicitly studied the effect of aging in the Granovetter-Watts model as a paradigmatic example of Complex Contagion processes. Aging implies a lower probability to change state when the internal time increases. We considered two aging mechanisms: endogenous aging, in which the internal time measures the persistence time in the current state, and exogenous aging, in which the internal time measures the time since the last update attempt.

Our theoretical framework with some approximations to attain analytical results provide a good description of the results from Monte Carlo simulations for Erdős-Rényi, random-regular and Barabási-Albert networks. For these three types of complex networks, we found that the cascade condition T_c (critical value of the threshold parameter T as a function of mean degree z of the network) for the full spreading from an initial seed is not changed by the aging mechanisms. However, aging modifies in non-trivial ways cascade dynamics of the process. The exponential growth with exponent $\alpha(z,T)$ of the density of adopters in the absence of aging becomes a power law with exponent $\delta(z,T)$ for endogenous aging, and a stretched exponential characterized by an exponent $\gamma(z,T)$ for exogenous aging. We have analyzed the exponents' dependence with the order parameters $\alpha(z,T)$, $\delta(z,T)$, $\gamma(z,T)$ and shown that $\delta(z,T) = \alpha(z,T)$, for which an analytical expression is obtained.

Our general theoretical framework, based on the assumption of a tree-like network, is not appropriate for a regular lattice. In this case, we have been only able to run Monte Carlo simulations. Our results indicate that exogenous aging gives rise to adoption dynamics characterized by an increase in the interface roughness, by the presence of non-adopters in the bulk, and by a power law growth of the density of adopters with exponent $\zeta(T)$, while in the absence of aging $\zeta = 2$ independently of T. Endogenous aging, on the other hand, produces very slow (logarithmic-like) dynamics, with a threshold-dependent exponent $\nu(T)$.

This study highlights the importance of non-Markovian dynamics in general binary-state dynamics and, specifically, in the Granovetter-Watts model. For the problem of innovation adoption that this model addresses, we show how persistence times have an important impact on the adoption cascade. Further work in this direction would be to categorize technologies according to the adoption curve, to show if the system has important resistance to the previous technology (endogenous aging) or a balance between memory and external influence or advertisement (exogenous aging). Furthermore, the theoretical framework presented here gives a basis for further investigations of the memory effects and non-Markovian dynamics in networks, and in particular for binary-state models with aging. Still, a number of theoretical developments remain open for future work, such as the consideration of stochastic finite size effects (124), or extending this framework to tri-state models. Also, proper approximations need to be developed to account for some of our numerical results for random-regular networks with high degree, as well as for high clustering, degree-degree correlations networks and for regular lattices, including continuous field equations for this latter case.

6A. Symmetrical Threshold model: Ordering dynamics

The results in this chapter are published as:

David Abella et al. "Ordering dynamics and aging in the symmetrical threshold model". In: *New Journal of Physics* 26.1 (Jan. 2024), page 013033. DOI: 10.1088/1367-2630/ad1ad4. URL: https://dx.doi.org/10.1088/1367-2630/ad1ad4

In the previous chapters, we have studied the aging effects in two different models: the Sakoda-Schelling segregation model, a 3-state threshold model with 2 symmetric states, and the Granovetter-Watts model, a binary-state threshold asymmetric model. Despite both models are threshold models, the aging implications are different in both models. In this chapter and the next, we investigate a symmetric version of the threshold model and the aging implications in this model. In this first chapter, we explore the Symmetrical Threshold model in different network topologies and for different initial conditions. We find that the model exhibits three different phases: a mixed one (dynamically active disordered state), an ordered one, and a heterogeneous frozen phase. For random interaction networks, we develop a theoretical description based on an AME that describes with good accuracy the results of numerical simulations for the model.

6A.1 Introduction

In recent decades, various techniques of probability and statistical physics have been employed to measure and explain social phenomena (18, 24, 93). A variety of social collective phenomena can be well understood through models of interacting agents. For example, the consensus problem consists of determining under which circumstances the agents end up sharing the same state or when the coexistence of both states prevails. This is characterized by a phase diagram that provides the boundaries separating domains of different behaviors in the control parameter space.

As we have seen in this thesis, an important binary-state model is the Granovetter-Watts model (72, 167), In this model, multiple exposures, or group interaction, are necessary to update the current state, a characteristic of complex contagion models (30, 86). A main difference between the Granovetter-Watts model and other binary-state models, such as the Voter (102), majority vote (MV) (22, 117, 129), and nonlinear Voter model (26, 90, 104, 106, 109, 125), is the lack of symmetry between the two states. In the Granovetter-Watts model, changing state is only possible in one direction, representing the adoption forever of a new state that initially starts in a small minority of agents. A symmetric version of the Granovetter-Watts threshold model, with possible changes of states in both directions, shows hysteresis when the noise is introduced into the model (114, 115). However, a complete characterization of the Symmetrical Threshold model and its ordering dynamics have not been addressed so far.

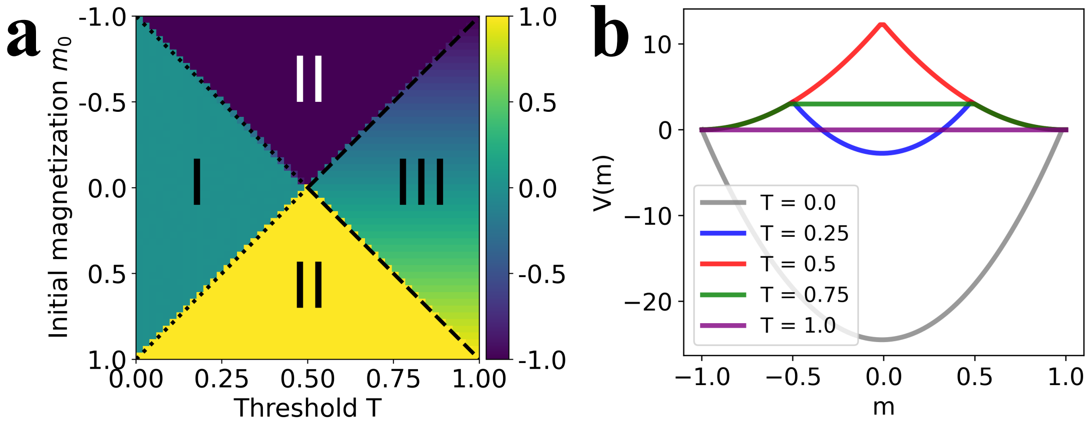

Figure 6A.1: **(a)** Phase diagram of the Symmetrical Threshold model in a Complete graph of $N = 2500$ nodes. Dotted and dashed lines correspond to $T = (1-|m_0|)/2$ and $T = (1+|m_0|)/2$, respectively. Average performed over 5000 realizations. **(b)** Potential representation from Eq. (6A.2) for a set of values of the threshold T, shown in different colors.

In this chapter, we present a comprehensive analysis of the Symmetrical Threshold model, including its full phase diagram. The model is examined in various network topologies, such as the complete graph, Erdős-Rényi (ER) (52), random regular (RR) (170), and a two-dimensional Moore lattice. The possible phases of the system are defined by the final stationary state as well as by the ordering/disordering dynamics characterized by the time-dependent magnetization, interface density, persistence, and mean internal time. The results of Monte Carlo numerical simulations are compared with results from the theoretical framework provided by the Approximate Master Equation (AME) (see details in chapter 4), which is general for any random network. We also derive a mean-field analysis to describe the outcomes in a complete graph.

6A.2 Symmetrical Threshold model

The system consists of a set of N agents located at the nodes of a network. The variable describing the state of each agent i takes one of the two possible values: $s_i = \pm 1$. Every agent has assigned a fixed threshold $0 \leq T \leq 1$, which determines the fraction of different neighbors required to change state. Even though this value might be agent-dependent, we will consider here homogeneous T for all the agents. In each update attempt, an agent i (called active agent) is randomly selected, and if the fraction of neighbors with a different state is larger than the threshold T, the active agent changes state $s_i \to -s_i$. In other words, if m is the number of neighbors in state -1 out of the total number of neighbors k, the condition to change is $\theta(m/k - T)$, for a node in state $+1$, and $\theta((k-m)/k - T)$, for a node in state -1, where $\theta(x)$ is the Heaviside step function. Notice that this update rule is equivalent to "shifted" Glauber dynamics (63), with swapping probability $1/(1+\exp[\beta(\Delta E + C)])$ (where β is the inverse temperature, ΔE the energy loss to swap the state of a node according to Ising Hamiltonian and C a shifting constant), at the limit of zero temperature ($\beta \to \infty$). Numerical simulations of the model run until the system reaches a frozen configuration (absorbing state) or until the average magnetization, $m = (1/N)\sum_i s_i$, fluctuates around a constant value. Simulation time is measured in Monte Carlo (MC) steps, i.e., N update attempts.

6A.3 Results on Complex networks

6A.3.1 Mean-field

We first consider the mean-field case of the complete graph (all-to-all connections). We take an initial random configuration with magnetization m_0 and run numerical simulations for various values of T to construct the phase diagram (shown in Fig. 6A.1a). We find three different phases based on the final state:

- **Phase I or Mixed**: The system reaches an active disordered state (final magnetization $m_f = 0$) where the agents change their state continuously;
- **Phase II or Ordered**: The system reaches the ordered absorbing states ($m_f = \pm 1$) according to the initial magnetization m_0;
- **Phase III or Frozen**: The system freezes at the initial random state $m_f = m_0$.

For a given initial magnetization $m_0 \neq 0$ and increasing T, the system undergoes a mixed-ordered transition at a critical threshold $T_c = (1-|m_0|)/2$, and an ordered-frozen transition at a critical threshold $T_c^* = (1+|m_0|)/2 > T_c$ (indicated by dotted and dashed black lines in Fig. 6A.1a, respectively). In this mean-field scheme, if the fraction of nodes in state $+1$ is denoted by x, the condition for a node in state -1 to change its state is given by $\theta(x-T)$, where θ is the Heaviside step function. Thus, in the thermodynamic limit ($N \to \infty$), the variable x evolves over time according to the following mean-field equation:

$$\frac{dx}{dt} = (1-x)\,\theta(x-T) - x\,\theta(1-x-T) = -\frac{\partial V(x)}{\partial x}. \tag{6A.1}$$

Here, $V(x)$ is the potential function. The stationary value of x, x_{st}, is the solution of the implicit equation resulting from setting the time derivative equal to 0. The stationary solutions are $x_{\text{st}} = 1/2$ ($m = 0$), the absorbing states $x_{\text{st}} = 0, 1$ ($m = \pm 1$) or a degenerate continuum of solutions. The stability of these solutions can be understood in terms of the potential $V(x)$:

$$\begin{aligned} V(x) &= -\int (1-x)\,\theta(x-T) - x\,\theta(1-x-T)\,dx \\ &= \frac{x^2}{2} + \frac{1}{2}\left(T^2 - 2T - x^2 + 1\right)\,\theta(T+x-1) - \frac{1}{2}\left(T^2 - 2T - x(x-2)\right)\,\theta(x-T) \end{aligned} \tag{6A.2}$$

The minimum and maximum values of $V(x)$ correspond to stable and unstable solutions, respectively. Figure 6A.1b shows the potential's dependence on the magnetization, obtained after a variable change $m = 2x-1$ in Eq. (6A.2). For $T < 0.5$, $m = 0$ is a stable solution, but increasing the threshold reduces the range of values of the initial magnetization from which this solution is reached, enclosing Phase I between the unstable solutions $m = 1-2T$ and $2T-1$. In fact, if $m_0 > 1-2T$, the system reaches the absorbing solution $m = +1$, while if $m_0 < -1+2T$, it reaches $m = -1$ (Phase II). For $T = 0.5$, there is just one unstable solution at $m = 0$, and all the initial magnetization values reach the absorbing states $m = \pm 1$. For $T > 0.5$, the potential is equal to a constant value for a range of m_0, which means that an initial condition will remain in this state forever (Phase III). The range of values of the initial condition from which this phase is reached grows linearly with T until $T = 1$, where all initial conditions fulfill $\frac{dm}{dt} = 0$.

Note that the mean-field Symmetrical Threshold model for $T = 1$ shows the same potential profile as the mean-field Voter model (25, 102, 158). The important difference is that for the Voter model, any initial magnetization is marginally stable, while in our model any initial magnetization is an absorbing state in Phase III. In the Voter model finite size fluctuations will take the system to the absorbing states $m = \pm 1$.

6A.3.2 Random networks

We analyze the phase diagram of the Symmetrical Threshold model in two random networks: Erdős-Rényi (ER) (52) and random regular (RR) (170) graphs with mean degree $\langle k \rangle = 8$. Figures

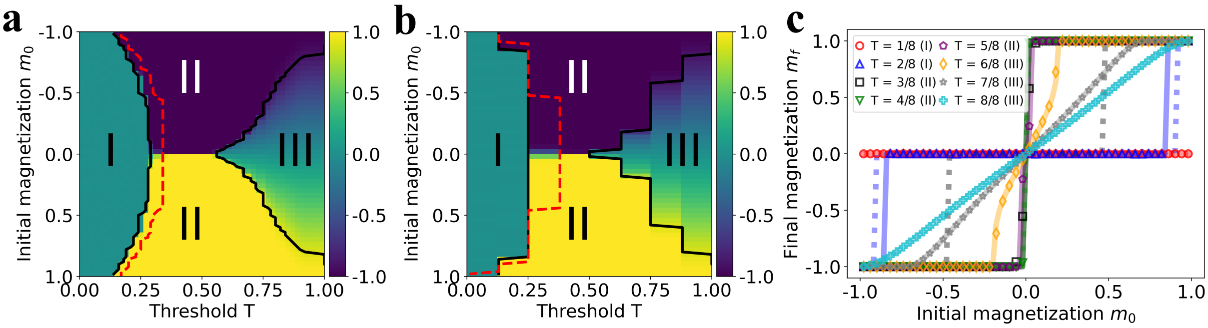

Figure 6A.2: Phase diagram of the Symmetrical Threshold model in an ER **(a)** and a RR **(b)** graph, both of $N = 4\cdot 10^4$ nodes and mean degree $\langle k\rangle = 8$. The color map indicates the value of the average final magnetization m_f. The red dashed line is the HMF prediction of the mixed-ordered critical line. The black solid lines correspond to the AME prediction of the borders of Phase II. **(c)** Average final magnetization m_f as a function of the initial magnetization m_0 for different T values (indicated with different colors and markers) in the RR graph. The average is performed over 5000 realizations. The dotted and solid lines are the HMF (for $T = 1/8 - 4/8$) and AME predictions (for all T), respectively.

6A.2a and 6A.2b show the phase diagram for both networks, where it is shown that the existence of the three phases previously described is robust to changes in network structure. The main difference from the all-to-all scenario is that Phase III does not freeze exactly at the same initial magnetization. Instead, the system reaches an absorbing state with a higher magnetization $m_f > m_0$. In this phase, the value of m_f depends on the threshold such that increasing T, increases the disorder in the system, until $T = 1$, where $m_f = m_0$ (see Fig. 6A.2c). On the other hand, phases I and II reach the same stationary state as in the mean-field case. Furthermore, the critical thresholds T_c and T_c^* show a different dependence on m_0 depending on the network structure. To explain the transitions exhibited by the model, we use the AME, described in detail in chapter 4, which considers agents in both states ± 1 with degree k, m neighbors in state -1 that have been j time steps in the current state (called "internal time" or "age") as different sets in a compartmental model. For the Symmetrical Threshold model, the dynamics are Markovian, since the rates do not depend on the internal time. Nevertheless, we keep this formalism to study the evolution of the mean internal time $\bar{\tau}(t)$, and to compare with the version with aging in the next chapter. According to the update rules of the model, the rates are defined as follows:

$$T^{+}_{k,m,j} = \theta(m/k - T) \qquad T^{-}_{k,m,j} = \theta((k-m)/k - T) \qquad A^{\pm}_{k,m,j} = 1 - T^{\pm}_{k,m,j} \qquad R^{\pm}_{k,m,j} = 0. \tag{6A.3}$$

Thus, the AME for the Symmetrical Threshold model is:

$$\begin{aligned}
\frac{d}{dt}x^{\pm}_{k,m,0}(t) &= -x^{\pm}_{k,m,0}(t) + \sum_{l} T^{\mp}_{k,m,l}\, x^{\mp}_{k,m,l}(t) - (k-m)\,\beta^{\pm}\, x^{\pm}_{k,m,0}(t) - m\,\gamma^{\pm}\, x^{\pm}_{k,m,0}(t), \\
\frac{d}{dt}x^{\pm}_{k,m,j}(t) &= -x^{\pm}_{k,m,j}(t) + A^{\pm}_{k,m,j}\, x^{\pm}_{k,m,j-1}(t) - (k-m)\,\beta^{\pm}\, x^{\pm}_{k,m,j}(t) + (k-m+1)\,\beta^{\pm}\, x^{\pm}_{k,m-1,j-1}(t) \\
&\quad + (m+1)\,\gamma^{\pm}\, x^{\pm}_{k,m+1,j-1}(t) - m\,\gamma^{\pm}\, x^{\pm}_{k,m,j}(t),
\end{aligned} \tag{6A.4}$$

where variables $x^{+}_{k,m,j}(t)$ and $x^{-}_{k,m,j}(t)$ are the fractions of k-degree nodes that are in state $+1$ (respectively, -1), have m neighbours in state -1, and have age j. The configuration-dependent rates $\beta^{\pm}$ account for the change of state of neighbors ($\pm$) of a node in state $+1$. The rates $\gamma^{\pm}$ are equivalent but for nodes in state -1. If we were not concerned with the internal time dynamics, we can simplify our AME to the one reduced Markovian binary-state models (see the reduction in the section 4.3).

The mixed-ordered and ordered-frozen transitions predicted (solid black lines in Figs. 6A.2a and 6A.2b, respectively) are in agreement with the numerical simulations. The predicted lines

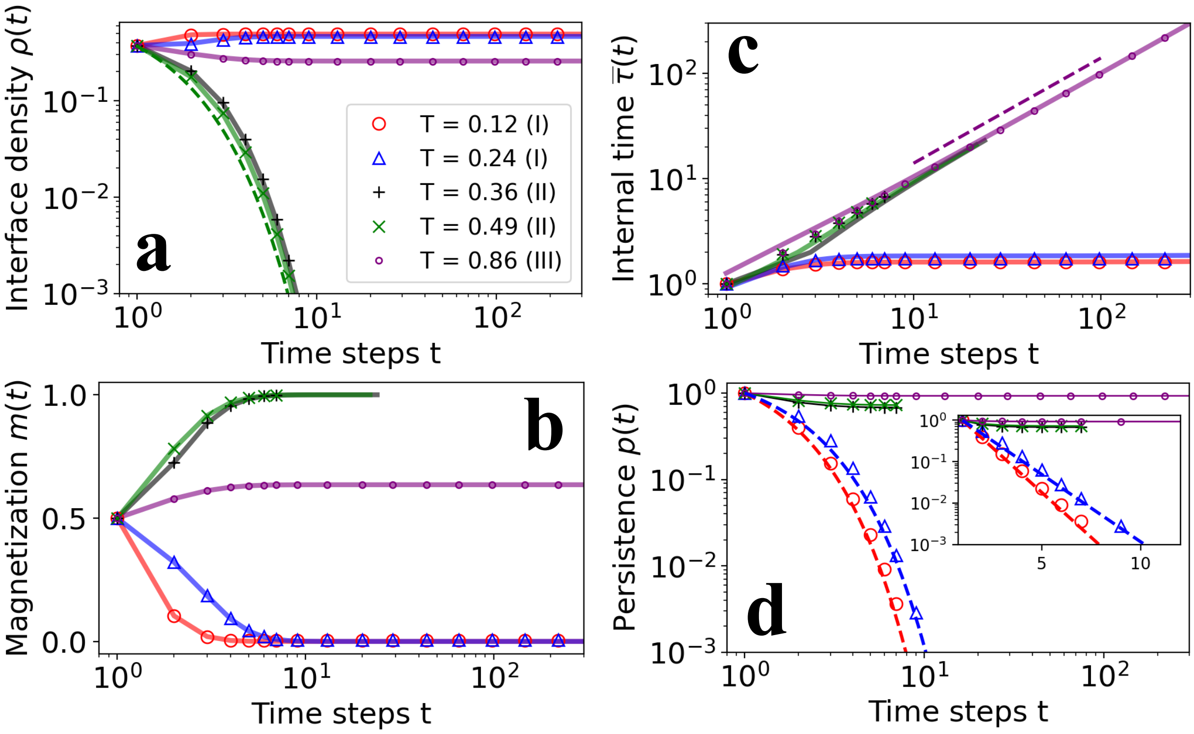

Figure 6A.3: Evolution of the average interface density $\rho(t)$ **(a)**, the average magnetization $m(t)$ **(b)**, the mean internal time $\bar{\tau}(t)$ **(c)**, and the persistence $p(t)$ **(d)** for the Symmetrical Threshold model. The average is computed over 5000 surviving trajectories (simulations stop when the system reaches the absorbing ordered states). Results for different values of T are plotted with diverse markers and colors: red ($T = 0.12$) and blue ($T = 0.24$) belong to Phase I, green ($T = 0.36$) and grey ($T = 0.49$) belong to Phase II and purple ($T = 0.86$) belongs to Phase III. Solid colored lines are the AME integrated solutions, using Eqs. (6A.5)-(6A.7). The initial magnetization is $m_0 = 0.5$. The system is on an ER graph with $N = 4 \cdot 10^4$ and mean degree $\langle k \rangle = 8$. The dashed green line in (a) shows $\rho(t) \sim \rho_0 e^{-t}$, the dashed purple line in (c) shows $\bar{\tau}(t) = t$ and the dashed lines in (d) show $p(t) \sim e^{-\alpha t}$, where $\alpha = 1$ (red) and $\alpha = 3/4$ (blue).

represent the initial and final values of T at which the AME reaches the ordered absorbing states $m_f = \pm 1$. In Fig. 6A.2c, we also observe a good agreement between numerically integrated solutions (solid colored lines) and numerical simulations (markers).

An alternative simpler approximation is to consider a heterogeneous mean-field approximation (HMF) (refer to section 4.4). This approximation is very useful when we work with networks with high clustering, close to the complete graph scenario ($\langle k \rangle / N \to 1$), a regime where the AME does not work properly because the clustering is not negligible. For our networks, HMF captures the qualitative behavior but the numerically integrated solutions do not agree with numerical simulations (see red dashed lines in Figs. 6A.2a and 6A.2b, and the colored dotted lines in Fig. 6A.2c), and the frozen phase is not predicted by this framework. These findings demonstrate that threshold models (in networks far from $\langle k \rangle / N = 1$) need approximations beyond mean-field to achieve accuracy (66, 67).

Beyond the stationary states, the previous phases can be characterized by their ordering dynamical regimes. To describe the coarsening process, we use the time-dependent average interface density $\rho(t)$ (fraction of links between nodes in different states), the average magnetization $m(t)$, the mean internal time $\bar{\tau}(t)$ (mean time spent in the current state over all the nodes) and the persistence $p(t)$ (fraction of nodes that remain in their initial state at time t) (16). Fig. 6A.3 shows the average results obtained from the numerical simulations, starting from an initial magnetization $m_0 = 0.5$. There are 3 regimes with different dynamical properties:

- **Mixed regime (Phase I in the static diagram):** It is characterized by fast disordering dynamics, which is reflected by an exponential decay of the persistence. The interface density, the magnetization, and the mean internal time exhibit fast dynamics towards their asymptotic values in the dynamically active stationary state (see $T = 0.12, 0.24$ in Fig. 6A.3);
- **Ordered regime (Phase II in the static diagram):** It is characterized by an exponential decay of the interface density. The magnetization tends to the ordered absorbing state based on the initial majority, and the mean internal time scales as $\bar{\tau}(t) \sim t$. Persistence in this phase decays until a plateau that corresponds to the initial majority that reaches consensus (since this fraction of nodes does not change state from the initial condition). When consensus is reached, the surviving trajectory is stopped (see $T = 0.36, 0.49$ in Fig. 6A.3);
- **Frozen regime (Phase III in the static diagram):** It is characterized by an initial ordering process followed by the stop of the dynamics, with constant values of the metrics. The only exceptions are the mean internal time that grows as $\bar{\tau}(t) \sim t$ (see $T = 0.86$ in Fig. 6A.3) and the persistence.

Using the numerically integrated solutions of AME ($x^{\pm}_{k,m,j}(t)$) from eq. 6A.4, we can compute the magnetization $m(t)$, the interface density $\rho(t)$, and the mean internal time $\bar{\tau}$:

$$\rho(t) = \frac{\sum_j \sum_k p_k \sum_m m x^{+}_{k,m,j}}{\frac{1}{2}\sum_j \sum_k p_k \sum_m k(x^{+}_{k,m,j} + x^{-}_{k,m,j})}, \tag{6A.5}$$

$$m(t) = 2\sum_j \sum_k p_k \sum_m x^{+}_{k,m,j} - 1 = -2\sum_j \sum_k p_k \sum_m x^{-}_{k,m,j} + 1, \tag{6A.6}$$

$$\bar{\tau}(t) = \sum_j \sum_k p_k \sum_m j\left(x^{+}_{k,m,j} + x^{-}_{k,m,j}\right), \tag{6A.7}$$

where p_k is the degree distribution of the network. All metrics exhibit a strong agreement between the numerical simulations and the integrated solutions (see solid lines in Fig. 6A.3). However, the persistence cannot be directly calculated from the integrated solutions. This is because the fraction of persistent nodes at time t corresponds to the fraction of nodes with internal time $j = t$, which is at an extreme of the age distribution at each time step, since $x^{\pm}_{k,m,j}(t) = 0$ for $j > t$. Therefore, the computation of this measure requires a more sophisticated analysis using extreme value theory (79).

We note that the dynamical characterization discussed above holds for all possible m_0 except for the symmetric initial condition $m_0 = 0$. In this case, an order-disorder transition arises at a critical mean degree k_c, whose value depends on the size of the system N (131).

6A.4 Results on a Moore Lattice

In this section, we consider the Symmetrical Threshold model in a Moore lattice, which is a regular 2-dimensional lattice with interactions among nearest and next-nearest neighbors ($k = 8$). From numerical simulations, we obtain a phase diagram (Fig. 6A.4a) that is consistent with our previous results in random networks. The system undergoes a mixed-ordered transition at a threshold value $T_c = 2/8$ which is independent of the value of the initial magnetization m_0. When $T > 4/8$, the system undergoes an ordered-frozen transition at a critical threshold T_c^*, which depends on m_0 (similarly to what happens in random networks). The final magnetization $m_f(m_0)$ (Fig. 6A.4b) also shows a dependence on m_0 similar to the one found in RR networks (Fig. 6A.2c).

Fig. 6A.5 shows the results from numerical simulations (for $m_0 = 0$ and 0.5) for the average interface density $\rho(t)$, the magnetization $m(t)$, and the persistence $(p(t))$ (the internal time shows the same results as in random graphs). Dynamical properties change significantly for different values of the threshold and initial magnetization m_0. Similarly to the case of random networks,

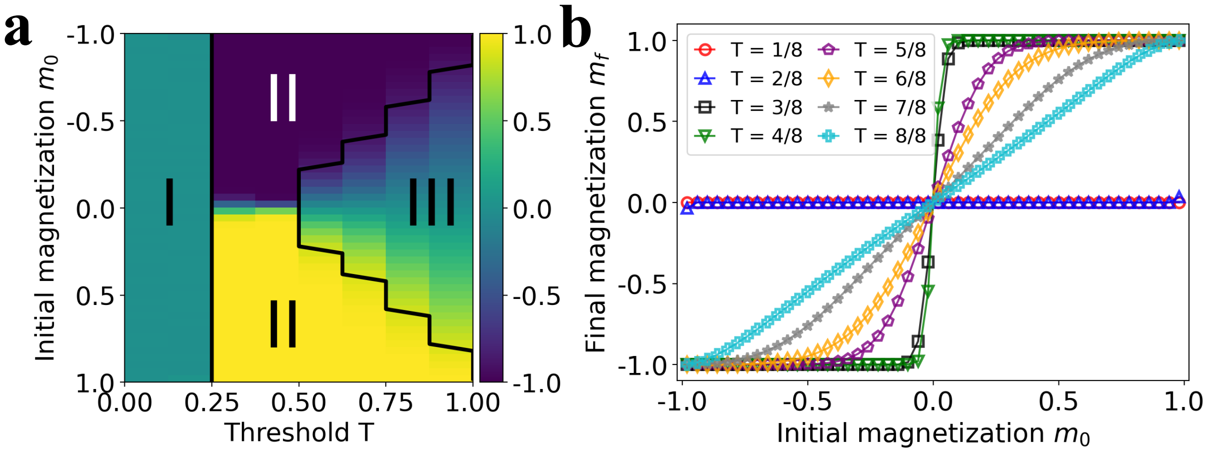

Figure 6A.4: **(a)** Phase diagram of the Symmetrical Threshold model in a Moore lattice of size $N = L \times L$, with $L = 100$. The color map indicates the value of the average final magnetization m_f. Solid black lines are the borders of Phase II (first and last value of T where the system reaches the absorbing ordered state for each m_0), computed from the numerical simulations. **(b)** Average final magnetization m_f as a function of the initial magnetization m_0 for the discrete values of the threshold T (indicated with different colors and markers) in a Moore lattice of the same size. Average performed over 5000 realizations.

we find three different regimes corresponding to the three phases, but with some properties different from the results on random networks:

- **Mixed regime (Phase I):** It is characterized by fast disordering dynamics with a persistence decay $p(t) \sim \exp(-\ln(t)^2)$, consistent with the results of the Voter model (16). The interface density and the magnetization exhibit fast dynamics towards their asymptotic values in the dynamically active stationary state (see $T = 1/8, 2/8$ in Fig. 6A.5);
- **Ordered regime (Phase II):** It is characterized by an exponential or power-law decay of the interface density, depending on the initial condition (see details below). The magnetization tends to the absorbing ordered state (see $T = 3/8, 4/8$ in Fig. 6A.5);
- **Frozen regime (Phase III):** It is characterized by an initial ordering process, but the system freezes fast (see $T = 5/8$ in Fig. 6A.5).

In particular, in Phase II for $m_0 = 0$ the persistence and interface density decay are found to decay as a power law, $p(t) \sim t^{-0.22}$ and $\rho(t) \sim t^{-1/2}$, respectively (consistent with the results of the Ising model (43, 44, 45, 154)). For a biased initial condition ($m_0 = 0.5$), $p(t)$ decays to the initial majority fraction (which corresponds to the state reaching consensus), and $\rho(t)$ follows an exponential-like decay. Note that, for $m_0 = 0$, not all trajectories reach the ordered absorbing states ($m_f = \pm 1$). There exist other absorbing configurations as, for example, a flat interface configuration for $T = 4/8$, no agent will be able to change, and the system remains trapped in this state. This result is not observed for $m_0 > 0$. Contrary, phases I and III show similar dynamics for balanced ($m_0 = 0$) and unbalanced ($m_0 = 0.5$) initial conditions. In Phase I, the system shows disordering dynamics with a persistence decay similar to the one exhibited for the Voter model in a lattice (16) while in Phase III, the system exhibited freezing dynamics with an initial tendency towards the majority consensus. Due to the lattice structure and high clustering, the mathematical tools employed in the previous sections for random networks are inapplicable to regular lattices. Consequently, we limit ourselves to the results of numerical simulations.

6A.5 Summary and discussion

In this chapter, we have studied with Monte Carlo numerical simulations and analytical calculations the phase diagram of the Symmetrical Threshold Model. In this model, the agents, nodes

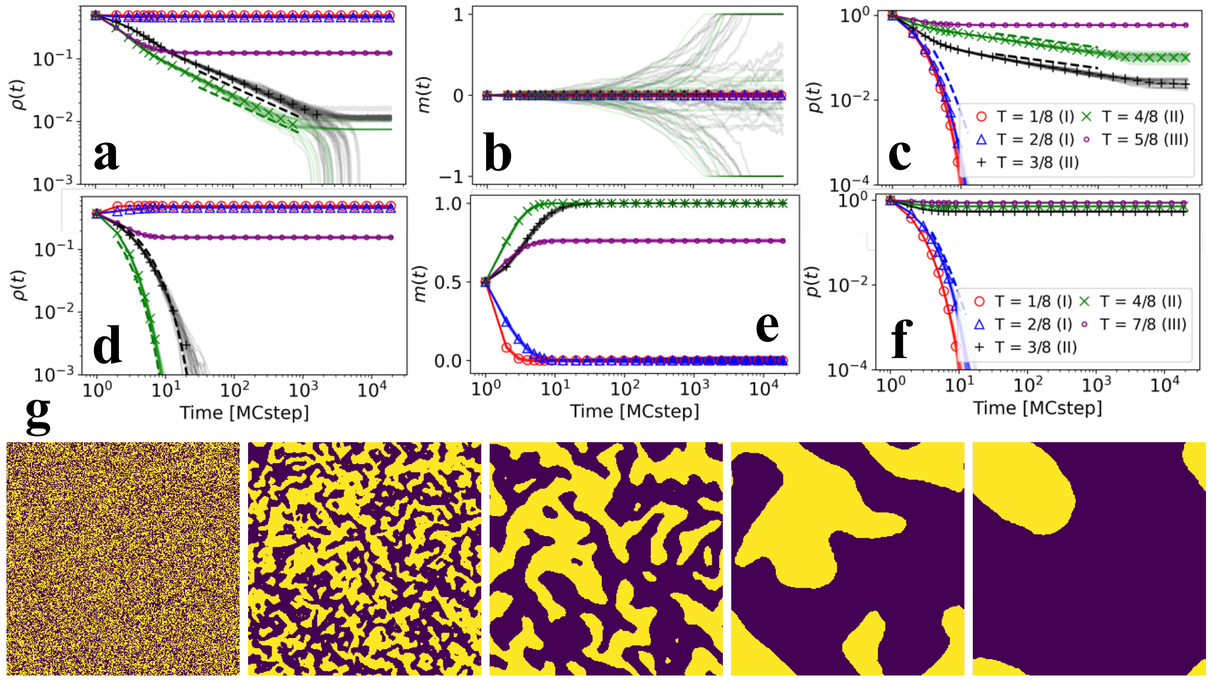

Figure 6A.5: Evolution of the average interface density $\rho(t)$ **(a-d)**, the average magnetization $m(t)$ **(b-e)**, and the persistence $p(t)$ **(c-f)** for the Symmetrical model in a Moore lattice starting from a random configuration with $m_0 = 0$ (a-b-c) and $m_0 = 0.5$ (d-e-f). We plot 50 different trajectories in solid lines and the average of 5000 surviving trajectories (simulations stop when the system reaches the absorbing ordered states) in different markers. Different colors and markers indicate different threshold values: red ($T = 1/8$) and blue ($T = 2/8$) belong to Phase I, green ($T = 3/8$) and black ($T = 4/8$) belong to Phase II, and purple ($T = 5/8, 7/8$) belong to Phase III. The average magnetization $m(t)$ is computed according to the two symmetric absorbing states. System size is fixed at $N = L \times L$, $L = 200$. The dashed lines in (a) are $\rho \sim \exp(-\alpha \cdot t)$ with $\alpha = 0.5$ (black) and $\alpha = 0.8$ (green), in (d) are $\rho(t) \sim at^{-1/2}$ with $a = 0.36$ (black) and $a = 0.2$ (green), in (c-f) are $p(t) \sim \exp(-\ln(t)^2)$ (blue) and $p(t) \sim c * t^{-0.22}$, with $b = 0.12$ (black) and $b = 0.56$ (green). **(g)** Evolution of a single realization for $T = 0.5$ and $m_0 = 0$ using the Symmetrical Threshold model. Snapshots are taken after $1, 10, 60, 440$ and 3300 time steps increasing from left to right. System size is fixed to $N = L \times L$, $L = 256$.

of a contact network, can be in one of the two symmetric states ± 1. System dynamics follows a complex contagion process in which a node changes state when the fraction of neighboring nodes in the opposite state is above a given threshold T. For $T = 1/2$, the model reduces to a majority rule or the zero temperature Spin Flip Kinetic Ising Model. When the change of state is only possible in one direction, say from 1 to -1, it reduces to the Threshold model (72, 167). We have considered the cases of a fully connected network, Erdős-Rényi, and random regular networks, as well as a regular two-dimensional Moore lattice.

We have found that, in the parameter space of threshold T and initial magnetization m_0, the model exhibits three distinct phases, namely Phase I or mixed, Phase II or ordered, and Phase III or frozen. The existence of these three phases is robust for different network structures. These phases are well characterized by the final state (m_f), and by dynamical properties such as the interface density $\rho(t)$, time-dependent average magnetization $m(t)$, persistence $p(t)$, and mean internal time $\bar{\tau}(t)$. These phases can be obtained analytically in the mean-field case of a fully connected network. For the random networks considered, we derive an approximate master equation (AME) (66) considering agents in each state according to their degree k, neighbors in state -1, m, and age j. From this AME, we have also derived a heterogeneous mean-field (HMF) approximation. While the AME reproduces with great accuracy the results of Monte Carlo numerical simulations of the model (both static and dynamic), the HMF shows an important lack of agreement, highlighting the importance of high-accuracy methods necessary for threshold models.

The model exhibits a rich dynamical behavior, with different regimes for the interface density, magnetization, and persistence. In the mixed phase, the system shows fast disordering dynamics, with an exponential decay of the persistence. In the ordered phase, the system exhibits an decay of the interface density, which can be exponential or power-law, depending on the initial condition and the topology. The magnetization tends to the ordered absorbing state, and the persistence decays to a plateau that corresponds to the initial majority that reaches consensus. In the frozen phase, the system shows an initial ordering process followed by the stop of the dynamics, with constant values of the metrics, except for the mean internal time that grows linearly with time.

Further research with the general AME used in this study would involve to incorporate finite size effects (124), which are relevant when m_0 is close to zero for ER graphs, and would provide a mathematical framework for further analyisis of the results in Ref. (131). Regarding the model, this chapter reports the main features of the Symmetrical Threshold model dynamics. However, there are several areas for future research along this lines, such as investigating the impact of strongly heterogeneous (12) or coevolving networks (163, 175).

6B. Symmetrical Threshold model: Aging implications

The results in this chapter are published as:

David Abella et al. "Ordering dynamics and aging in the symmetrical threshold model". In: *New Journal of Physics* 26.1 (Jan. 2024), page 013033. DOI: 10.1088/1367-2630/ad1ad4. URL: https://dx.doi.org/10.1088/1367-2630/ad1ad4

In this second part of chapter 6, we explore the effects of introducing aging in the Symmeytrical Threshold model, where agents become increasingly resistant to change their state the longer they remain in it. When aging is present, the mixed phase is replaced, for sparse networks, by a new phase with different dynamical properties. This new phase is characterized by an initial disordering stage followed by a slow ordering process towards a fully ordered absorbing state. In the ordered phase, aging modifies the dynamical properties. For random contact networks, we use a theoretical description based on the Approximate Master Equation that describes with good accuracy the results of numerical simulations for the model with and without aging. The aging implications in this model show similarities with the results in both the Granovetter-Watts model and the Sakoda-Schelling model.

6B.1 Introduction

As it was introduced in previous chapter, the Symmetrical Threshold model is a binary-state model where agents change their state if the fraction of neighbors in a different state exceeds a threshold T. The phase diagram of this model shows 3 different dynamical regimes: Phase I or mixed, Phase II or ordered and phase III or frozen. In the mixed phase, the system shows fast disordering dynamics, with an exponential decay of the persistence. In the ordered phase, the system exhibits an exponential decay of the interface density. The magnetization tends to the ordered absorbing state, and the persistence decays to a plateau that corresponds to the initial majority that reaches consensus. In the frozen phase, the system shows an initial ordering process followed by the stop of the dynamics, since the system gets trapped in a configuration where no threshold is exceeded.

In this chapter, we investigate the effects of aging in the Symmetrical threshold model. The model is examined in the same network topologies as in the previous chapter, complete graph, Erdős-Rényi (ER) (52), random regular (RR) (170), and a two-dimensional Moore lattice, such that we can compare the results with the version without aging. The possible phases of the system are defined by the final stationary state as well as by the ordering/disordering dynamics characterized by the time-dependent magnetization, interface density, persistence, and mean internal time, as in previous chapter for the original model. The results of Monte Carlo numerical simulations are compared with results from the Approximate Master Equation (AME). We also derive a heterogeneous mean-field framework to account for the effects of aging in a complete

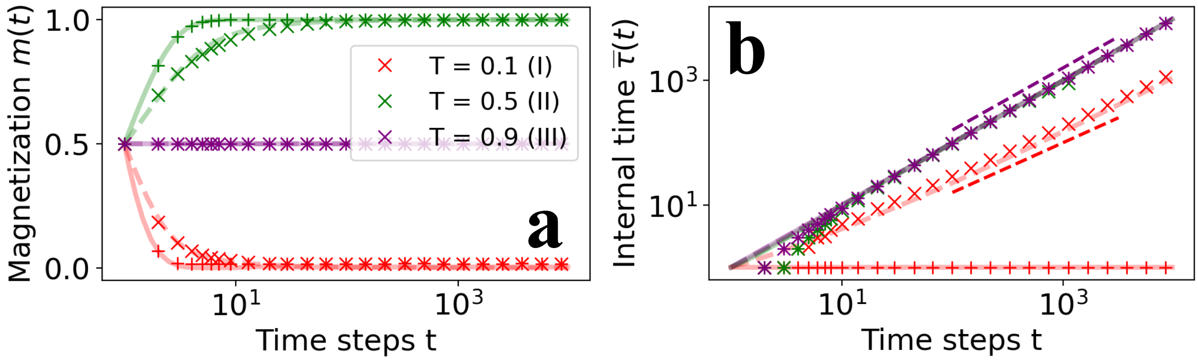

Figure 6B.1: Evolution of the average magnetization $m(t)$ **(a)** and the mean internal time $\bar{\tau}(t)$ **(b)** in a complete graph of $N = 2500$ nodes. Results are shown for the Symmetrical Threshold Model (pluses) and the version with aging (crosses) obtained from simulations. Different colors correspond to different values of the threshold T: red ($T = 0.1$) belongs to Phase I, green ($T = 0.5$) belongs to Phase II, and purple ($T = 0.9$) to Phase III. The initial magnetization is fixed at $m_0 = 0.5$. The solid and dashed lines correspond to the numerically integrated solutions from Eq. 6B.3 for the original model ($p_A(j) = 1$) and the version with aging ($p_A(j) = 1/(t+2)$), respectively. The dashed lines in (b) show $\bar{\tau}(t) = t$ (purple) and the solution from the recursive relation in Eq. (C.2) (red).

graph, where the AME cannot be used (does not fullfil the tree-like approximation).

6B.2 Symmetrical Threshold model with aging

In contrast to the original Symmetrical Threshold model, which assumes that agents update their state at a constant rate, the Symmetrical Threshold model with aging introduces an activation function $p_A(j)$ that is inversely proportional to the agent's internal time j. At each time step, the following two steps are performed:

1. A node i with age j is selected at random and activated with probability $p_A(j)$;
2. If the fraction of neighbors in a different state is greater than the threshold T, the activated node changes its state from s_i to $-s_i$ and resets its internal time to $j = 0$.

As in previous chapters in this thesis, we make the choice of $p_A(j) = 1/(j+2)$ for the aging probability. This particular choice is motivated by the fact that it allows to reproduce inter-event time distributions observed empirically (9, 136).

6B.3 Results on Complex networks

6B.3.1 Mean-field

Figure 6B.1 compares the evolution of the average magnetization and mean internal time on a complete graph of the original Symmetrical Threshold model and the version with aging in phases I, II, and III. We observe that, for all considered threshold values, aging introduces a delay. However, the final stationary magnetization coincides with the one observed for the original model. To explain these dynamics, we use a heterogeneous mean-field approach that considers the effects of aging (HMFA) (31). Notice that, for a complete graph, the AME cannot be used, as it does not fulfill the tree-like approximation $\langle k \rangle = N$. We derive here this formalism for heterogeneous degree networks, such that we can compare the results with the AME in the next section. For a general network with degree distribution p_k, we define the fraction of agents in state ± 1 with k neighbors and age j at time t as $x^{\pm}_{k,j}(t)$. The probability of finding a neighbor in state ± 1 is $\tilde{x}^{\pm}$, which can be written as

$$\tilde{x}^{\pm} = \sum_k p_k \frac{k}{\langle k \rangle} \sum_{j=0}^{\infty} x^{\pm}_{k,j}, \tag{6B.1}$$

where $\langle k \rangle$ is the mean degree of the network. The transition rate $\omega^{\pm}_{k,j}$ for a node with state ± 1, degree k and age j to change state is given by

$$\omega^{\pm}_{k,j} = p_A(j) \sum_{m=0}^{k} \theta\left(\frac{m}{k} - T\right) B_{k,m}[\tilde{x}^{\mp}], \tag{6B.2}$$

where $B_{k,m}[x]$ is the binomial distribution with k attempts, m successes, and with the probability of success x. In our model, there are two possible events for a node with degree k and age j:

- It changes state and the age is reset to $j = 0$;
- It remains at its state and the age increases by one time step $j = j + 1$.

According to these possible events, we can write the rate equations for the variables $x^{\pm}_{k,j}$ and $x^{\pm}_{k,0}$ as

$$\begin{aligned}
\frac{dx^{\pm}_{k,0}}{dt} &= \sum_{j=0}^{\infty} x^{\mp}_{k,j}\, \omega^{\mp}_{k,j} - x^{\pm}_{k,0}, \\
\frac{dx^{\pm}_{k,j}}{dt} &= x^{\pm}_{k,j-1}\,(1 - \omega^{\pm}_{k,j-1}) - x^{\pm}_{k,j} \qquad j > 0.
\end{aligned} \tag{6B.3}$$

It can be shown from Eq. (6B.3) that the stationary solution for the fraction of agents in state $+1$, x_f, obeys the following implicit equation for a complete graph (see Appendix B for a detailed explanation):

$$x_f = \frac{F(1-x_f)}{F(x_f) + F(1-x_f)}, \tag{6B.4}$$

where,

$$F(x) = 1 + \sum_{j=1}^{\infty} \prod_{a=0}^{j-1} \left(1 - p_A(a) \sum_{m=(N-1)T}^{N-1} B_{N-1,m}[x] \right). \tag{6B.5}$$

A solution of Eq. (6B.4) can be obtained numerically using standard methods. The final magnetization is calculated as $m_f = 2x_f - 1$. With this method, we obtain that the phase diagram for the model with aging is the same as for the model without aging (refer to Fig. 6A.1a). As a technical point, we note that a truncation of the summation of the variable j in Eq. (6B.5) is required for the numerical resolution of the implicit equation. The higher the maximum age considered $j_{\max}$, the higher the accuracy. With $j_{\max} = 5 \cdot 10^4$, the transition lines predicted by this mean-field approach show great accuracy. Moreover, by numerically integrating Eqs. (6B.3), the dynamical evolution of the magnetization and mean internal time can be obtained. Fig. 6B.1 shows the agreement between integrated solutions and Monte Carlo simulations of the system both for the aging and non-aging versions. It should be noted that, while aging introduces only a dynamical delay for the magnetization $m(t)$, the mean internal time $\bar{\tau}(t)$ in Phase I shows a different dynamical behavior with aging than in the original model (where $\bar{\tau}(t)$ fluctuates around an stationary value). In this phase, due to the low value of T, the agents selected randomly will change their state (as they fulfill the threshold condition) and reset their internal time. Consequently, while the internal time fluctuates around a stationary value for the original model, when aging is incorporated, due to the activation probability $p_A(j)$ chosen, the mean internal time increases following a recursive relation (Eq. (C.2)). We refer to Appendix C for a derivation of this result.

6B.3.2 Random networks

In contrast to the results obtained in a complete graph, aging effects have a significant impact on the phase diagram of the model on random networks. In Fig. 6B.2, we show the borders

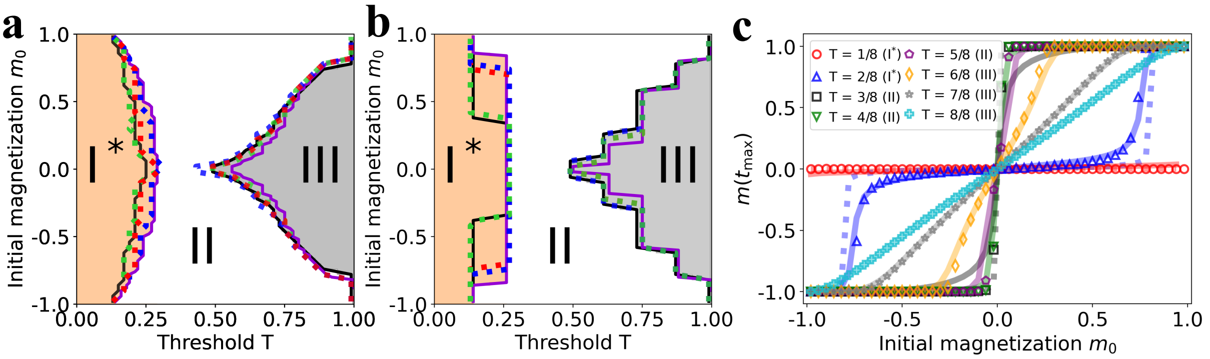

Figure 6B.2: Phase diagram of the Symmetrical Threshold with aging model in an ER **(a)** and RR **(b)** graph of $N = 4 \cdot 10^4$ nodes and $\langle k \rangle = 8$. The blue, red, and green dotted lines show the borders of Phase II (first and last value of T where the system reaches the absorbing ordered state for each m_0) computed from numerical simulations evolving until $t_{\max} = 10^3$, 10^4 and 10^5 time steps, respectively. Black solid lines show AME solution integrated 10^5 time steps. Phase I^*, II and III correspond with the orange, white and gray areas, respectively. The solid purple lines are the mixed-ordered and ordered-frozen critical lines for the non-aging version of the model. **(c)** Average magnetization at time $t_{\max}$ ($m(t_{\max})$) as a function of the initial magnetization m_0 for different values of the threshold T (indicated with different colors and markers) in an 8-regular graph of $N = 4 \cdot 10^4$. Average performed over 5000 realizations evolved until $t_{\max} = 10^4$ time steps. Dotted and solid lines are the HMFA (for $T = 1/8 - 4/8$) and AME (for all T) solutions integrated numerically 10^4 time steps.

of Phase II (first and last value of T where the system reaches the absorbing ordered state for each m_0) obtained from Monte Carlo simulations running up to a maximum time $t_{\max}$ (dotted colored lines). Reaching the stationary state in this model requires a large number of steps (with a corresponding high computational cost). The two borders of Phase II exhibit different behavior as we increase the time cutoff $t_{\max}$: while the ordered-frozen border does not change with different $t_{\max}$, the mixed-ordered border is shifted to lower values of T as we increase the time cutoff $t_{\max}$. Our results suggest that Phase I is actually replaced in a good part of the phase diagram by an ordered phase in which the absorbing state $m_f = \pm 1$ is reached after a large number of time steps. These results occur for both ER (Fig. 6B.2a) and RR (Fig. 6B.2b) graphs. The ordered-frozen border is now slightly shifted to lower values of the threshold T due to aging. Figure 6B.2c shows the average magnetization on RR graphs with simulations running up to a time $t_{\max} = 10^4$. Upon comparison with Figure 6A.2c, the dependence on m_0 is quite similar, indicating the persistence of a transient mixed phase. The dependence of the results with $t_{\max}$ calls for a characterization of different phases in terms of dynamical properties rather than by the asymptotic value of the magnetization.

Figure 6B.3 shows the time evolution of the average interface density $\rho(t)$, the average magnetization $m(t)$, the mean internal time $\bar{\tau}(t)$, and the persistence $p(t)$ for the Symmetrical Threshold model with aging in an ER graph. The dynamical properties are largely affected by the aging mechanism. In terms of the evolution, we find the following regimes:

- **Initial mixing regime (Phase I^*):** It is characterized by two dynamical transient regimes: a fast initial disordering dynamics followed by a slow ordering process. After the initial fast disordering stage, the average interface density exhibits a very slow (logarithmic-like) decay. Later, due to the finite size of the system, the average interface density follows a power law decay with time, where $\rho(t)$ scales as t^{-1}. This phase exists for the same domain of parameters (m_0, T) as Phase I (orange region in Fig. 6B.2) in the model without aging (see $T = 0.12, 0.24$ in Fig. 6B.3);
- **Ordered regime (Phase II):** According to the initial majority, the magnetization tends to the ordered absorbing state. This regime is characterized by a power-law interface decay, where $\rho(t)$ scales as t^{-1}. (see $T = 0.36, 0.49$ in Fig. 6B.3);

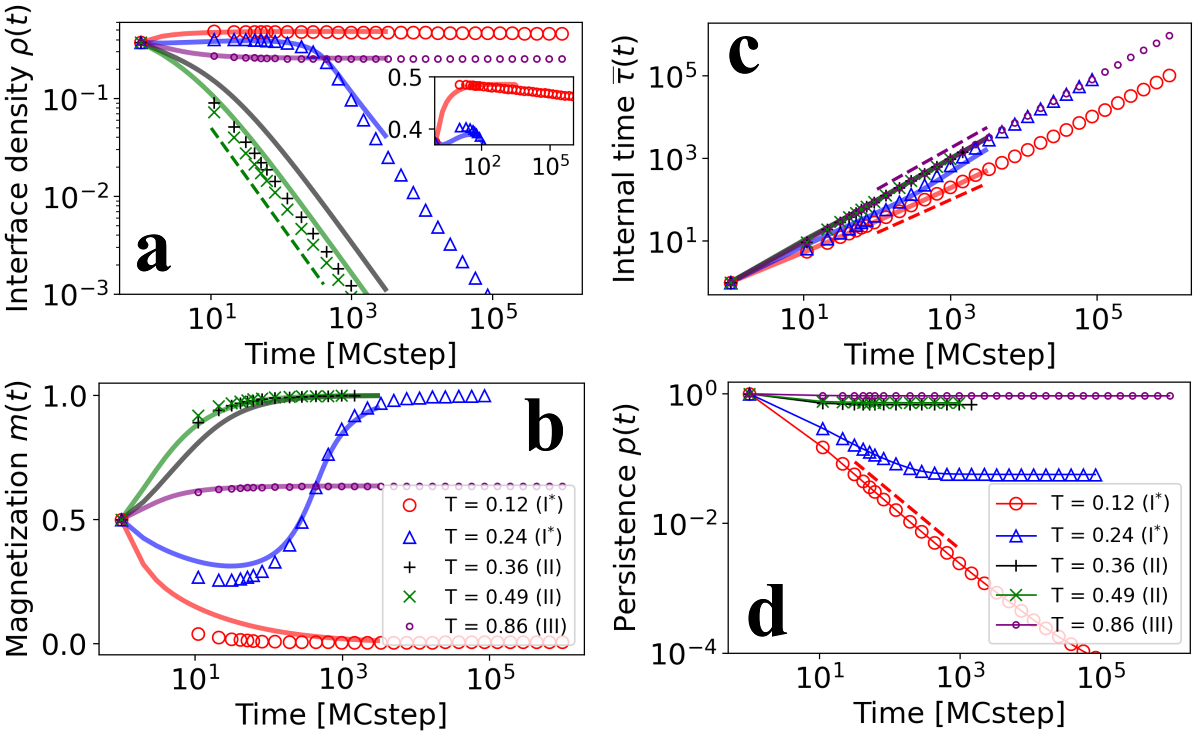

Figure 6B.3: Evolution of the average interface density $\rho(t)$ **(a)**, the average magnetization $m(t)$ **(b)**, the mean internal time $\bar{\tau}(t)$ **(c)** and the persistence $p(t)$ **(d)** for the Symmetrical Threshold model with aging. The average is computed over 5000 surviving trajectories (simulations stop when the system reaches the absorbing ordered states) for different values of T, shown by different markers and colors: red ($T = 0.12$) and blue ($T = 0.24$) belong to Phase I^*, green ($T = 0.36$) and grey ($T = 0.49$) belong to Phase II and purple ($T = 0.86$) belong to Phase III. The inset in (a) shows a close look to the evolution for $T = 0.12$, in linear-log scale. Solid colored lines are the AME integrated solutions for 10^4 time steps, using Eqs. 6A.5 - 6A.6. The initial magnetization is $m_0 = 0.5$. The system is on an ER graph with $N = 4 \cdot 10^4$ and mean degree $\langle k \rangle = 8$. The dashed green line in (a) shows $\rho(t) \sim \rho_0 t^{-1}$. The dashed lines in (c) $\bar{\tau}(t) = t$ (purple) and the solution from the recursive relation in Eq. (C.2) (red). The dashed red line in (d) shows $p(t) = t^{-1}$.

- **Frozen regime (Phase III):** Each individual realization is characterized by an initial tendency towards the majority consensus, but very fast reaches an absorbing frozen configuration (see $T = 0.86$ in Fig. 6B.3).

The main effect of aging is that the mixed states of Phase I are no longer present, at least not for the type of networks that we are analyzing here. We will show later that Phase I reemerges in denser graphs (consistently with the results in a complete graph). Instead, for sparse graphs, we observe a new Phase I^* in which the system initially disorders and later orders until reaching the absorbing states $m_f = \pm 1$. This behavior is shown in Fig. 6B.3 for $T = 0.12$ and 0.24. For $T = 0.12$, the system initially disorders, and then the interface density follows a logarithmic-like decay (see inset in Fig. 6B.3a). Due to the slow decay, the system stays in this transient regime even after 10^6 time steps, and the fall to the absorbing states is not observed in this figure. Similarly, for $T = 0.24$ the disordering process stops and then the system gradually evolves towards a fully ordered state. For this value of T, the logarithmic-like decay is not appreciated and we just observe the power-law decay due to the finite size of the system. The difference between $T = 0.12$ and $T = 0.24$ comes from the fact that in this Phase I^*, the interface decay becomes faster as we increase the threshold T (see Fig. 6B.4(c)). Notice the different interface decay in Fig. 6B.4c (inset) between values of $T < 0.3$ (Phase I^*), where all trajectories show a logarithmic-like decay of $\rho(t)$ in a transient regime, and $T \geq 0.3$ (Phase II), where trajectories from the initial condition

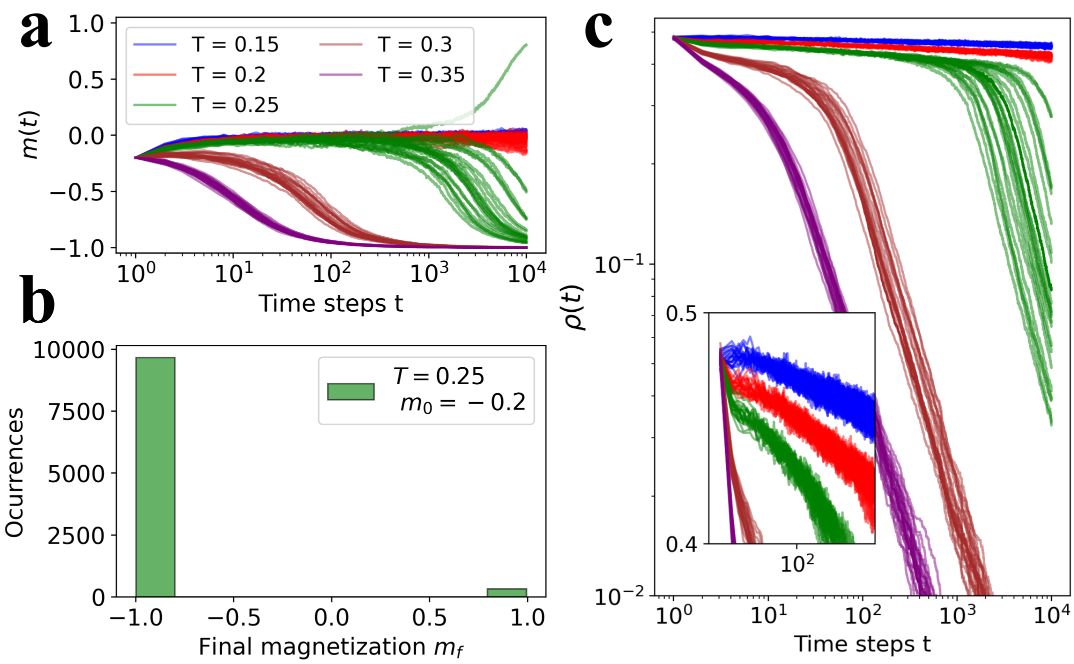

Figure 6B.4: Magnetization $m(t)$ **(a)** and interface density $\rho(t)$ **(c)** trajectories for different values of the threshold T ($m_0 = -0.2$) using the Symmetrical Threshold model with aging. **(b)** Final magnetization histogram of 1000 trajectories for the same system at $T = 0.25$. Different colors indicate different values of T. The inset at (b) shows a close look at the logarithmic-like decay, shown in linear-log scale. The system is an ER graph with $N = 4 \cdot 10^4$ and mean degree $\langle k \rangle = 8$.

exhibit fast ordering dynamics towards the majority consensus. Moreover, we observe that in Phase I^*, the initial magnetization m_0 introduces a bias to the stochastic process, implying that the larger m_0 in absolute value, the larger the number of realizations that reach the absorbing state with the same sign of m_0. However, the system can still reach the absorbing state of the opposite sign of m_0 (initial minority), as shown in the trajectories with $T = 0.25$ in Fig. 6B.4a. Due to the characteristic logarithmic decay of Phase I^*, a statistical analysis of the inversion process incurs a significant computational cost. In Fig. 6B.4b, we present the final magnetization histogram for $T = 0.25$, a value proximal to the $\mathrm{I}^* - \mathrm{II}$ boundary where this analysis is computationally feasible. As depicted in this figure, the proportion of realizations in which consensus is reached in the initial minority state is approximately 3.3%. Fig. 6B.3(c-d) shows the evolution of the temporal dynamics via the mean internal time and the persistence. The persistence in Phase I^* shows a power-law decay, where $p(t)$ scales as t^{-1}, and the internal time shows an increase following the recursive relation given in Appendix C, as it occurred for the mean-field scenario (Fig. 6B.1).

In Phase II, the system asymptotically orders for any initial condition as in the original model, but the dynamical properties are modified due to the presence of aging: the exponential decay of the interface density is replaced by a slow power-law decay, where the exponents of the exponential and the power-law are found to be similar. Contrary, the dynamical properties of Phase III are not affected by the presence of aging.

As it occurred for the non-aging version of the model, the dynamical characterization discussed above holds for all possible m_0 except for the symmetric initial condition $m_0 = 0$. The implications of the order-disorder transition (that occurs at a critical mean degree $k_c(N)$) (131) are still present in the model with aging. Moreover, as it ocurred for the Symmetrical Threshold model, the persistence cannot be predicted by this framework.

To account for the results of our Monte Carlo simulations, we use the same mathematical framework as described in Equation (6A.4). According to the update rules of the Symmetrical Threshold Model with aging, the transition probabilities now depend on the age j, as given by

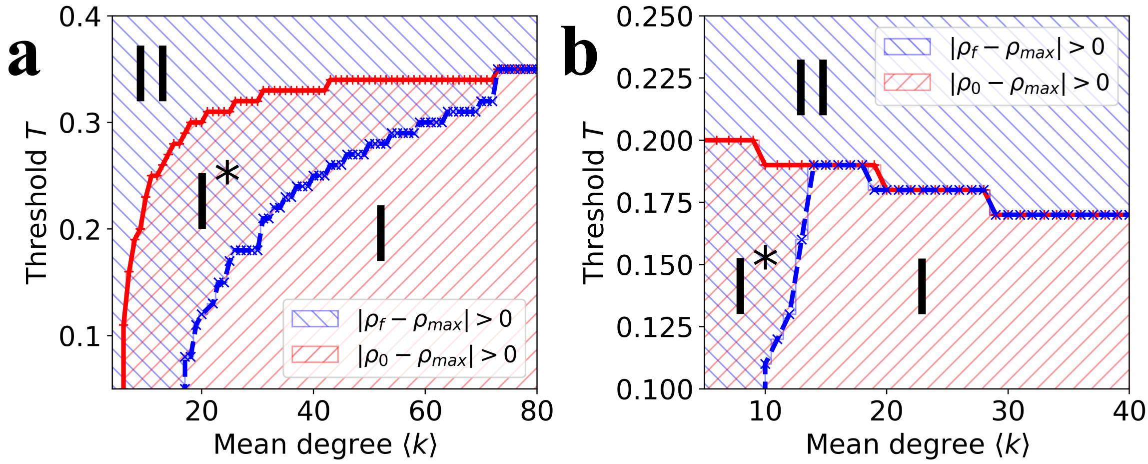

Figure 6B.5: Critical threshold T_c dependence with the mean degree $\langle k \rangle$ for the Symmetrical Threshold model with aging for an ER graph with $N = 4 \times 10^4$ nodes for an initial magnetization of $m_0 = 0.25$ **(a)** and $m_0 = 0.75$ **(b)**. The blue and red markers indicate the borders of phases I and II, which coincide for a sufficiently large value of the mean degree. The hatched area corresponds to the fulfillment of the inequality in the legend.

the activation probability $p_A(j)$:

$$T^{+}_{k,m,j} = p_A(j)\,\theta(m/k - T) \qquad T^{-}_{k,m,j} = p_A(j)\,\theta((k-m)/k - T) \qquad A^{\pm}_{k,m,j} = 1 - T^{\pm}_{k,m,j}. \tag{6B.6}$$

We show in Figure 6B.2 the mixed-ordered and ordered-frozen transition lines predicted by the integration of the AME equations until a time cutoff $t_{\max}$. We find good agreement between the theoretical predictions and the simulations both for ER and RR networks. Regarding dynamical properties, the AME integrated solutions exhibit a remarkable concordance with the evolution of all the metrics as shown in Figure 6B.3. Minor discrepancies between the numerical simulations and the integrated solutions are attributed to the different assumptions, discussed previously, on which the AME is based.

The numerical results discussed so far are for random networks with average degree $\langle k \rangle = 8$. According to them and to the analytical insights, one can conclude that aging significantly changes the phase diagram for sparse networks. However, we know that the model with aging shows the same phase diagram as the model without aging for a fully connected network. This implies that, for ER graphs, as the mean degree $\langle k \rangle$ approaches N, Phase I^* must disappear. Therefore, the combined effects of increasing the mean degree and introducing aging need to be investigated in more detail. Phase II is distinguishable from phases I and I^* because the system initially orders, i.e., $|\rho_0 - \rho_{\max}| = 0$, where $\rho_{\max}$ is the maximum value attained by the interface density during the dynamical evolution. In contrast, Phase I is distinguished from Phases I^* and II because the system remains disordered, i.e., $|\rho_{\max} - \rho(t_{\max})| \approx 0$. Thus, Phase I^* is the only phase among these three where $|\rho_0 - \rho_{\max}| > 0$ and $|\rho_{\max} - \rho(t_{\max})| > 0$. Using this criterion, we studied the dependence of the critical threshold T_c on the mean network degree defining the transition lines between phases I, I^*, and II (see Fig. 6B.5). In the absence of aging, the red line in Fig. 6B.5 gives the value of the mixed-ordered transition line T_c. When aging is included, at low degree values, Phase I is replaced by I^*, as expected. However, as the mean degree increases, Phase I emerges despite the presence of aging, leading to the range of mean degree values where the model exhibit 4 different phases: I, I^*, II and III. As the mean degree is further increased, a critical value is reached where Phase I^* is no longer present, and the discontinuous transition I-II occurs at the same value than in the model without aging. Importantly, this critical mean degree at which Phase I^* disappears, depends significantly on the initial magnetization m_0.

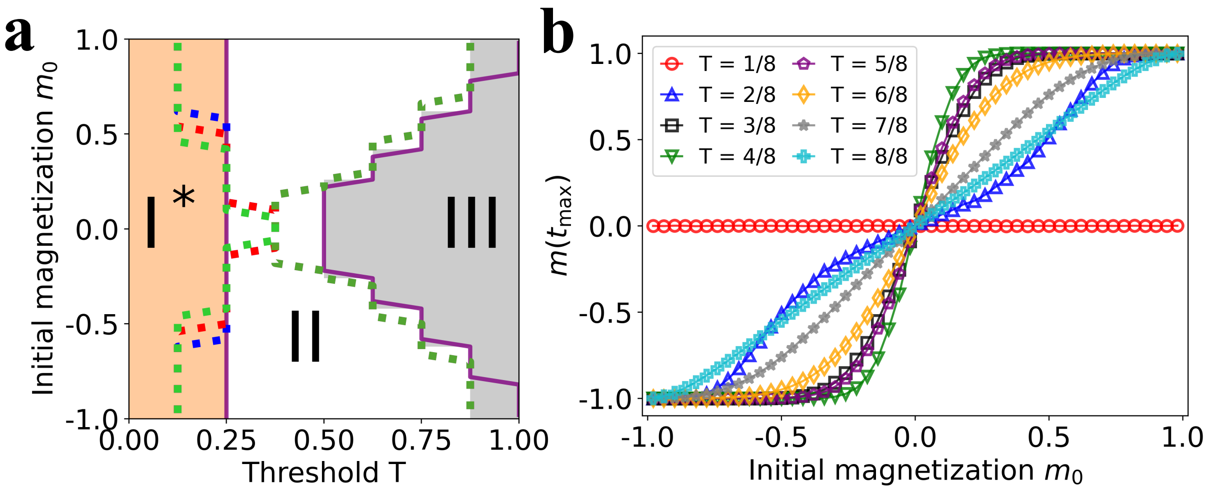

Figure 6B.6: **(a)** Phase diagram of the Symmetrical Threshold model with aging in a Moore lattice of $N = L \times L$, with $L = 100$. The blue, red and green dotted lines show the borders of Phase II (first and last value of T where the system reaches the absorbing ordered state for each m_0) from numerical simulations evolving until $t_{\max} = 10^3$, 10^4 and 10^5 time steps, respectively. Phase I*, II and III correspond with the orange, white and gray areas, respectively. The solid purple lines are the mixed-ordered and ordered-frozen critical lines for the Symmetrical threshold model (from Fig. 6A.4). **(b)** Average magnetization at time $t_{\max}$ ($m_f(t_{\max})$) as a function of the initial magnetization m_0 for different values of the threshold T (indicated with different colors and markers) in a Moore lattice of $N = L \times L$, with $L = 100$. The numerical simulations are obtained until $t_{\max} = 10^4$ time steps. Average performed over 5000 realizations.

6B.4 Results on a Moore Lattice

We show in Figure 6B.6a the borders of Phase II obtained from numerical simulations of the Symmetrical threshold model with aging running up to a time $t_{\max}$ (dotted colored lines) in a Moore lattice. Similarly to the behavior observed in random networks, the mixed-ordered border is shifted to lower values of T as we increase the simulation time cutoff $t_{\max}$. Thus, Phase I is replaced by an ordered phase due to the aging mechanism. Examining the dependence of the final value of the magnetization on its initial condition $m_f(m_0)$ (Figure 6B.6b), one can conclude that the mixed phase is still present, at least transiently, as in the initial disordering phase described in the previous section (Phase I*). Phase II is again characterized by an asymptotically ordered state where the initial majority reaches consensus. However, for this specific structure, near $m_0 = 0$ and $T = 1/2$, the ordered state is not reached for any threshold value. Furthermore, comparing with Fig. 6B.6b with the results from the model without aging (Fig. 6A.4b), the discontinuous jump at $m_0 = 0$ for $T = 3/8, 4/8$ is replaced by a continuous transition, where a range of states with $0 < |m_f| < 1$ are present around $m_0 = 0$. To determine whether these states belong to Phase I*, II or III, we need again a characterization of phases in terms of dynamical properties. According to the results in Figure 6B.7, we find here the same regimes identified for random networks:

- **Initial mixing regime (Phase I*):** After the initial disordering stage, the average interface density shows a very slow decay reflecting the slow growth of spatial domains in each binary state. The persistence in this phase shows a power-law decay $p(t) \sim t^{-1}$ (see $T = 1/8, 2/8$ in Fig. 6B.7);
- **Ordered regime (Phase II):** It is characterized by coarsening dynamics that end in the absorbing states $m_f = \pm 1$. The form of the decay of the interface density depends on the value of m_0 (see $T = 3/8, 4/8$ in Fig. 6B.7);
- **Frozen regime (Phase III):** It is characterized by an initial tendency to order but the system very fast reaches an absorbing frozen configuration (see $T = 5/8, 7/8$ in Fig. 6B.7).

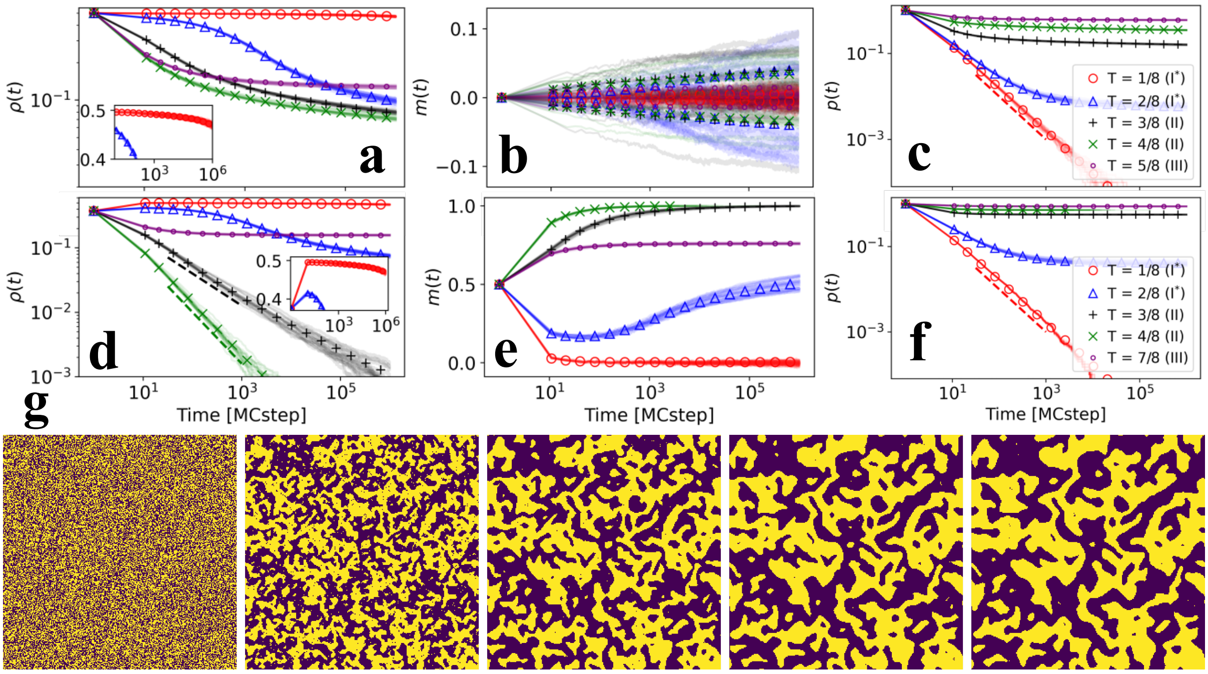

Figure 6B.7: Evolution of the average interface density $\rho(t)$ **(a-d)**, the average magnetization $m(t)$ **(b-e)**, and the persistence $p(t)$ **(c-f)** for the Symmetrical model with aging in a Moore lattice starting from a random configuration with $m_0 = 0$ (a-b-c) and $m_0 = 0.5$ (d-e-f). We plot 30 different trajectories in solid lines and the average of over 5000 surviving trajectories in symbols. Colors and symbols indicate different threshold values: red ($T = 1/8$) and blue ($T = 2/8$) belong to Phase I^*, green ($T = 3/8$), and black ($T = 4/8$) belong to Phase II, and purple ($T = 5/8, 7/8$) belong to Phase III. The average magnetization is computed according to the two symmetric absorbing states. The insets in (a-d) show a close look at the evolution for $T = 0.12$, in linear-log scale. System size is fixed at $N = L \times L$, $L = 200$. The dashed lines in (d) are $\rho \sim t^{-\alpha}$ with $\alpha = 0.5$ (black) and $\alpha = 0.8$ (green), and in (c-f) are $p(t) \sim t^{-1}$ (red). Simulations stop when the system reaches the absorbing ordered states. **(g)** Evolution of a single realization for $T = 0.5$ and $m_0 = 0$ using the Symmetrical threshold model with aging. Snapshots are taken after $1, 60, 3300, 2 \cdot 10^5$ and $5 \cdot 10^6$ time steps, increasing from left to right. System size is fixed to $N = L \times L$, $L = 256$.

The implications of aging become explicit by comparing the dynamical properties of the cases with aging (Figure 6B.7) and without aging (Figure 6A.5). When the threshold is $T < 3/8$, Phase I is replaced by Phase I^* in which there is an initial disordering process very fast followed by a slow coarsening process that accelerates when we increase the threshold. Although the aging implications in this phase are similar to those observed in the ER graph, the coarsening process is much slower in a Moore lattice (see insets in Fig. 6B.7a-d).

In Phase II ($T = 3/8, 4/8$) and when $m_0 = 0.5$, the system exhibits coarsening towards the ordered state $m_f = \pm 1$. In this case, the interface decay $\rho \sim \exp(-\alpha t)$, observed in the absence of aging is replaced, due to aging, by a power law decay $\rho \sim t^{-\alpha}$, as it ocurred in chapter 5 for the endogenous aging. We find $\alpha = 0.5$ and 0.8 for $T = 3/8$ and $4/8$, respectively. For $m_0 = 0$, the power law decay of the interface density vanishes with aging, and the system exhibits coarsening dynamics much slower than for an unbalanced initial condition. In this region of the phase diagram, spatial clusters start to grow from the initial condition, but once formed, it takes a long time for the system to reach the absorbing state $m_f = \pm 1$. We note that for these parameter values, the system is not able to reach $|m|$ over 0.1 even after 10^6 time steps, but since there is coarsening from the initial condition, the expected stationary state as $t \to \infty$ is $m_f = \pm 1$. There is neither initial disordering nor freezing, these values correspond to the defined Phase II, even though the system exhibits "long-lived segregation" long transient dynamics (compare the coarsening process in Fig.6A.5g with Fig.6B.7g). In Fig. 6B.6a, we differentiate Phase II from Phase

III by analyzing the activity in the system: If agents are changing, even though the interface decay is slow, the system is in Phase II. If agents are frozen, it lies in Phase III.

Finally, it should be noted that in Phase I^*, the initial disordering dynamics drive the system towards $m = 0$. Therefore, the subsequent coarsening dynamics follow the slow interface decay observed in Phase II for $m_0 \sim 0$. Thus, the presence of aging implies that the system asymptotically orders for any initial condition, but due to the initial disordering, the coarsening dynamics fall into the "long-lived segregation" regime independently of the initial condition.

6B.5 Summary and discussion

In this chapter, aging is incorporated in the model as a decreasing probability to modify the state as the time already spent by the agent in that state increases. The key finding is that the mixed phase (Phase I), characterized by an asymptotically disordered dynamically active state, does not always exist: the aging mechanism can drive the system to an asymptotic absorbing ordered state, regardless of how low the threshold T is set. A similar effect of aging was already described for the Sakoda-Schelling model in chapter 3. When the dynamics are examined in detail, a new Phase I^*, defined in terms of dynamical properties, emerges in the domain of parameters where the model without aging displays Phase I. This phase is characterized by an initial disordering regime ($m \to 0$) followed by a slow ordering dynamics, driving the system toward the ordered absorbing states (including the one with spins opposite to the majoritarian initial option). This result is counter-intuitive since aging incorporates memory into the system, yet in this phase, the system "forgets" its initial state. The network structure plays an important role in the emergence of Phase I^* since it does not exist for complete graphs. A detailed analysis reveals that Phase I^* replaces Phase I only for sparse networks, including the case of the Moore lattice. For ER networks we find that, as the mean degree increases, Phase I reappears and there is a range of values of the mean degree for which both phases, I and I^*, are present in the same phase diagram for different values of (m_0, T). Beyond a critical value of the mean degree, Phase I extends over the entire domain of parameters where Phase I^* was observed.

While aging favors reaching an asymptotic absorbing ordered state for low values of T (Phase I), in Phase II the ordering dynamics are slowed down by aging, changing, both in random networks and in the Moore lattice, the exponential decay of the interface density by a power law decay with the same exponent. The aging mechanism is found not to be important in the frozen Phase III. All these effects of aging in the three phases are well reproduced for random networks by the AME derived in this work, which is general for any chosen activation probability $p_A(j)$.

For the Moore lattice, we have also considered in detail the special case of the initial condition $m_0 = 0$. In this case, Phase I^* emerges, and Phase III is robust against aging effects. However, in Phase II aging destroys the characteristic power law decay of the interface density, $\rho(t) \sim at^{-1/2}$, associated with curvature reduction of domain walls. This would be a main effect of aging in the dynamics of the phase transition for the zero temperature spin flip Kinetic Ising model (78).

As a final remark on the general effects of aging in different models of collective behavior, we note that the replacement of a dynamically active disordered stationary phase by a dynamically ordering phase is generic. In this chaptrer, we find the replacement of Phase I by Phase I^*. Likewise in the Voter model, aging destroys long-lived dynamically active states characterized by a constant value of the average interface density, and it gives rise to coarsening dynamics with a power law decay of the average interface density (53). In the same way, in the Sakoda-Schelling segregation model, a dynamically active mixed phase is replaced, due to the aging effect, by an ordering phase with segregation in two main clusters (refer to chapter 3). Another aging effect that seems generic, in phases in which the system orders when there is no aging, is the replacement of dynamical exponential laws by power laws. This is what happens here in Phase II for the decay of the average interface density but, likewise, exponential cascades in the

Granovetter-Watts threshold model are replaced due to aging by a power-law growth with the same exponent (refer to chapter 5).

II Real estate market dynamics

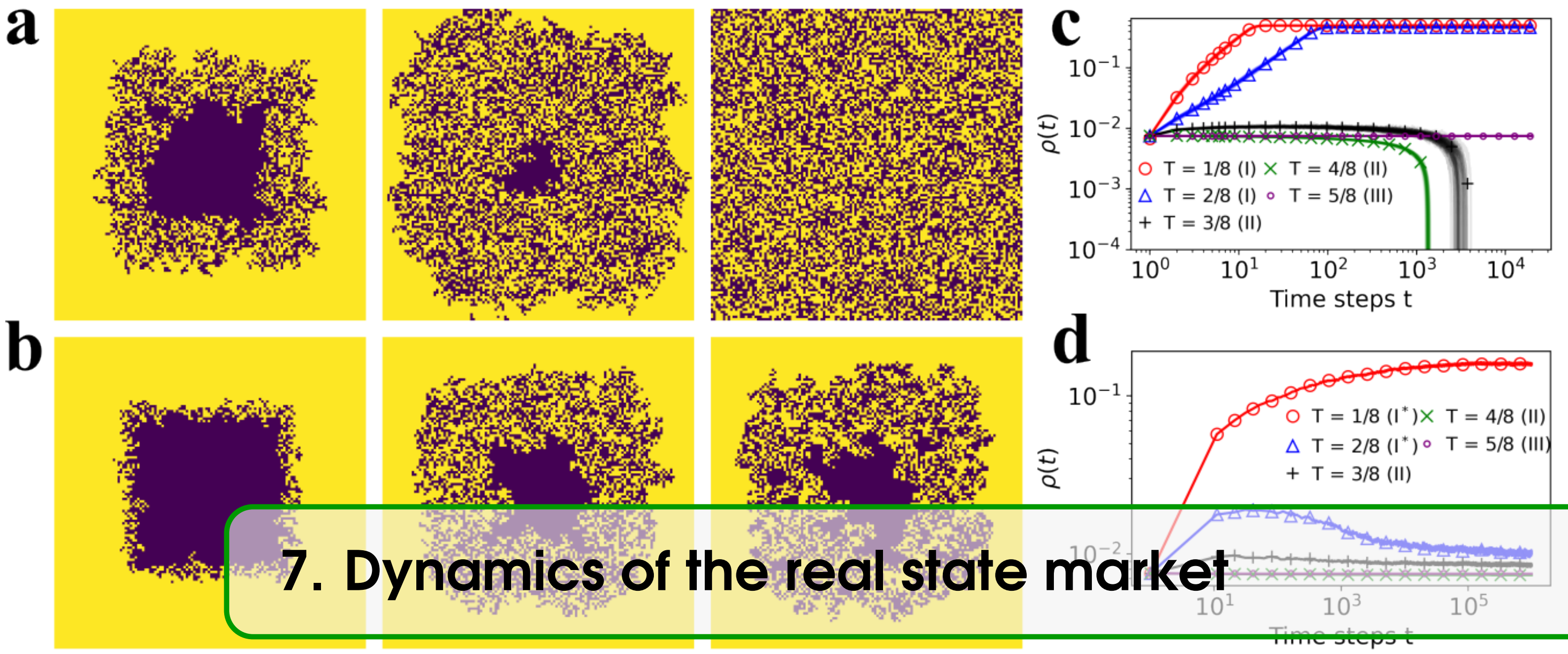

7. Dynamics of the real state market

The results in this chapter are published as:

David Abella et al. "Ordering dynamics and aging in the symmetrical threshold model". In: *New Journal of Physics* 26.1 (Jan. 2024), page 013033. DOI: 10.1088/1367-2630/ad1ad4. URL: https://dx.doi.org/10.1088/1367-2630/ad1ad4

7.1 Theorems

7.1.1 Several equations

This is a theorem consisting of several equations.

Update rules — Name of the theorem. In $E = \mathbb{R}^n$ all norms are equivalent. It has the properties:

$$\big| ||\mathbf{x}|| - ||\mathbf{y}|| \big| \leq ||\mathbf{x} - \mathbf{y}|| \tag{7.1}$$

$$|| \sum_{i=1}^{n} \mathbf{x}_i || \leq \sum_{i=1}^{n} ||\mathbf{x}_i|| \quad \text{where } n \text{ is a finite integer} \tag{7.2}$$

7.1.2 Single Line

This is a theorem consisting of just one line.

Update rules A set $\mathscr{D}(G)$ in dense in $L^2(G)$, $|\cdot|_0$.

7.2 Definitions

A definition can be mathematical or it could define a concept.

Definition 7.1 — Definition name. Given a vector space E, a norm on E is an application, denoted $||\cdot||$, E in $\mathbb{R}^+ = [0, +\infty[$ such that:

$$||\mathbf{x}|| = 0 \ \Rightarrow \ \mathbf{x} = \mathbf{0} \tag{7.3}$$

$$||\lambda \mathbf{x}|| = |\lambda| \cdot ||\mathbf{x}|| \tag{7.4}$$

$$||\mathbf{x} + \mathbf{y}|| \leq ||\mathbf{x}|| + ||\mathbf{y}|| \tag{7.5}$$

7.3 Notations

▪ **Notation 7.1** Given an open subset G of $\mathbb{R}^n$, the set of functions φ are:

1. Bounded support G;

2. Infinitely differentiable;

a vector space is denoted by $\mathscr{D}(G)$.

7.4 Remarks

This is an example of a remark.

R The concepts presented here are now in conventional employment in mathematics. Vector spaces are taken over the field $\mathbb{K} = \mathbb{R}$, however, established properties are easily extended to $\mathbb{K} = \mathbb{C}$.

7.5 Corollaries

Corollary 7.1 — Corollary name. The concepts presented here are now in conventional employment in mathematics. Vector spaces are taken over the field $\mathbb{K} = \mathbb{R}$, however, established properties are easily extended to $\mathbb{K} = \mathbb{C}$.

7.6 Propositions

7.6.1 Several equations

Proposition 7.1 — Proposition name. It has the properties:

$$\big| ||\mathbf{x}|| - ||\mathbf{y}|| \big| \leq ||\mathbf{x} - \mathbf{y}|| \tag{7.6}$$

$$|| \sum_{i=1}^{n} \mathbf{x}_i || \leq \sum_{i=1}^{n} ||\mathbf{x}_i|| \quad \text{where } n \text{ is a finite integer} \tag{7.7}$$

7.6.2 Single Line

Proposition 7.2 Let $f, g \in L^2(G)$; if $\forall \varphi \in \mathscr{D}(G)$, $(f, \varphi)_0 = (g, \varphi)_0$ then $f = g$.

7.7 Examples

7.7.1 Equation Example

■ **Example 7.1** Let $G = \{x \in \mathbb{R}^2 : |x| < 3\}$ and denoted by: $x^0 = (1, 1)$; consider the function:

$$f(x) = \begin{cases} \mathrm{e}^{|x|} & \text{si } |x - x^0| \leq 1/2 \\ 0 & \text{si } |x - x^0| > 1/2 \end{cases} \tag{7.8}$$

The function f has bounded support, we can take $A = \{x \in \mathbb{R}^2 : |x - x^0| \leq 1/2 + \varepsilon\}$ for all $\varepsilon \in]0; 5/2 - \sqrt{2}[$. ■

7.7.2 Text Example

■ **Example 7.2 — Example name.** Aliquam arcu turpis, ultrices sed luctus ac, vehicula id metus. Morbi eu feugiat velit, et tempus augue. Proin ac mattis tortor. Donec tincidunt, ante rhoncus luctus semper, arcu lorem lobortis justo, nec convallis ante quam quis lectus. Aenean tincidunt sodales massa, et hendrerit tellus mattis ac. Sed non pretium nibh. Donec cursus maximus luctus. Vivamus lobortis eros et massa porta porttitor. ■

7.8 Exercises

Exercise 7.1 This is a good place to ask a question to test learning progress or further cement ideas into students' minds. ■

7.9 Problems

Problem 7.1 What is the average airspeed velocity of an unladen swallow?

7.10 Vocabulary

Define a word to improve a students' vocabulary.

- **Vocabulary 7.1 — Word.** Definition of word.

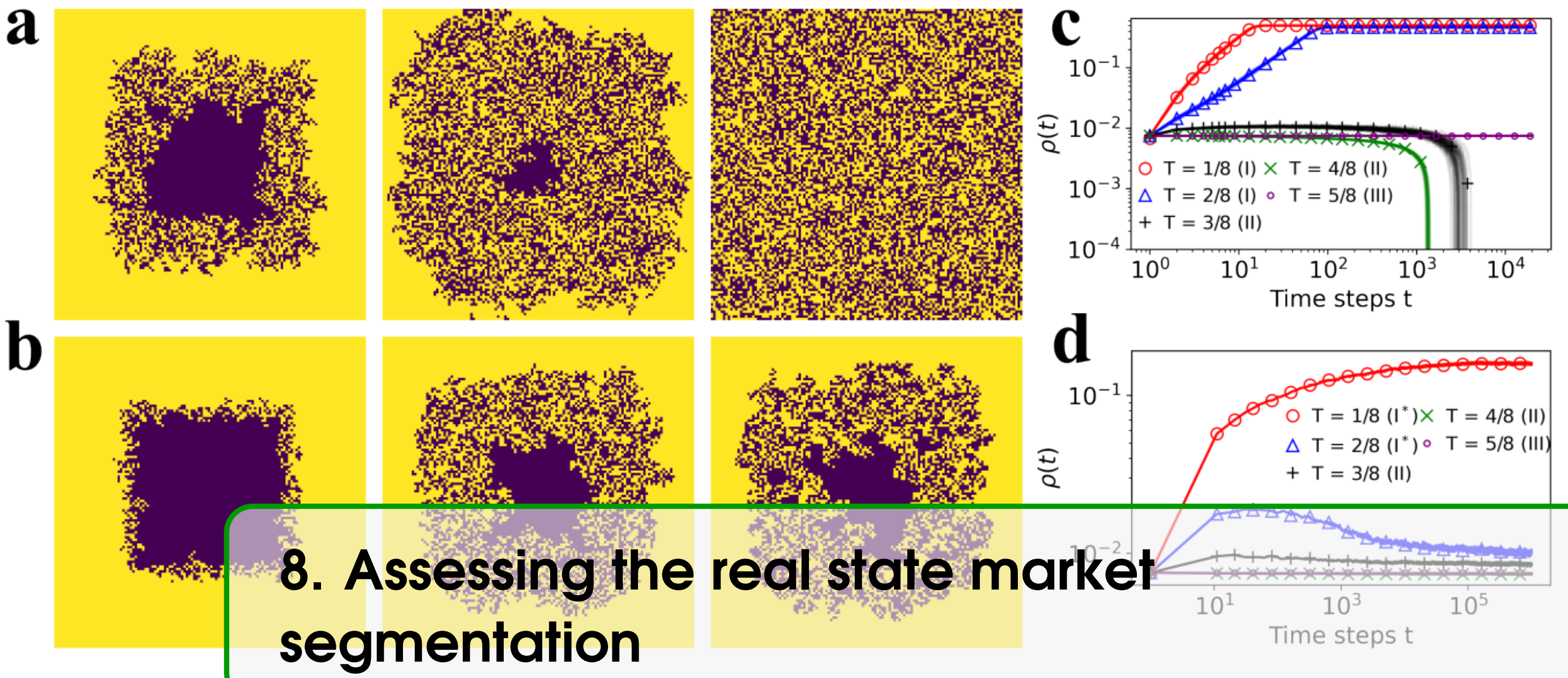

8. Assessing the real state market segmentation

The results in this chapter are published as:

David Abella et al. "Ordering dynamics and aging in the symmetrical threshold model". In: *New Journal of Physics* 26.1 (Jan. 2024), page 013033. DOI: 10.1088/1367-2630/ad1ad4. URL: https://dx.doi.org/10.1088/1367-2630/ad1ad4

8.1 Table

Lorem ipsum dolor sit amet, consectetur adipiscing elit. Praesent porttitor arcu luctus, imperdiet urna iaculis, mattis eros. Pellentesque iaculis odio vel nisl ullamcorper, nec faucibus ipsum molestie. Sed dictum nisl non aliquet porttitor. Etiam vulputate arcu dignissim, finibus sem et, viverra nisl. Aenean luctus congue massa, ut laoreet metus ornare in. Nunc fermentum nisi imperdiet lectus tincidunt vestibulum at ac elit. Nulla mattis nisl eu malesuada suscipit.

8.2 Figure

Lorem ipsum dolor sit amet, consectetur adipiscing elit. Praesent porttitor arcu luctus, imperdiet urna iaculis, mattis eros. Pellentesque iaculis odio vel nisl ullamcorper, nec faucibus ipsum molestie. Sed dictum nisl non aliquet porttitor. Etiam vulputate arcu dignissim, finibus sem et, viverra nisl. Aenean luctus congue massa, ut laoreet metus ornare in. Nunc fermentum nisi imperdiet lectus tincidunt vestibulum at ac elit. Nulla mattis nisl eu malesuada suscipit.

creodocs

Figure 8.1: Figure caption.

Referencing Figure 8.1 in-text using its label.

Figure 8.2: Floating figure.

Bibliography

Bibliography

[1] David Abella, Giancarlo Franzese, and Javier Hernández-Rojas. "Many-Body Contributions in Water Nanoclusters". In: *ACS Nano* 17.3 (Jan. 2023), pages 1959–1964. ISSN: 1936-086X. DOI: 10.1021/acsnano.2c06077. URL: http://dx.doi.org/10.1021/acsnano.2c06077 (cited on page 19).

[2] David Abella, Maxi San Miguel, and José J. Ramasco. "Aging effects in Schelling segregation model". In: *Scientific Reports* 12.1 (Nov. 2022). ISSN: 2045-2322. DOI: 10.1038/s41598-022-23224-7. URL: http://dx.doi.org/10.1038/s41598-022-23224-7 (cited on pages 19, 13).

[3] David Abella, Maxi San Miguel, and José J. Ramasco. "Aging in binary-state models: The Threshold model for complex contagion". In: *Phys. Rev. E* 107 (2 Feb. 2023), page 024101. DOI: 10.1103/PhysRevE.107.024101. URL: https://link.aps.org/doi/10.1103/PhysRevE.107.024101 (cited on pages 19, 23, 29).

[4] David Abella et al. "Ordering dynamics and aging in the symmetrical threshold model". In: *New Journal of Physics* 26.1 (Jan. 2024), page 013033. DOI: 10.1088/1367-2630/ad1ad4. URL: https://dx.doi.org/10.1088/1367-2630/ad1ad4 (cited on pages 19, 43, 53, 67, 71).

[5] Aishwarya Agarwal et al. "Swap Stability in Schelling Games on Graphs". In: *Proceedings of the AAAI Conference on Artificial Intelligence* 34.02 (2020), pages 1758–1765. DOI: 10.1609/aaai.v34i02.5541 (cited on page 13).

[6] Ezequiel Albano. "Interfacial roughening, segregation and dynamic behaviour in a generalized Schelling model". In: *Journal of Statistical Mechanics-theory and Experiment - J STAT MECH-THEORY EXP* 2012 (Mar. 2012). DOI: 10.1088/1742-5468/2012/03/P03013 (cited on pages 13, 18, 21).

[7] R Amato et al. "Opinion competition dynamics on multiplex networks". In: *New Journal of Physics* 19.12 (2017), page 123019. DOI: 10.1088/1367-2630/aa936a (cited on pages 5, 23).

[8] Guilherme Ferraz de Arruda, Giovanni Petri, and Yamir Moreno. "Social contagion models on hypergraphs". In: *Physical Review Research* 2.2 (2020). DOI: 10.1103/physrevresearch.2.023032 (cited on pages 5–8, 23, 29).

[9] Oriol Artime, José J. Ramasco, and Maxi San Miguel. "Dynamics on networks: competition of temporal and topological correlations". In: *Scientific Reports* 7.1 (2017). DOI: 10.1038/srep41627 (cited on pages 24, 31, 54).

[10] Oriol Artime et al. "Aging-induced continuous phase transition". In: *Physical Review E* 98.3 (2018). DOI: 10.1103/physreve.98.032104 (cited on pages 10, 14, 31, 32).

[11] A. L. Barabasi. "The origin of bursts and heavy tails in human dynamics". In: *Nature* 435 (2005), page 207 (cited on pages 10, 14).

[12] Albert-László Barabási. "Scale-free networks: a decade and beyond". In: *Science* 325.5939 (2009), pages 412–413 (cited on pages 5, 31, 51).

[13] George Barmpalias, Richard Elwes, and Andrew Lewis-Pye. "Minority Population in the One-Dimensional Schelling Model of Segregation". In: *Journal of Statistical Physics* 173.5 (2018), pages 1408–1458. DOI: 10.1007/s10955-018-2146-2 (cited on page 13).

[14] Frank M Bass. "A new product growth for model consumer durables". In: *Management science* 15.5 (1969), pages 215–227 (cited on page 30).

[15] Federico Battiston et al. "The physics of higher-order interactions in complex systems". In: *Nature Physics* 17.10 (Oct. 2021), pages 1093–1098. DOI: 10.1038/s41567-021-01371-4. URL: https://doi.org/10.1038/s41567-021-01371-4 (cited on page 7).

[16] E. Ben-Naim, L. Frachebourg, and P. L. Krapivsky. "Coarsening and persistence in the voter model". In: *Physical Review E* 53.4 (1996), pages 3078–3087. DOI: 10.1103/physreve.53.3078 (cited on pages 47, 49).

[17] L. Berthier and A. P. Young. "Aging dynamics of the Heisenberg spin glass". In: *Physical Review B* 69.18 (May 2004). ISSN: 1550-235X. DOI: 10.1103/physrevb.69.184423. URL: http://dx.doi.org/10.1103/PhysRevB.69.184423 (cited on page 20).

[18] Ginestra Bianconi et al. "Complex systems in the spotlight: next steps after the 2021 Nobel Prize in Physics". In: *Journal of Physics: Complexity* 4.1 (2023), page 010201 (cited on page 43).

[19] M. Blume, V.J. Emery, and Robert B. Griffiths. "Ising Model for the Lambda Transition and Phase Separation in He3-He4 Mixtures". In: *Phys. Rev. A* 4 (1971), page 1071. DOI: https://doi.org/10.1103/PhysRevA.4.1071 (cited on page 9).

[20] Marian Boguñá et al. "Simulating non-Markovian stochastic processes". In: *Physical Review E* 90.4 (2014). DOI: 10.1103/physreve.90.042108 (cited on page 10).

[21] Bryan Bollinger and Kenneth Gillingham. "Peer effects in the diffusion of solar photovoltaic panels". In: *Marketing science (Providence, R.I.)* 31.6 (Nov. 2012), pages 900–912. DOI: 10.1287/mksc.1120.0727. URL: https://doi.org/10.1287/mksc.1120.0727 (cited on page 6).

[22] Paulo RA Campos, Viviane M de Oliveira, and FG Brady Moreira. "Small-world effects in the majority-vote model". In: *Physical Review E* 67.2 (2003), page 026104 (cited on page 43).

[23] Adrián Carro, Raúl Toral, and Maxi San Miguel. "The noisy Voter model on complex networks". In: *Scientific Reports* 6.1 (2016). DOI: 10.1038/srep24775 (cited on pages 5, 23).

[24] Claudio Castellano, Santo Fortunato, and Vittorio Loreto. "Statistical physics of social dynamics". In: *Rev. Mod. Phys.* 81 (2 May 2009), pages 591–646. DOI: 10.1103/RevModPhys.81.591. URL: https://link.aps.org/doi/10.1103/RevModPhys.81.591 (cited on page 43).

[25] Claudio Castellano, Santo Fortunato, and Vittorio Loreto. "Statistical physics of social dynamics". In: *Rev. Mod. Phys.* 81 (2 May 2009), pages 591–646. DOI: 10.1103/RevModPhys.81.591. URL: https://link.aps.org/doi/10.1103/RevModPhys.81.591 (cited on page 45).

[26] Claudio Castellano, Miguel A. Muñoz, and Romualdo Pastor-Satorras. "Nonlinearq-Voter model". In: *Physical Review E* 80.4 (2009). DOI: 10.1103/physreve.80.041129 (cited on pages 5, 23, 43).

[27] Giulia Cencetti et al. "Temporal properties of higher-order interactions in social networks". In: *Scientific Reports* 11.1 (2021). DOI: 10.1038/s41598-021-86469-8 (cited on pages 5, 23).

[28] Giulia Cencetti et al. "Distinguishing Simple and Complex Contagion Processes on Networks". In: *Phys. Rev. Lett.* 130 (24 June 2023), page 247401. DOI: 10.1103/PhysRevLett.130.247401. URL: https://link.aps.org/doi/10.1103/PhysRevLett.130.247401 (cited on page 7).

[29] Damon Centola. "The Spread of Behavior in an Online Social Network Experiment". In: *Science* 329.5996 (2010), pages 1194–1197. DOI: 10.1126/science.1185231 (cited on pages 6–8, 29).

[30] Damon Centola, Víctor M. Eguíluz, and Michael W. Macy. "Cascade dynamics of complex propagation". In: *Physica A: Statistical Mechanics and its Applications* 374.1 (2007), pages 449–456. DOI: 10.1016/j.physa.2006.06.018 (cited on pages 6–8, 29, 32, 39, 43).

[31] Hanshuang Chen et al. "Non-Markovian majority-vote model". In: *Physical Review E* 102.6 (2020). DOI: 10.1103/physreve.102.062311 (cited on pages 5, 10, 23, 31, 32, 54, 91).

[32] Ling-Jiao Chen et al. "Complex contagions with social reinforcement from different layers and neighbors". In: *Physica A: Statistical Mechanics and its Applications* 503 (2018), pages 516–525. DOI: 10.1016/j.physa.2018.03.017 (cited on page 8).

[33] Raj Chetty, Nathaniel Hendren, and Lawrence F. Katz. "The Effects of Exposure to Better Neighborhoods on Children: New Evidence from the Moving to Opportunity Experiment". In: *American Economic Review* 106.4 (Apr. 2016), pages 855–902. DOI: 10.1257/aer.20150572. URL: http://dx.doi.org/10.1257/aer.20150572 (cited on page 14).

[34] Nicholas A. Christakis and James H. Fowler. “The Spread of Obesity in a Large Social Network over 32 Years”. In: *The New England Journal of Medicine* 357.4 (July 2007), pages 370–379. DOI: 10.1056/nejmsa066082. URL: https://doi.org/10.1056/nejmsa066082 (cited on page 6).

[35] Terry Nichols Clark et al. “Amenities Drive Urban Growth”. In: *Journal of Urban Affairs* 24.5 (Dec. 2002), pages 493–515. DOI: 10.1111/1467-9906.00134. URL: http://dx.doi.org/10.1111/1467-9906.00134 (cited on page 14).

[36] W. A. V. Clark and M. Fossett. “Understanding the social context of the Schelling segregation model”. In: *Proceedings of the National Academy of Sciences* 105.11 (2008), pages 4109–4114. DOI: 10.1073/pnas.0708155105 (cited on page 13).

[37] W.A.V. Clark. “Residential preferences and neighborhood racial segregation: A test of the schelling segregation model”. In: *Demography* 28.1 (1991), pages 1–19. DOI: 10.2307/2061333 (cited on page 13).

[38] William A.V. Clark, Youqin Huang, and Suzanne Withers. “Does commuting distance matter?” In: *Regional Science and Urban Economics* 33.2 (Mar. 2003), pages 199–221. DOI: 10.1016/s0166-0462(02)00012-1. URL: http://dx.doi.org/10.1016/s0166-0462(02)00012-1 (cited on page 14).

[39] “Creating social contagion through viral product design: a randomized trial of peer influence in networks on JSTOR”. In: *www.jstor.org* (). URL: https://www.jstor.org/stable/41261920 (cited on page 5).

[40] Agnieszka Czaplicka, Raul Toral, and Maxi San Miguel. “Competition of simple and complex adoption on interdependent networks”. In: *Physical Review E* 94.6 (2016). DOI: 10.1103/physreve.94.062301 (cited on pages 8, 29).

[41] L Dall’Asta, C Castellano, and M Marsili. “Statistical physics of the Schelling model of segregation”. In: *Journal of Statistical Mechanics: Theory and Experiment* 2008.07 (July 2008), page L07002. ISSN: 1742-5468. DOI: 10.1088/1742-5468/2008/07/l07002. URL: http://dx.doi.org/10.1088/1742-5468/2008/07/L07002 (cited on pages 9, 13, 15, 16, 18, 21).

[42] Nancy A Denton. “The persistence of segregation: Links between residential segregation and school segregation”. In: *Minn. L. Rev.* 80 (1995), page 795 (cited on page 14).

[43] B Derrida. “Exponents appearing in the zero-temperature dynamics of the 1D Potts model”. In: *Journal of Physics A: Mathematical and General* 28.6 (1995), pages 1481–1491. DOI: 10.1088/0305-4470/28/6/006 (cited on page 49).

[44] B. Derrida. “How to extract information from simulations of coarsening at finite temperature”. In: *Phys. Rev. E* 55 (3 Mar. 1997), pages 3705–3707. DOI: 10.1103/PhysRevE.55.3705. URL: https://link.aps.org/doi/10.1103/PhysRevE.55.3705 (cited on page 49).

[45] Bernard Derrida, Vincent Hakim, and Vincent Pasquier. “Exact First-Passage Exponents of 1D Domain Growth: Relation to a Reaction-Diffusion Model”. In: *Physical Review Letters* 75.4 (1995), pages 751–754. DOI: 10.1103/physrevlett.75.751 (cited on page 49).

[46] Marina Diakonova, Maxi San Miguel, and Víctor M. Eguíluz. “Absorbing and shattered fragmentation transitions in multilayer coevolution”. In: *Physical Review E* 89.6 (2014). DOI: 10.1103/physreve.89.062818 (cited on pages 5, 23).

[47] Marina Diakonova et al. “Irreducibility of multilayer network dynamics: the case of the Voter model”. In: *New Journal of Physics* 18.2 (2016), page 023010. DOI: 10.1088/1367-2630/18/2/023010 (cited on pages 5, 23).

[48] Fernando Diaz-Diaz, Maxi San Miguel, and Sandro Meloni. “Echo chambers and information transmission biases in homophilic and heterophilic networks”. In: *Scientific Reports* 12.1 (2022). DOI: 10.1038/s41598-022-13343-6 (cited on pages 7, 8, 29).

[49] Peter Sheridan Dodds, Kameron Decker Harris, and Christopher M. Danforth. “Limited Imitation Contagion on Random Networks: Chaos, Universality, and Unpredictability”. In: *Physical Review Letters* 110.15 (2013). DOI: 10.1103/physrevlett.110.158701 (cited on pages 8, 29).

[50] Peter Sheridan Dodds and Duncan J. Watts. "Universal Behavior in a Generalized Model of Contagion". In: *Physical Review Letters* 92.21 (2004). DOI: 10.1103/physrevlett.92.218701 (cited on pages 7, 24, 29).

[51] Nicolás Goles Domic, Eric Goles, and Sergio Rica. "Dynamics and complexity of the Schelling segregation model". In: *Physical Review E* 83.5 (2011). DOI: 10.1103/physreve.83.056111 (cited on page 13).

[52] Paul Erdős, Alfréd Rényi, et al. "On the evolution of random graphs". In: *Publ. Math. Inst. Hung. Acad. Sci* 5.1 (1960), pages 17–60 (cited on pages 31, 44, 45, 53).

[53] J. Fernández-Gracia, V. M. Eguíluz, and M. San Miguel. "Update rules and interevent time distributions: Slow ordering versus no ordering in the voter model". In: *Physical Review E* 84.1 (2011). DOI: 10.1103/physreve.84.015103 (cited on pages 10, 14, 31, 32, 62).

[54] Juan Fernández-Gracia, Víctor M. Eguíluz, and Maxi San Miguel. "Timing Interactions in Social Simulations: The Voter Model". In: *Understanding Complex Systems* (2013), pages 331–352 (cited on pages 31, 32).

[55] Juan Fernández-Gracia et al. "Is the Voter Model a Model for Voters?" In: *Physical Review Letters* 112.15 (2014). DOI: 10.1103/physrevlett.112.158701 (cited on pages 5, 23).

[56] Emilio Ferrara and Zeyao Yang. "Measuring emotional contagion in social media". In: *PLOS ONE* 10.11 (Nov. 2015), e0142390. DOI: 10.1371/journal.pone.0142390. URL: https://doi.org/10.1371/journal.pone.0142390 (cited on page 5).

[57] Daniel S. Fisher and David A. Huse. "Ordered Phase of Short-Range Ising Spin-Glasses". In: *Phys. Rev. Lett.* 56 (15 Apr. 1986), pages 1601–1604. DOI: 10.1103/PhysRevLett.56.1601. URL: https://link.aps.org/doi/10.1103/PhysRevLett.56.1601 (cited on page 20).

[58] James H. Fowler and Nicholas A. Christakis. "Cooperative behavior cascades in human social networks". In: *Proceedings of the National Academy of Sciences of the United States of America* 107.12 (Mar. 2010), pages 5334–5338. DOI: 10.1073/pnas.0913149107. URL: https://doi.org/10.1073/pnas.0913149107 (cited on page 6).

[59] SERGE GALAM. "SOCIOPHYSICS: A REVIEW OF GALAM MODELS". In: *International Journal of Modern Physics C* 19.03 (Mar. 2008), pages 409–440. DOI: 10.1142/s0129183108012297. URL: http://dx.doi.org/10.1142/s0129183108012297 (cited on page 30).

[60] L. Gauvin, J. Vannimenus, and J.-P. Nadal. "Phase diagram of a Schelling segregation model". In: *The European Physical Journal B* 70.2 (July 2009), pages 293–304. ISSN: 1434-6036. DOI: 10.1140/epjb/e2009-00234-0. URL: http://dx.doi.org/10.1140/epjb/e2009-00234-0 (cited on pages 9, 13–16).

[61] Laetitia Gauvin, Jean-Pierre Nadal, and Jean Vannimenus. "Schelling segregation in an open city: A kinetically constrained Blume-Emery-Griffiths spin-1 system". In: *Physical Review E* 81.6 (June 2010). ISSN: 1550-2376. DOI: 10.1103/physreve.81.066120. URL: http://dx.doi.org/10.1103/PhysRevE.81.066120 (cited on pages 9, 13).

[62] *GitHub repository*. https://github.com/davidabbu/Aging-in-binary-state-models (cited on page 26).

[63] Roy J Glauber. "Time-dependent statistics of the Ising model". In: *Journal of mathematical physics* 4.2 (1963), pages 294–307 (cited on page 44).

[64] James P. Gleeson. "Cascades on correlated and modular random networks". In: *Physical Review E* 77.4 (2008). DOI: 10.1103/physreve.77.046117 (cited on pages 8, 29, 34, 37).

[65] James P. Gleeson. "High-Accuracy Approximation of Binary-State Dynamics on Networks". In: *Physical Review Letters* 107.6 (2011). DOI: 10.1103/physrevlett.107.068701 (cited on page 24).

[66] James P. Gleeson. "Binary-State Dynamics on Complex Networks: Pair Approximation and Beyond". In: *Physical Review X* 3.2 (2013). DOI: 10.1103/physrevx.3.021004 (cited on pages 24, 25, 27, 34, 36, 47, 50).

[67] James P. Gleeson and Diarmuid J. Cahalane. “Seed size strongly affects cascades on random networks”. In: *Physical Review E* 75.5 (2007). DOI: 10.1103/physreve.75.056103 (cited on pages 8, 27, 29, 32, 34, 37, 47).

[68] James P. Gleeson et al. “Effects of Network Structure, Competition and Memory Time on Social Spreading Phenomena”. In: *Physical Review X* 6.2 (2016). DOI: 10.1103/physrevx.6.021019 (cited on pages 24, 30).

[69] S. Gonçalves, M. F. Laguna, and J. R. Iglesias. “Why, when, and how fast innovations are adopted”. In: *The European Physical Journal B* 85.6 (June 2012). DOI: 10.1140/epjb/e2012-30082-6. URL: http://dx.doi.org/10.1140/epjb/e2012-30082-6 (cited on page 30).

[70] C. Gracia-Lázaro et al. “Residential segregation and cultural dissemination: An Axelrod-Schelling model”. In: *Physical Review E* 80.4 (2009). DOI: 10.1103/physreve.80.046123 (cited on page 13).

[71] M. Granovetter. “Threshold models of collective behavior”. In: *American Journal of Sociology* 83 (1978), page 1420 (cited on page 13).

[72] Mark Granovetter. “Threshold Models of Collective Behavior”. In: *American Journal of Sociology* 83.6 (1978), pages 1420–1443. DOI: 10.1086/226707 (cited on pages 5–7, 23, 29, 30, 43, 50).

[73] Mark Granovetter. “Economic Action and Social Structure: The Problem of Embeddedness”. In: *American Journal of Sociology* 91.3 (Nov. 1985), pages 481–510. DOI: 10.1086/228311. URL: http://dx.doi.org/10.1086/228311 (cited on page 13).

[74] Mark S. Granovetter. “The Strength of Weak Ties”. In: *American Journal of Sociology* 78.6 (1973), pages 1360–1380. DOI: 10.1086/225469 (cited on page 7).

[75] S. Grauwin et al. “Competition between collective and individual dynamics”. In: *Proceedings of the National Academy of Sciences* 106.49 (2009), pages 20622–20626. DOI: 10.1073/pnas.0906263106 (cited on page 13).

[76] Douglas Guilbeault and Damon Centola. “Topological measures for identifying and predicting the spread of complex contagions”. In: *Nature Communications* 12 (2021), page 4430. DOI: 10.1038/s41467-021-24704-6 (cited on pages 8, 29).

[77] D. Gunton, M. San Miguel, and P.S. Sahni. “The dynamics of first order phase transitions”. In: *Phase transitions and critical phenomena* 8 (1983), pages 267–466 (cited on page 18).

[78] JD Gunton. “The dynamics of first-order phase transitions”. In: *Phase transitions and critical phenomena* 8 (1983), page 267 (cited on page 62).

[79] Laurens Haan and Ana Ferreira. *Extreme value theory: an introduction*. Volume 3. Springer, 2006 (cited on page 48).

[80] Adam Hackett and James P. Gleeson. “Cascades on clique-based graphs”. In: *Physical Review E* 87.6 (2013). DOI: 10.1103/physreve.87.062801 (cited on pages 8, 29).

[81] Adam Hackett, Sergey Melnik, and James P. Gleeson. “Cascades on a class of clustered random networks”. In: *Physical Review E* 83.5 (2011). DOI: 10.1103/physreve.83.056107 (cited on pages 8, 29).

[82] Rainer Hegselmann. “Thomas C. Schelling and James M. Sakoda: The Intellectual, Technical,and Social History of a Model”. In: *Journal of Artificial Societies and Social Simulation* 20.3 (2017), page 15. DOI: 10.18564/jasss.3511 (cited on page 9).

[83] A. D. Henry, P. Pralat, and C.-Q. Zhang. “Emergence of segregation in evolving social networks”. In: *Proceedings of the National Academy of Sciences* 108.21 (2011), pages 8605–8610. DOI: 10.1073/pnas.1014486108 (cited on page 13).

[84] Nina Holden and Scott Sheffield. “Scaling limits of the Schelling model”. In: *Probability Theory and Related Fields* 176.1-2 (2019), pages 219–292. DOI: 10.1007/s00440-019-00918-0 (cited on page 13).

[85] J. Hoshen and R. Kopelman. “Percolation and cluster distribution. I. Cluster multiple labeling technique and critical concentration algorithm”. In: *Phys. Rev. B* 14 (8 Oct. 1976), pages 3438–3445. DOI: 10.1103/PhysRevB.14.3438. URL: https://link.aps.org/doi/10.1103/PhysRevB.14.3438 (cited on page 15).

[86] "How Behavior Spreads: The Science of Complex Contagions How Behavior Spreads: The Science of Complex Contagions Damon Centola Princeton University Press, 2018. 308 pp." In: *Science* 361.6409 (2018), pages 1320–1320. DOI: 10.1126/science.aav1974 (cited on page 43).

[87] Iacopo Iacopini et al. "Simplicial models of social contagion". In: *Nature Communications* 10.1 (2019). DOI: 10.1038/s41467-019-10431-6 (cited on pages 5, 7, 23).

[88] J. L. Iribarren and E. Moro. "Impact of human activity patterns on the dynamics of information diffusion." In: *Physical Review Letters* 103 (2009), page 038702 (cited on page 10).

[89] José Luis Iribarren and Esteban Moro. "Impact of Human Activity Patterns on the Dynamics of Information Diffusion". In: *Physical Review Letters* 103.3 (2009). DOI: 10.1103/physrevlett.103.038702 (cited on page 24).

[90] A Jedrzejewski. "Pair approximation for the q-voter model with independence on complex networks". In: *Phys. Rev. E* 95 (1 Jan. 2017), page 012307. DOI: 10.1103/PhysRevE.95.012307. URL: https://link.aps.org/doi/10.1103/PhysRevE.95.012307 (cited on page 43).

[91] Michaeline Jensen and Thomas J. Dishion. "Mechanisms and processes of peer contagion". In: *Psychology* (Jan. 2015). DOI: 10.1093/obo/9780199828340-0165. URL: https://doi.org/10.1093/obo/9780199828340-0165 (cited on page 5).

[92] Pablo Jensen et al. "Giant Catalytic Effect of Altruists in Schelling's Segregation Model". In: *Physical Review Letters* 120.20 (2018). DOI: 10.1103/physrevlett.120.208301 (cited on page 13).

[93] Marko Jusup et al. "Social physics". In: *Physics Reports* 948 (2022), pages 1–148 (cited on page 43).

[94] Fariba Karimi and Petter Holme. "Threshold model of cascades in empirical temporal networks". In: *Physica A: Statistical Mechanics and its Applications* 392.16 (2013), pages 3476–3483. DOI: 10.1016/j.physa.2013.03.050 (cited on pages 8, 29).

[95] M. Karsai et al. "Small but slow world: How network topology and burstiness slow down spreading". In: *Physical Review E* 83.2 (2011). DOI: 10.1103/physreve.83.025102 (cited on page 24).

[96] Márton Karsai et al. "Complex contagion process in spreading of online innovation". In: *Journal of The Royal Society Interface* 11.101 (2014), page 20140694. DOI: 10.1098/rsif.2014.0694 (cited on pages 8, 29).

[97] Márton Karsai et al. "Local cascades induced global contagion: How heterogeneous thresholds, exogenous effects, and unconcerned behaviour govern online adoption spreading". In: *Scientific Reports* 6.1 (2016). DOI: 10.1038/srep27178 (cited on pages 8, 29).

[98] Leah A. Keating, James P. Gleeson, and David J. P. O'Sullivan. "Multitype branching process method for modeling complex contagion on clustered networks". In: *Phys. Rev. E* 105 (3 Mar. 2022), page 034306. DOI: 10.1103/PhysRevE.105.034306. URL: https://link.aps.org/doi/10.1103/PhysRevE.105.034306 (cited on page 38).

[99] Pinaki Kumar et al. "On interevent time distributions of avalanche dynamics". In: *Scientific Reports* 10.1 (2020). DOI: 10.1038/s41598-019-56764-6 (cited on pages 10, 24).

[100] Fabio Lamanna et al. "Immigrant community integration in world cities". In: *PLOS ONE* 13.3 (2018), e0191612. DOI: 10.1371/journal.pone.0191612 (cited on page 13).

[101] Maxime Lenormand et al. "Comparing and modelling land use organization in cities". In: *Royal Society Open Science* 2.12 (2015), page 150449. DOI: 10.1098/rsos.150449 (cited on pages 13, 15).

[102] Thomas M Liggett et al. *Stochastic interacting systems: contact, Voter and exclusion processes*. Volume 324. springer science & Business Media, 1999 (cited on pages 5, 23, 43, 45).

[103] Quan-Hui Liu et al. "Impacts of opinion leaders on social contagions". In: *Chaos: An Interdisciplinary Journal of Nonlinear Science* 28.5 (2018), page 053103. DOI: 10.1063/1.5017515 (cited on pages 8, 29).

[104] Andrew Mellor, Mauro Mobilia, and RKP Zia. "Characterization of the nonequilibrium steady state of a heterogeneous nonlinear q-voter model with zealotry". In: *EPL (Europhysics Letters)* 113.4 (2016), page 48001 (cited on page 43).

[105] Byungjoon Min and M. San Miguel. "Competition and dual users in complex contagion processes". In: *Scientific reports* 8.1 (Oct. 2018). DOI: 10.1038/s41598-018-32643-4. URL: https://doi.org/10.1038/s41598-018-32643-4 (cited on page 29).

[106] Byungjoon Min and Maxi San Miguel. "Fragmentation transitions in a coevolving nonlinear voter model". In: *Scientific Reports* 7 (2017), page 12864. DOI: 10.1038/s41598-017-13047-2 (cited on page 43).

[107] Byungjoon Min and Maxi San Miguel. "Competing contagion processes: Complex contagion triggered by simple contagion". In: *Scientific Reports* 8.1 (2018). DOI: 10.1038/s41598-018-28615-3 (cited on pages 7, 8, 29).

[108] Byungjoon Min and Maxi San Miguel. "Threshold Cascade Dynamics in Coevolving Networks". In: *Entropy* 25.6 (2023), page 929 (cited on page 29).

[109] Mauro Mobilia. "Nonlinear q-voter model with inflexible zealots". In: *Physical Review E* 92.1 (2015), page 012803 (cited on page 43).

[110] Michael Molloy and Bruce Reed. "A critical point for random graphs with a given degree sequence". In: *Random Structures and Algorithms* 6.2-3 (1995), pages 161–180. DOI: 10.1002/rsa.3240060204 (cited on page 24).

[111] Bjarke Mønsted et al. "Evidence of complex contagion of information in social media: An experiment using Twitter bots". In: *PLOS ONE* 12.9 (2017), e0184148. DOI: 10.1371/journal.pone.0184148 (cited on pages 8, 29).

[112] M. E. J. Newman. "Spread of epidemic disease on networks". In: *Phys. Rev. E* 66 (1 July 2002), page 016128. DOI: 10.1103/PhysRevE.66.016128. URL: https://link.aps.org/doi/10.1103/PhysRevE.66.016128 (cited on page 6).

[113] M. E. J. Newman, S. H. Strogatz, and D. J. Watts. "Random graphs with arbitrary degree distributions and their applications". In: *Physical Review E* 64.2 (2001). DOI: 10.1103/physreve.64.026118 (cited on page 24).

[114] B. Nowak and Katarzyna Sznajd-Weron. "Homogeneous Symmetrical Threshold Model with Nonconformity: Independence versus Anticonformity". In: *Complexity* 2019 (Apr. 2019), pages 1–14. DOI: 10.1155/2019/5150825. URL: https://doi.org/10.1155/2019/5150825 (cited on page 43).

[115] Bartłomiej Nowak and Katarzyna Sznajd-Weron. "Symmetrical threshold model with independence on random graphs". In: *Physical Review E* 101.5 (2020), page 052316 (cited on page 43).

[116] Se-Wook Oh and Mason A. Porter. "Complex contagions with timers". In: *Chaos: An Interdisciplinary Journal of Nonlinear Science* 28.3 (2018), page 033101. DOI: 10.1063/1.4990038 (cited on pages 24, 30).

[117] Mario J de Oliveira. "Isotropic majority-vote model on a square lattice". In: *Journal of Statistical Physics* 66.1 (1992), pages 273–281 (cited on page 43).

[118] *Online platforms: Economic and societal effects | Panel for the Future of Science and Technology (STOA) | European Parliament*. URL: https://www.europarl.europa.eu/stoa/en/document/EPRS_STU%282021%29656336 (cited on page 5).

[119] Maxi San Miguel Oriol Artine Jose J. Ramasco. "Dynamics on networks: competition of temporal and topological correlations." In: *Scientific Reports* 7 (2017), page 41627 (cited on page 10).

[120] Diego Ortega, Javier Rodríguez-Laguna, and Elka Korutcheva. "A Schelling model with a variable threshold in a closed city segregation model. Analysis of the universality classes". In: *Physica A: Statistical Mechanics and its Applications* 574 (2021), page 126010. DOI: 10.1016/j.physa.2021.126010 (cited on page 13).

[121] Diego Ortega, Javier Rodríguez-Laguna, and Elka Korutcheva. "Avalanches in an extended Schelling model: An explanation of urban gentrification". In: *Physica A: Statistical Mechanics and its Applications* 573 (2021), page 125943. DOI: 10.1016/j.physa.2021.125943 (cited on page 13).

[122] Romualdo Pastor-Satorras and Alessandro Vespignani. "Epidemic Spreading in Scale-Free Networks". In: *Phys. Rev. Lett.* 86 (14 Apr. 2001), pages 3200–3203. DOI: 10.1103/PhysRevLett.86.3200. URL: https://link.aps.org/doi/10.1103/PhysRevLett.86.3200 (cited on page 6).

[123] Romualdo Pastor-Satorras et al. “Epidemic processes in complex networks”. In: *Reviews of Modern Physics* 87.3 (2015), pages 925–979. DOI: 10.1103/revmodphys.87.925 (cited on pages 5, 23).

[124] A. F. Peralta and R. Toral. “Binary-state dynamics on complex networks: Stochastic pair approximation and beyond”. In: *Physical Review Research* 2.4 (2020). DOI: 10.1103/physrevresearch.2.043370 (cited on pages 24, 41, 51).

[125] A. F. Peralta et al. “Analytical and numerical study of the non-linear noisy Voter model on complex networks”. In: *Chaos: An Interdisciplinary Journal of Nonlinear Science* 28.7 (2018), page 075516. DOI: 10.1063/1.5030112 (cited on pages 5, 23, 43).

[126] Antonio F Peralta, Nagi Khalil, and Raúl Toral. “Reduction from non-Markovian to Markovian dynamics: the case of aging in the noisy-Voter model”. In: *Journal of Statistical Mechanics: Theory and Experiment* 2020.2 (2020), page 024004. DOI: 10.1088/1742-5468/ab6847 (cited on pages 5, 10, 23, 24, 29, 31, 32, 34).

[127] Antonio F. Peralta, Nagi Khalil, and Raúl Toral. “Ordering dynamics in the Voter model with aging”. In: *Physica A: Statistical Mechanics and its Applications* 552 (2020), page 122475. DOI: 10.1016/j.physa.2019.122475 (cited on pages 10, 24, 27, 29, 31, 32, 34).

[128] Antonio F. Peralta, Nagi Khalil, and Raúl Toral. “Ordering dynamics in the voter model with aging”. In: *Physica A: Statistical Mechanics and its Applications* 552 (2020), page 122475. DOI: 10.1016/j.physa.2019.122475 (cited on page 10).

[129] Luiz FC Pereira and FG Brady Moreira. “Majority-vote model on random graphs”. In: *Physical Review E* 71.1 (2005), page 016123 (cited on page 43).

[130] Toni Pérez, Konstantin Klemm, and Víctor M. Eguíluz. “Competition in the presence of aging: dominance, coexistence, and alternation between states”. In: *Scientific Reports* 6.1 (2016). DOI: 10.1038/srep21128 (cited on pages 10, 31, 32).

[131] Armin Pournaki et al. *Order-disorder transition in the zero-temperature Ising model on random graphs*. May 2023. DOI: 10.1103/PhysRevE.107.054112. URL: https://link.aps.org/doi/10.1103/PhysRevE.107.054112 (cited on pages 48, 51, 58).

[132] Sidney Redner. “Reality-inspired Voter models: A mini-review”. In: *Comptes Rendus Physique* 20.4 (2019), pages 275–292. DOI: 10.1016/j.crhy.2019.05.004 (cited on pages 5, 23).

[133] Everett M Rogers, Arvind Singhal, and Margaret M Quinlan. “Diffusion of innovations”. In: *An integrated approach to communication theory and research*. Routledge, 2014, pages 432–448 (cited on pages 6, 30).

[134] Tim Rogers and Alan J McKane. “A unified framework for Schelling’s model of segregation”. In: *Journal of Statistical Mechanics: Theory and Experiment* 2011.07 (July 2011), P07006. ISSN: 1742-5468. DOI: 10.1088/1742-5468/2011/07/p07006. URL: http://dx.doi.org/10.1088/1742-5468/2011/07/P07006 (cited on page 13).

[135] Sara Brin Rosenthal et al. “Revealing the hidden networks of interaction in mobile animal groups allows prediction of complex behavioral contagion”. In: *Proceedings of the National Academy of Sciences* 112.15 (2015), pages 4690–4695. DOI: 10.1073/pnas.1420068112 (cited on pages 8, 29).

[136] Diego Rybski et al. “Scaling laws of human interaction activity”. In: *Proceedings of the National Academy of Sciences* 106.31 (2009), pages 12640–12645. DOI: 10.1073/pnas.0902667106. eprint: https://www.pnas.org/doi/pdf/10.1073/pnas.0902667106. URL: https://www.pnas.org/doi/abs/10.1073/pnas.0902667106 (cited on page 54).

[137] Diego Rybski et al. “Communication activity in a social network: relation between long-term correlations and inter-event clustering”. In: *Scientific Reports* 2.1 (2012). DOI: 10.1038/srep00560 (cited on pages 10, 24).

[138] Meghdad Saeedian et al. “Memory effects on epidemic evolution: The susceptible-infected-recovered epidemic model”. In: *Physical Review E* 95.2 (2017), page 022409 (cited on page 27).

[139] S. Sassen. “The global city: introducing a concept”. In: *Brown Journal of World Affairs* 11 (2005), pages 27–43 (cited on page 13).

[140] D. M. Saul, Michael Wortis, and D. Stauffer. “Tricritical behavior of the Blume-Capel model”. In: *Phys. Rev. B* 9 (11 June 1974), pages 4964–4980. DOI: 10.1103/PhysRevB.9.4964. URL: https://link.aps.org/doi/10.1103/PhysRevB.9.4964 (cited on page 9).

[141] T Schelling. *Micromotives and Macrobehavior*. Norton, New York, 1978 (cited on page 9).

[142] Thomas Schelling. “Models of Segregation”. In: *American Economic Review* 59.2 (1969), page 488 (cited on page 9).

[143] Thomas C Schelling. “Dynamic models of segregation”. In: *The Journal of Mathematical Sociology* 1.2 (1971), pages 143–186. DOI: 10.1080/0022250X.1971.9989794. URL: https://doi.org/10.1080/0022250X.1971.9989794 (cited on page 9).

[144] Egemen Sert, Yaneer Bar-Yam, and Alfredo J. Morales. “Segregation dynamics with reinforcement learning and agent based modeling”. In: *Scientific Reports* 10.1 (2020). DOI: 10.1038/s41598-020-68447-8 (cited on page 13).

[145] Munik Shrestha and Cristopher Moore. “Message-passing approach for threshold models of behavior in networks”. In: *Physical Review E* 89.2 (2014). DOI: 10.1103/physreve.89.022805 (cited on pages 24, 29).

[146] Daniel Silver, Ultan Byrne, and Patrick Adler. “Venues and segregation: A revised Schelling model”. In: *PLOS ONE* 16.1 (Jan. 2021), e0242611. DOI: 10.1371/journal.pone.0242611. URL: http://dx.doi.org/10.1371/journal.pone.0242611 (cited on pages 13, 14).

[147] Daniel Aaron Silver and Terry Nichols Clark. *Scenescapes: How qualities of place shape social life*. University of Chicago Press, 2016 (cited on page 14).

[148] P. Singh et al. “Threshold-limited spreading in social networks with multiple initiators”. In: *Scientific Reports* 3.1 (2013). DOI: 10.1038/srep02330 (cited on pages 8, 29, 32).

[149] V. Sood and S. Redner. “Voter Model on Heterogeneous Graphs”. In: *Physical Review Letters* 94.17 (2005). DOI: 10.1103/physrevlett.94.178701 (cited on pages 5, 23).

[150] Sandro Sousa and Vincenzo Nicosia. *Quantifying ethnic segregation in cities through random walks*. 2020. arXiv: 2010.10462 [physics.soc-ph] (cited on page 15).

[151] Hans-Ulrich Stark, Claudio J. Tessone, and Frank Schweitzer. “Decelerating Microdynamics Can Accelerate Macrodynamics in the Voter Model”. In: *Phys. Rev. Lett.* 101 (1 June 2008), page 018701. DOI: 10.1103/PhysRevLett.101.018701. URL: https://link.aps.org/doi/10.1103/PhysRevLett.101.018701 (cited on page 10).

[152] Hans-Ulrich Stark, Claudio J. Tessone, and Frank Schweitzer. “Decelerating Microdynamics Can Accelerate Macrodynamics in the Voter Model”. In: *Physical Review Letters* 101.1 (2008). DOI: 10.1103/physrevlett.101.018701 (cited on pages 10, 31, 32).

[153] Michele Starnini, James P. Gleeson, and Marián Boguñá. “Equivalence between Non-Markovian and Markovian Dynamics in Epidemic Spreading Processes”. In: *Physical Review Letters* 118.12 (2017). DOI: 10.1103/physrevlett.118.128301 (cited on pages 5, 23, 24, 29).

[154] D Stauffer, J Adler, and A Aharony. “Universality at the three-dimensional percolation threshold”. In: *Journal of Physics A: Mathematical and General* 27.13 (1994), pages L475–L480. DOI: 10.1088/0305-4470/27/13/003 (cited on page 49).

[155] D. Stauffer and S. Solomon. “Ising, Schelling and self-organising segregation”. In: *The European Physical Journal B* 57.4 (2007), pages 473–479. DOI: 10.1140/epjb/e2007-00181-8 (cited on pages 9, 13).

[156] Dietrich Stauffer. “A Biased Review of Sociophysics”. In: *Journal of Statistical Physics* 151.1-2 (2013), pages 9–20. DOI: 10.1007/s10955-012-0604-9 (cited on pages 9, 13).

[157] Steffen Steinert and Matthew Dennis. “Emotions and Digital Well-Being: on Social Media’s Emotional Affordances”. In: *Philosophy and Technology* 35.2 (Apr. 2022). DOI: 10.1007/s13347-022-00530-6. URL: https://doi.org/10.1007/s13347-022-00530-6 (cited on page 5).

[158] Krzysztof Suchecki, Vı************************************ctor M. Eguı************************************lu and Maxi San Miguel. "Voter model dynamics in complex networks: Role of dimensionality, disorder, and degree distribution". In: *Phys. Rev. E* 72 (3 Sept. 2005), page 036132. DOI: 10.1103/PhysRevE.72.036132. URL: https://link.aps.org/doi/10.1103/PhysRevE.72.036132 (cited on page 45).

[159] Raúl Toral and Pere Colet. *Stochastic numerical methods: an introduction for students and scientists*. John Wiley & Sons, 2014 (cited on page 24).

[160] Samuel Unicomb, Gerardo Iñiguez, and Márton Karsai. "Threshold driven contagion on weighted networks". In: *Scientific Reports* 8.1 (2018). DOI: 10.1038/s41598-018-21261-9 (cited on pages 8, 29).

[161] Thomas W. Valente. "Social network thresholds in the diffusion of innovations". In: *Social Networks* 18.1 (1996), pages 69–89. ISSN: 0378-8733. DOI: https://doi.org/10.1016/0378-8733(95)00256-1. URL: https://www.sciencedirect.com/science/article/pii/0378873395002561 (cited on page 6).

[162] P. Van Mieghem and R. van de Bovenkamp. "Non-Markovian Infection Spread Dramatically Alters the Susceptible-Infected-Susceptible Epidemic Threshold in Networks". In: *Physical Review Letters* 110.10 (2013). DOI: 10.1103/physrevlett.110.108701 (cited on pages 5, 23, 24, 29).

[163] Federico Vazquez, Víctor M. Eguíluz, and Maxi San Miguel. "Generic Absorbing Transition in Coevolution Dynamics". In: *Physical Review Letters* 100.10 (2008). DOI: 10.1103/physrevlett.100.108702 (cited on pages 5, 23, 51).

[164] André P Vieira, Eric Goles, and Hans J Herrmann. "Dynamics of extended Schelling models". In: *Journal of Statistical Mechanics: Theory and Experiment* 2020.1 (2020), page 013212. DOI: 10.1088/1742-5468/ab5b8d (cited on page 13).

[165] D. Vinkovic and A. Kirman. "A physical analogue of the Schelling model". In: *Proceedings of the National Academy of Sciences* 103.51 (2006), pages 19261–19265. DOI: 10.1073/pnas.0609371103 (cited on pages 9, 13).

[166] Henry Wasserman and Gary Yohe. "Segregation and the Provision of Spatially Defined Local Public Goods". In: *The American Economist* 45.2 (Oct. 2001), pages 13–24. DOI: 10.1177/056943450104500202. URL: http://dx.doi.org/10.1177/056943450104500202 (cited on page 14).

[167] D. J. Watts. "A simple model of global cascades on random networks". In: *Proceedings of the National Academy of Sciences* 99.9 (2002), pages 5766–5771. DOI: 10.1073/pnas.082090499 (cited on pages 7, 8, 29, 30, 32, 43, 50).

[168] Duncan J Watts and Steven H Strogatz. "Collective dynamics of 'small-world' networks". In: *nature* 393.6684 (1998), pages 440–442 (cited on page 5).

[169] N. C. Wormald. "Models of Random Regular Graphs". In: *Surveys in Combinatorics, 1999*. Edited by J. D. Lamb and D. A.Editors Preece. London Mathematical Society Lecture Note Series. Cambridge University Press, 1999, pages 239–298. DOI: 10.1017/CBO9780511721335.010 (cited on page 38).

[170] Nicholas C Wormald et al. "Models of random regular graphs". In: *London Mathematical Society Lecture Note Series* (1999), pages 239–298 (cited on pages 31, 44, 45, 53).

[171] Yang Xu et al. "Quantifying segregation in an integrated urban physical-social space". In: *Journal of the Royal Society Interface* 16.160 (2019), page 20190536. ISSN: 17425662. DOI: 10.1098/rsif.2019.0536. URL: https://royalsocietypublishing.org/doi/abs/10.1098/rsif.2019.0536 (cited on page 15).

[172] A P Young. *Spin glasses and random fields*. World Scientific, 1997. URL: libgen.li/file.php?md5=5941f917f91576aa2f77de1c40712f2c (cited on page 20).

[173] Junfu Zhang. "Residential segregation in an all-integrationist world". In: *Journal of Economic Behavior and Organization* 54.4 (2004), pages 533–550. ISSN: 0167-2681. DOI: https://doi.org/10.1016/j.jebo.2003.03.005. URL: https://www.sciencedirect.com/science/article/pii/S0167268103001768 (cited on page 21).

[174] Matteo Zignani et al. "Walls-in-one: usage and temporal patterns in a social media aggregator". In: *Applied Network Science* 1.1 (2016). DOI: 10.1007/s41109-016-0009-9 (cited on pages 10, 24).

[175] Martı************************************n G. Zimmermann, Vı************************************cto M. Eguı************************************luz, and Maxi San Miguel. "Coevolution of dynamical states and interactions in dynamic networks". In: *Phys. Rev. E* 69 (6 June 2004), page 065102. DOI: 10.1103/PhysRevE.69.065102. URL: https://link.aps.org/doi/10.1103/PhysRevE.69.065102 (cited on page 51).

Index

A. Vacancy density effect on the Schelling model dynamics

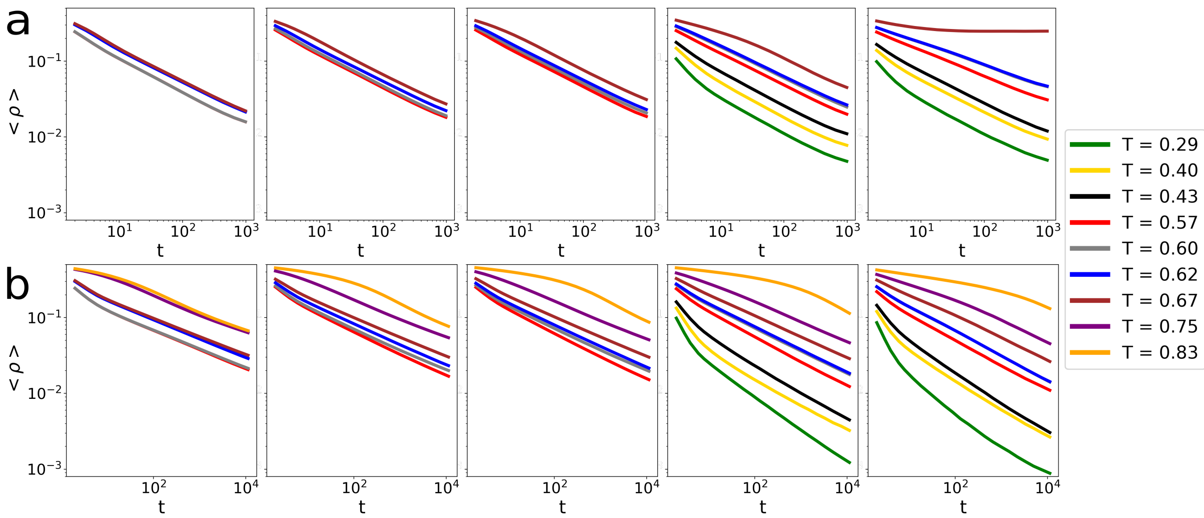

Figure A.1: Average interface density $\langle \rho(t) \rangle$ as a function of time steps for different values of the tolerance parameter T fr the Schelling model (**a**) and the version with aging (**b**). The different plots show a the evolution at a different value of the vacancy density, increasing from left to right $\rho_v = 0.005$, 0.15, 0.2, 0.3 and 0.45. Average performed over 10^3 realisations with system size 100 x 100.

Since we restrain ourselves to the region $\rho_v < 0.5$, the increase/decrease of the number of vacancies does not change dramatically the behaviour. Above this value, we approach the segregated-dilute transition ($\rho_v \sim 0.62$). Nevertheless, it is worth to mention a few features we observe on the coarsening dynamics. Essentially, when we set a higher vacancy density, the number of agents which see vacancies at their surroundings increases. This results in a family of similar power-law decays towards the segregated state for every meaningful value of T (see Fig. A.1).

Moreover, a higher ρ_v allows us to study the coarsening phenomena for lower values of T according to the phase diagram for the original Schelling model. For those particular cases, when the aging is introduced, we observe a power law decay faster than without aging (Fig. A.1b). Therefore, the aging effect accelerates segregation in this region of the phase diagram, contrary as for lower values of ρ_v. This acceleration is not caused by reaching the 2-clusters state in less time. Since there is a large presence of vacancies, aging causes a formation of vacancy clusters at the interface. Fig. A.2 shows the final segregated state with and without aging. This

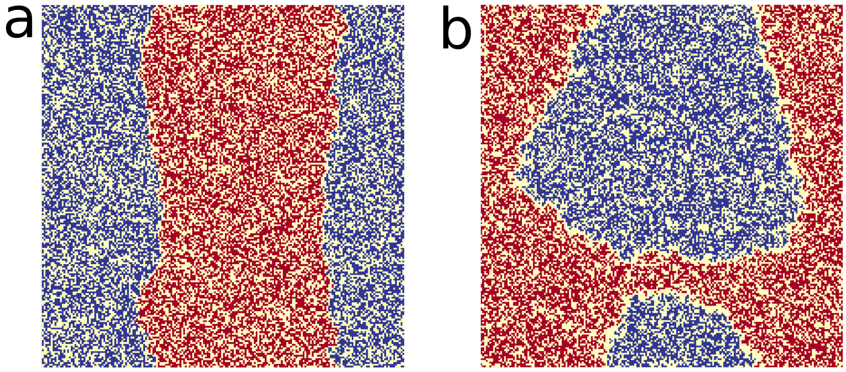

Figure A.2: Snapshots of the system at the final segregated state (after 10^6 MC steps) for the Schelling model (**a**) and the version with (**b**). System size 200 x 200 with $\rho_v = 0.45$ and $T = 0.29$.

spontaneous behaviour is result of the low tolerance combined with the persistence of clusters (once formed) due to aging effect and the large number of vacancies that allows the possibility of the formation of clusters at the interface.

In order to quantify this vacancy cluster formation, we define a measure inspired in the segregation coefficient:

$$s_v = \frac{1}{(L^2\rho_v)^2} \sum_{\{c\}} n_c^2 \tag{A.1}$$

where c is the size of a vacancy cluster and n_c is the number of clusters with size c. The sample average of s_v after reaching equilibrium is called the cluster coefficient of vacancies $\langle s_v \rangle$.

The results of this measure as a function of ρ_v for a few values of T are represented in Fig.A.3 for the Schelling model with and without aging. We observe an increasing dependence of $\langle s_v \rangle$ with ρ_v for both models, but the effect reducing tolerance changes dramatically the behaviour for the case with aging, highlighting the vacancy cluster formation.

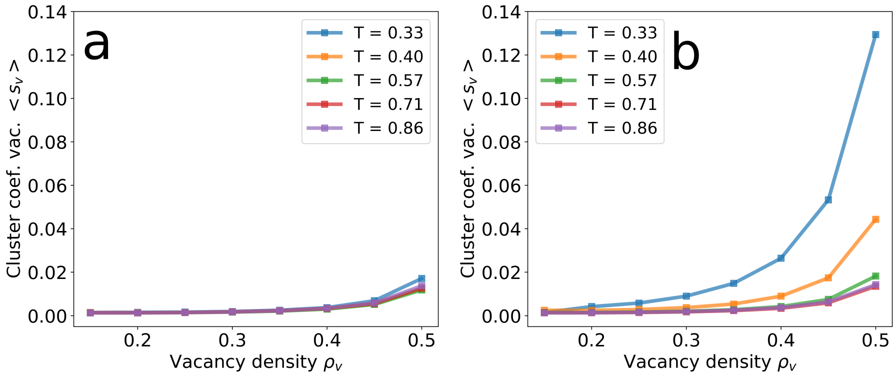

Figure A.3: Cluster coefficient of vacancies as a function of the vacancy density ρ_v for the Schelling model (**a**) and the version with (**b**) for different values of the tolerance T.

B. Heterogeneous mean-field taking into account aging (HMFA)

Setting the time derivatives to 0 in Eqs. (6B.3), we obtain the relations for the stationary state:

$$x^{\pm}_{k,0} = \sum_{j=0}^{\infty} x^{\mp}_{k,j}\,\omega^{\mp}_{k,j}, \qquad x^{\pm}_{k,j} = x^{\pm}_{k,j-1}\,(1-\omega^{\pm}_{k,j-1}) \qquad j>0, \tag{B.1}$$

from where we extract the stationary condition $x^{-}_{k,0} = x^{+}_{k,0}$, as in Ref. (31). Notice that by setting $p_A(j) = 1$ and summing over all ages j, we recover the HMF approximation (Eq. 4.12) for the model without aging. Defining $x^{\pm}_{j}(t)$ as the fraction of agents in state ± 1 with age j:

$$x^{\pm}_{j} = \sum_{k} p_k\, x^{\pm}_{k,j}, \tag{B.2}$$

and using the degree distribution of a complete graph $p_k = \delta(k-N+1)$ (where $\delta(\cdot)$ is the Dirac delta), we sum over the variable k and rewrite Eq. (B.1) in terms of $x^{\pm}_{j}$:

$$x^{\pm}_{0} = \sum_{j=0}^{\infty} x^{\mp}_{j}\,\omega^{\mp}_{j}, \qquad x^{\pm}_{j} = x^{\pm}_{j-1}\,(1-\omega^{\pm}_{j-1}) \qquad j>0, \tag{B.3}$$

where $\omega^{\pm}_{j} \equiv \omega^{\pm}_{N-1,j}$. Note that the stationary condition $x^{-}_{0} = x^{+}_{0}$ remains valid after summing over the degree variable. We compute the solution $x^{\pm}_{j}$ recursively as a function of $x^{\pm}_{0}$:

$$x^{\pm}_{j} = x^{\pm}_{0}\,F^{\pm}_{j} \qquad \text{where} \qquad F^{\pm}_{j} = \prod_{a=0}^{j-1}(1-\omega^{\pm}_{a}), \tag{B.4}$$

and summing all j,

$$x^{\pm} = x^{\pm}_{0}\,F^{\pm} \qquad \text{where} \qquad F^{\pm} = 1 + \sum_{j=1}^{\infty} F^{\pm}_{j}. \tag{B.5}$$

Using the stationary condition $x^{-}_{0} = x^{+}_{0}$, we reach:

$$\frac{x^{+}}{x^{-}} = \frac{F^{+}}{F^{-}}. \tag{B.6}$$

Notice that, for the complete graph, $\tilde{x}^{+} = x$, $\tilde{x}^{-} = 1-x$. Therefore, $F^{\pm}$ is a function of the variable $x^{\mp}$ ($F^{+} = F(1-x)$). Thus, we rewrite the previous expression just in terms of the variable x:

$$\frac{x}{1-x} = \frac{F(1-x)}{F(x)}. \tag{B.7}$$

C. Internal time recursive relation in Phase $\mathbf{I/I^*}$

In Phase I and I^*, the exceeding threshold condition ($m/k > T$) is full-filled for almost all agents in the system. Thus, agents will change their state and reset the internal time once activated. For the original model, all agents are activated once in a time step on average, but for the model with aging, the activation probability plays an important role. We consider here a set of N agents that are activated randomly with an activation probability $p_A(j)$ and, once activated, they reset their internal time. Being $n_i(t)$ the fraction of agents with internal time i at the time step t, we build a recursive relation for the previously described dynamics in terms of variables i and t:

$$n_1(t) = \sum_{i=1}^{t-1} p_A(i) n_i(t-1) \qquad n_i(t) = (1 - p_A(i-1)) n_{i-1}(t-1) \qquad i > 1. \tag{C.1}$$

This recursion relation can be solved numerically from the initial condition ($n_1(0) = 1$, $n_i(0) = 0$ for $i > 1$). To obtain the mean internal time at time t, we just need to compute the following:

$$\bar{\tau}(t) = \sum_{i=1}^{t} i n_i(t). \tag{C.2}$$

The solution from this recursive relation describes the mean internal time dynamics with great agreement with the numerical simulations performed at Phase I (for the complete graph) and Phase I^* (for the Erdős-Rényi and Moore lattice).